



SEA
GRANT
PROJECT
OFFICE

CIRCULATING COPY
Sea Grant Depository

MATHEMATICAL MODELS OF THE MASSACHUSETTS BAY

Part I.

by

**Jerome J. Connor
and John D. Wang**

Part II.

by

**Douglas A. Briggs
and Ole S. Madsen**

NATIONAL SEA GRANT DEPOSITORY
PELL LIBRARY BUILDING
URL MASSACHUSETTS BAY CAMPUS
NARRAGANSETT, RI 02882



Massachusetts Institute of Technology

Cambridge, Massachusetts 02139

Report No. MITSG 74-4

October 15, 1973

CIRCULATING COPY
Sea Grant Depository

MATHEMATICAL MODELS OF THE MASSACHUSETTS BAY

**PART I. FINITE ELEMENT MODELING OF TWO-
DIMENSIONAL HYDRODYNAMIC CIRCULATION**

by

Jerome J. Connor

and

John D. Wang

**PART II. ANALYTICAL MODELS FOR ONE- AND TWO-
LAYER SYSTEMS IN RECTANGULAR BASINS**

by

Douglas A. Briggs

and

Ole S. Madsen

Report No. MITSG 74-4
Index No. 74-304-Cbs

MATHEMATICAL MODELS OF THE MASSACHUSETTS BAY

PART I

FINITE ELEMENT MODELING OF TWO-DIMENSIONAL
HYDRODYNAMIC CIRCULATION IN SHALLOW WATER MASSES

BY

JEROME J. CONNOR

and

JOHN D. WANG

RALPH M. PARSONS LABORATORY

FOR WATER RESOURCES AND HYDRODYNAMICS

Department of Civil Engineering

Massachusetts Institute of Technology

Prepared with the Support of

Sea Grant Office
National Oceanographic and Atmospheric Administration
Department of Commerce
Washington, D.C.

MATHEMATICAL MODELS OF THE MASSACHUSETTS BAY

ABSTRACT - PART I

FINITE ELEMENT MODELING OF TWO-DIMENSIONAL
HYDRODYNAMIC CIRCULATION IN SHALLOW WATER MASSES

BY

JEROME J. CONNOR

and

JOHN D. WANG

The vertically integrated conservation of mass and momentum equations for shallow water bodies are reviewed. The equations used in this study are based on only two assumptions: hydrostatic pressure and squares of surface elevation gradients negligible with respect to unity. The finite element method is applied to reduce the governing equations to a system of ordinary non-linear differential equations in time for which two different numerical integration schemes are described. Model results are compared with analytical solutions. Also, numerical predictions of the tidal response for Massachusetts Bay are presented.

PART I

ACKNOWLEDGEMENTS

This study constitutes a part of a series of investigations in a major environmental research program on the "Sea Environment in Massachusetts Bay and Adjacent Waters". This program consists of theoretical and field investigations and is under the administrative and technical direction of Dr. Arthur T. Ippen, Institute Professor, Department of Civil Engineering and of Dr. Erik L. Mollo-Christensen, Professor, Department of Meteorology as co-principal investigators. Support of the program is provided in part by the Sea Grant Office of NOAA, Department of Commerce, Washington, D.C. through Grant No. NG-43-72, in part by the Henry L. and Grace Doherty Charitable Foundation, Inc., and in part by the Department of Natural Resources, Commonwealth of Massachusetts through Project No. DMR-73-1. The project which is the subject of this report was conducted by staff members of the Ralph M. Parsons Laboratory for Water Resources and Hydrodynamics and was administered under Project No. DSR 80344 and DSR 81100 at M.I.T.

This report was prepared by Mr. John D. Wang, Research Assistant, and Dr. Jerome J. Connor, Professor of Civil Engineering. The advice and guidance of Dr. Arthur T. Ippen is hereby gratefully acknowledged.

Appreciation is expressed here to Ms. Stephanie M. Demeris for her excellent typing of this manuscript.

TABLE OF CONTENTS

	<u>Page</u>
ABSTRACT	1
TABLE OF CONTENTS	2
LIST OF FIGURES	3
LIST OF SYMBOLS	5
CHAPTER 1 INTRODUCTION	9
CHAPTER 2 BASIC HYDRODYNAMIC EQUATIONS	11
CHAPTER 3 VARIATIONAL STATEMENT	20
CHAPTER 4 FINITE ELEMENT MODEL	22
CHAPTER 5 NUMERICAL INTEGRATION SCHEMES	27
CHAPTER 6 MODEL COMPARISONS AND RESULTS	31
REFERENCES	56

LIST OF FIGURES

<u>Figure</u>		<u>Page</u>
1	Geometrical and Surface Force Notation	12
2	Boundary Notation	17
3	Finite Element Geometric Discretization	23
4	Sketch of Rectangular Channel	32
5	Comparison of Numerical and Analytical Solutions	34
6	Rectangular Model of Massachusetts Bay Analytical Solutions	36
7	Rectangular Model of Massachusetts Bay Dimensions and Element Layout	37
8	Rectangular Model of Massachusetts Bay Finite Element Solution. Surface Elevations	38
9	Rectangular Model of Massachusetts Bay Finite Element Solution. Currents	39
10	Massachusetts Bay. Geographical Boundaries and Finite Element Grid	41
11	Massachusetts Bay Surface Contour Lines at High Tide	42
12	Massachusetts Bay Surface Contour Lines at Low Tide	43
13	Massachusetts Bay Currents at Ebbing Tide	44
14	Massachusetts Bay Currents at Flooding Tide	45
15	Time History of Computed Elevations at Boston and in Cape Cod Bay	46
16	Time History of Computed Currents a. Center of Cape Cod Bay b. 15 km East of Boston	47

<u>Figure</u>		<u>Page</u>
17	Computed Current Field due to Wind Forcing from the North. No Tidal Motion. Steady-state Reached	50
18	Computed Current Field due to Wind Forcing from the South-West. No Tidal Motion. Steady-state Reached	51
19	Superposition of Computed Flood Tide Currents and Wind Driven Currents	52
20	Superposition of Computed Ebb Tide Currents and Wind Driven Currents	53
21	Flood Tide and Wind Driven Current Field	54
22	Ebb Tide and Wind Driven Current Field	55

LIST OF SYMBOLS

A	area
a	tidal amplitude
B_x^*	sum of surface and bottom stress terms in x-direction
B_y^*	sum of surface and bottom stress terms in y-direction
B_x	sum of surface, bottom, coriolis and nonlinear force measures in x-direction
B_y	sum of surface, bottom, coriolis and nonlinear force measures in y-direction
b	superscript signifying bottom
C_f	bottom friction factor
c	wave velocity = \sqrt{gh}
E	truncation error
e	mass source per unit volume
e	superscript signifying eddy viscosity term
(e)	superscript signifying element
f	coriolis parameter = $2\Omega \sin \phi$
f	function
F_p	pressure force resultant
F_{nn}	} internal stress resultants
F_{ns}	
F_{xx}	
F_{yy}	
$F_{xy} = F_{yx}$	

g	gravitational acceleration
g	function
H	total depth = $h+\eta$
h	mean low water (chart) depth
i	subscript signifying node i
k_1, k_2 k_3, k_4	integration variables
L	channel length
M	"mass" matrix
n_1, n_2, n_3	modes of element n
n	normal (outward) coordinate
P	force matrix
p	pressure
Q	velocity component matrix
q_x	mass flux in x-direction
q_y	mass flux in y-direction
q_I	distributed mass inflow per unit area
R	residual
S	boundary
S_f	flux boundary
S_o	ocean boundary
s	tangential coordinate
s	supercript signifying surface
T	tidal period

T	superscript signifying transpose of matrix
t	time
u	x-velocity
v	y-velocity
w	z-velocity
x, y, z	orthogonal coordinates forming a right-handed system. z vertical upwards, x towards east
α	direction cosine
Δt	time increment
$\Delta H, \Delta q_x,$ $\Delta q_y, \Delta Q$	weighting functions
δ	grid dimension measure
δ_ρ	incremental density
$\epsilon_{xx}, \epsilon_{yy},$ ϵ_{xy}	eddy viscosities
ϵ_h	convergence tolerance for heights
ϵ_Q	convergence tolerance for velocities
ζ	function
η	surface elevation above MLW
θ_h	relaxation factor for heights
θ_Q	relaxation factor for velocities
ρ	density
ρ_o	average density
τ	stress
ϕ	expansion function
ϕ	latitude

Ω phase velocity of earth's rotation
 ω phase velocity of tidal excitation
, (comma) subscript signifying partial differentiation
. (punctuation) superscript signifying time derivative

CHAPTER 1

INTRODUCTION

Mathematical modelling of circulation and dispersion in water bodies has developed rapidly during the past decade. The major impetus has been the concern for the environment which has necessitated more detailed studies of water quality and especially the development of transient predictive models.

This study is restricted to the development and evaluation of finite element models for predicting the transient response of water bodies due to tidal and wind excitation. Three dimensional solutions are most desirable but the uncertainty of boundary conditions and in the magnitudes of the eddy viscosities and turbulent diffusion coefficients does not justify the effort at this time. Therefore, this study is further restricted to vertically well-mixed two dimensional flow. Irregularity of the boundary geometry and depth are allowed for but the velocities are assumed to be approximately uniform over the depth.

There are a number of recent reports [1-7] describing finite difference models for circulation and dispersion in well-mixed estuaries and coastal waters. The proposed models by Leendertse et al. [3] and Abbot et al [7] appear to be well documented and have extensive supporting software for data generation and plotting.

Finite difference models employ rectangular grids and one has to resort to approximating an irregular boundary with orthogonal segments. This requires a small mesh spacing throughout the domain. Approximate techniques for expanding the mesh in the interior have

been employed but they can introduce additional numerical difficulties.

The finite element method was first applied to fluid flow by Martin [8] who treated two-dimensional steady potential flow. It has since been extended to Navier-Stokes flow [9], lake circulation [10,11], and long wave propagation (12). The method has proven to be particularly convenient for problems involving irregular boundaries since the mesh can be chosen to "fit" the boundary. However, relatively little experience with finite element transient solutions of hyperbolic equations has been accumulated in contrast to finite difference models where stability has been studied extensively [15,16].

In what follows, a consistent derivation of the vertically averaged equations for long wave propagation is presented. The formulation is sufficiently different from existing formulations (Pritchard, Ref. 2) to warrant its inclusion here. Next, the method of weighted residuals [14] is applied to generate a "quasi" variational statement which is the basis for the finite element discretization. Three numerical integration schemes are evaluated for one and two-dimensional test problems discretized with first order triangular elements. The scheme is also applied to Massachusetts Bay, a fairly complex coastal area, and a solution strategy for "adjusting" the bottom friction is discussed.

CHAPTER 2

BASIC HYDRODYNAMIC EQUATIONS

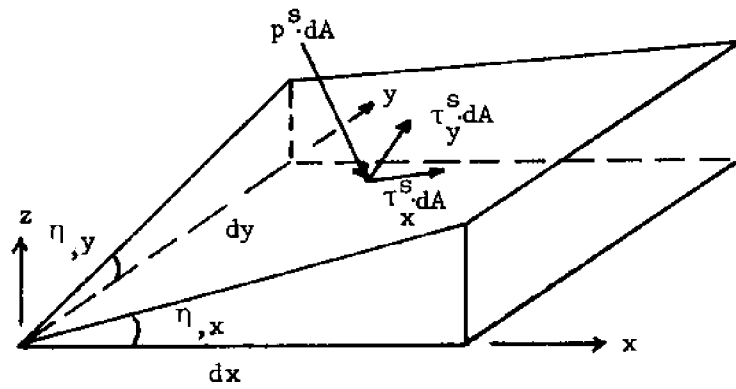
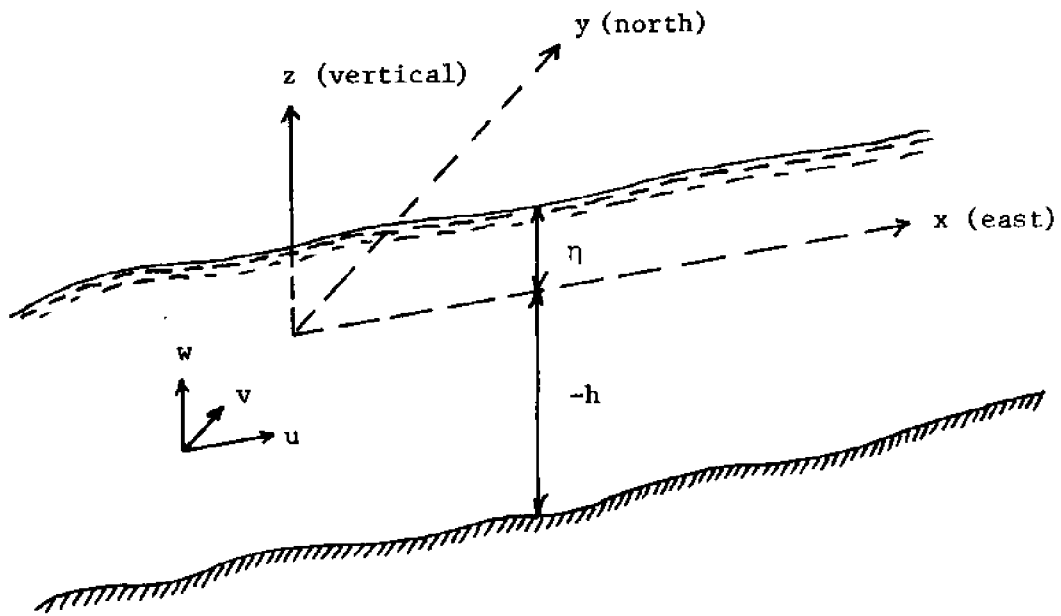
The 3-dimensional forms of the ensemble averaged continuity and momentum equations constitute the basis for the present formulation.

They are

$$\begin{aligned}
 \frac{\partial \rho}{\partial t} + (\rho u)_{,x} + (\rho v)_{,y} + (\rho w)_{,z} &= e \\
 (\rho u)_{,t} + (\rho u^2)_{,x} + (\rho uv)_{,y} + (\rho uw)_{,z} \\
 &= \rho f v - p_{,x} + \tau_{xx,x} + \tau_{yx,y} + \tau_{zx,z} \\
 (\rho v)_{,t} + (\rho uv)_{,x} + (\rho v^2)_{,y} + (\rho vw)_{,z} \\
 &= -\rho f u - p_{,y} + \tau_{xy,x} + \tau_{yy,y} + \tau_{zy,z}
 \end{aligned} \tag{1}$$

where u, v, w are the averaged velocities, e is a source of mass inflow per unit volume, τ are the sums of viscous and Reynolds stresses, ρ is mass density and f is the Coriolis parameter. By definition, the stress components are symmetrical with respect to the subscripts, i.e., $\tau_{xy} = \tau_{yx}$, etc.

A set of 2-dimensional equations is obtained by integrating (1) over the total depth and applying Leibnitz's rule. The notation and the applied surface forces are shown in Figure 1. We assume the surface slope is small and neglect $(\eta_{,x})^2, (\eta_{,y})^2$ with respect to unity. With this approximation, the surface force-interior stress relations for the upper surface reduce to



$$[\eta_{,x}]^2 \ll 1$$

$$[\eta_{,y}]^2 \ll 1$$

$$dA \approx dx dy$$

Figure 1. Geometrical and surface force notation.

$$\begin{aligned}
 \tau_x^s + \eta_{,x} p^s &= \left| -\eta_{,x} (-p + \tau_{xx}) - \eta_{,y} \tau_{yx} + \tau_{zx} \right|_{z=\eta} \\
 \tau_y^s + \eta_{,y} p^s &= \left| -\eta_{,x} \tau_{xy} - \eta_{,y} (-p + \tau_{yy}) + \tau_{zy} \right|_{z=\eta} \\
 -p^s + \eta_{,x} \tau_x^s + \eta_{,y} \tau_y^s &= \left| -p + \tau_{zz} - \eta_{,x} \tau_{xz} - \eta_{,y} \tau_{yz} \right|_{z=\eta}
 \end{aligned} \tag{2}$$

where τ^s are the applied tangential wind stresses and p^s is the external pressure. A similar set applies for the bottom surface.

Leibnitz's rule defines partial differentiation of an integral having variable limits. Its form for x differentiation is

$$\frac{\partial}{\partial x} \int_{g_1}^{g_2} f dz = \int_{g_1}^{g_2} \frac{\partial f}{\partial x} dz + f \Big|_{g_2} \frac{\partial g_2}{\partial x} - f \Big|_{g_1} \frac{\partial g_1}{\partial x} \tag{3}$$

Using the general form of (3) and applying the kinematic relation

$$w \Big|_{z=\zeta} = \frac{D\zeta}{Dt} = \frac{\partial \zeta}{\partial t} + u \frac{\partial \zeta}{\partial x} + v \frac{\partial \zeta}{\partial y} \tag{4}$$

at $\zeta = \eta$ and $\zeta = -h$, assuming the density is constant over depth results in the following "integrated" equations:

$$\begin{aligned}
 \frac{\partial}{\partial t}(\rho H) + \frac{\partial}{\partial x} q_x + \frac{\partial}{\partial y} q_y &= q_I \\
 \frac{\partial}{\partial t} q_x + \frac{\partial}{\partial x} \left(\rho \int_{-h}^{\eta} u^2 dz \right) + \frac{\partial}{\partial y} \left(\rho \int_{-h}^{\eta} uv dz \right) \\
 &= f q_y + \tau_x^s + \tau_x^b + p^s \frac{\partial \eta}{\partial x} + p^b \frac{\partial h}{\partial x} \\
 &+ \frac{\partial}{\partial x} \int_{-h}^{\eta} (-p + \tau_{xx}) dz + \frac{\partial}{\partial y} \int_{-h}^{\eta} \tau_{yx} dz
 \end{aligned} \tag{5}$$

$$\begin{aligned}
 \frac{\partial}{\partial t} q_y + \frac{\partial}{\partial x} \left(\rho \int_{-h}^{\eta} u v dz \right) + \frac{\partial}{\partial y} \left(\rho \int_{-h}^{\eta} v^2 dz \right) \\
 = - f q_x + \tau_y^s + \tau_y^b + p^s \frac{\partial \eta}{\partial y} + p^b \frac{\partial h}{\partial y} \\
 + \frac{\partial}{\partial x} \int_{-h}^{\eta} \tau_{xy} dz + \frac{\partial}{\partial y} \int_{-h}^{\eta} (-p + \tau_{yy}) dz
 \end{aligned}$$

where

$$H = h + \eta$$

$$q_x = \rho \int_{-h}^{\eta} u dz$$

$$q_y = \rho \int_{-h}^{\eta} v dz$$

and q_I is the distributed mass inflow per unit area.

To integrate the nonlinear advective terms we express the velocity components as

$$\begin{aligned}
 u &= \bar{u}(x, y, t) + u'(x, y, z, t) \\
 v &= \bar{v}(x, y, t) + v'(x, y, z, t)
 \end{aligned} \tag{6}$$

where \bar{u} , \bar{v} denote the vertically averaged velocities and u' , v' represent the vertical deviations. By definition,

$$\begin{aligned}
 q_x &\equiv \rho H \bar{u} \\
 q_y &\equiv \rho H \bar{v} \\
 \int_{-h}^{\eta} u' dz &= \int_{-h}^{\eta} v' dz = 0
 \end{aligned} \tag{7}$$

Introducing (6) in (5) and grouping terms in a form similar to the 3-dimensional momentum equations, we write the "integrated" momentum equations as

$$\begin{aligned}
 \frac{\partial}{\partial t}(\rho H) + \frac{\partial}{\partial x} q_x + \frac{\partial}{\partial y} q_y &= q_I \\
 \frac{\partial}{\partial t} q_x + \frac{\partial}{\partial x}(\bar{u}q_x) + \frac{\partial}{\partial y}(\bar{u}q_y) &= f q_y + B_x^* + \frac{\partial}{\partial x}(F_{xx} - F_p) + \frac{\partial}{\partial y} F_{yx} \\
 \frac{\partial}{\partial t} q_y + \frac{\partial}{\partial x}(\bar{v}q_x) + \frac{\partial}{\partial y}(\bar{v}q_y) &= -f q_x + B_y^* + \frac{\partial}{\partial x} F_{xy} + \frac{\partial}{\partial y}(F_{yy} - F_p)
 \end{aligned} \tag{8}$$

where B_x^* , B_y^* contain the surface and bottom stress terms, F_p is the pressure force resultant and F_{xx} , F_{xy} , F_{yy} are "equivalent" internal stress resultants due to turbulent and dispersive momentum flux.

$$\begin{aligned}
 F_p &= \int_{-h}^{\eta} p dz \\
 F_{xx} &= \int_{-h}^{\eta} (\tau_{xx} - \rho(u')^2) dz \\
 F_{yy} &= \int_{-h}^{\eta} (\tau_{yy} - \rho(v')^2) dz \\
 F_{xy} &= F_{yx} = \int_{-h}^{\eta} (\tau_{xy} - \rho u'v') dz
 \end{aligned} \tag{9}$$

We approximate the flux terms with

$$\begin{aligned}
 F_{xx} &= \epsilon_{xx} \frac{\partial}{\partial x} q_x \\
 F_{yy} &= \epsilon_{yy} \frac{\partial}{\partial y} q_y \\
 F_{yx} &= F_{xy} = \epsilon_{xy} \left(\frac{\partial}{\partial y} q_x + \frac{\partial}{\partial x} q_y \right)
 \end{aligned} \tag{10}$$

One can interpret the ϵ 's as either equivalent Fickian diffusion coefficients or generalized eddy viscosities. In (10) we have allowed for orthotropic behavior. For isotropic flow, (10) applies for arbitrary orientation of x , y , and therefore one has

$$\begin{aligned}\epsilon_{xx} &= \epsilon_{yy} = 2\epsilon \\ \epsilon_{xy} &= \epsilon\end{aligned}\tag{11}$$

Next, we assume the pressure variation with z is hydrostatic,

$$p = \rho g(\eta - z) + p^s\tag{12}$$

and the bottom shear is predicted by a quadratic relation,

$$\begin{aligned}\tau_x^b &= -\frac{C_f}{\rho H^2} q_x (q_x^2 + q_y^2)^{1/2} \\ \tau_y^b &= -\frac{C_f}{\rho H^2} q_y (q_x^2 + q_y^2)^{1/2}\end{aligned}\tag{13}$$

where C_f is a friction factor.

The corresponding forces are

$$\begin{aligned}F_p &= \int_{-h}^{\eta} p dz = p^s H + \frac{\rho g}{2} H^2 \\ B_x^* &= \tau_x^s + \tau_x^b + p^s \frac{\partial H}{\partial x} + \rho g H \frac{\partial h}{\partial x} \\ B_y^* &= \tau_y^s + \tau_y^b + p^s \frac{\partial H}{\partial y} + \rho g H \frac{\partial h}{\partial y}\end{aligned}\tag{14}$$

Lastly, we express the mass density as

$$\rho_0 + \delta\rho\tag{15}$$

where ρ_0 is constant. The incremental density $\delta\rho$ is small in comparison to ρ_0 for circulation in coastal waters and estuaries. Therefore, we set $\rho = \rho_0$ except for the pressure force terms. This is the Boussinesq approximation.

To complete the formulation, we need to establish the boundary conditions. The total boundary, S , consists of flux segments, S_f , and ocean segments, S_o , as shown in Figure 2. We refer the flux and

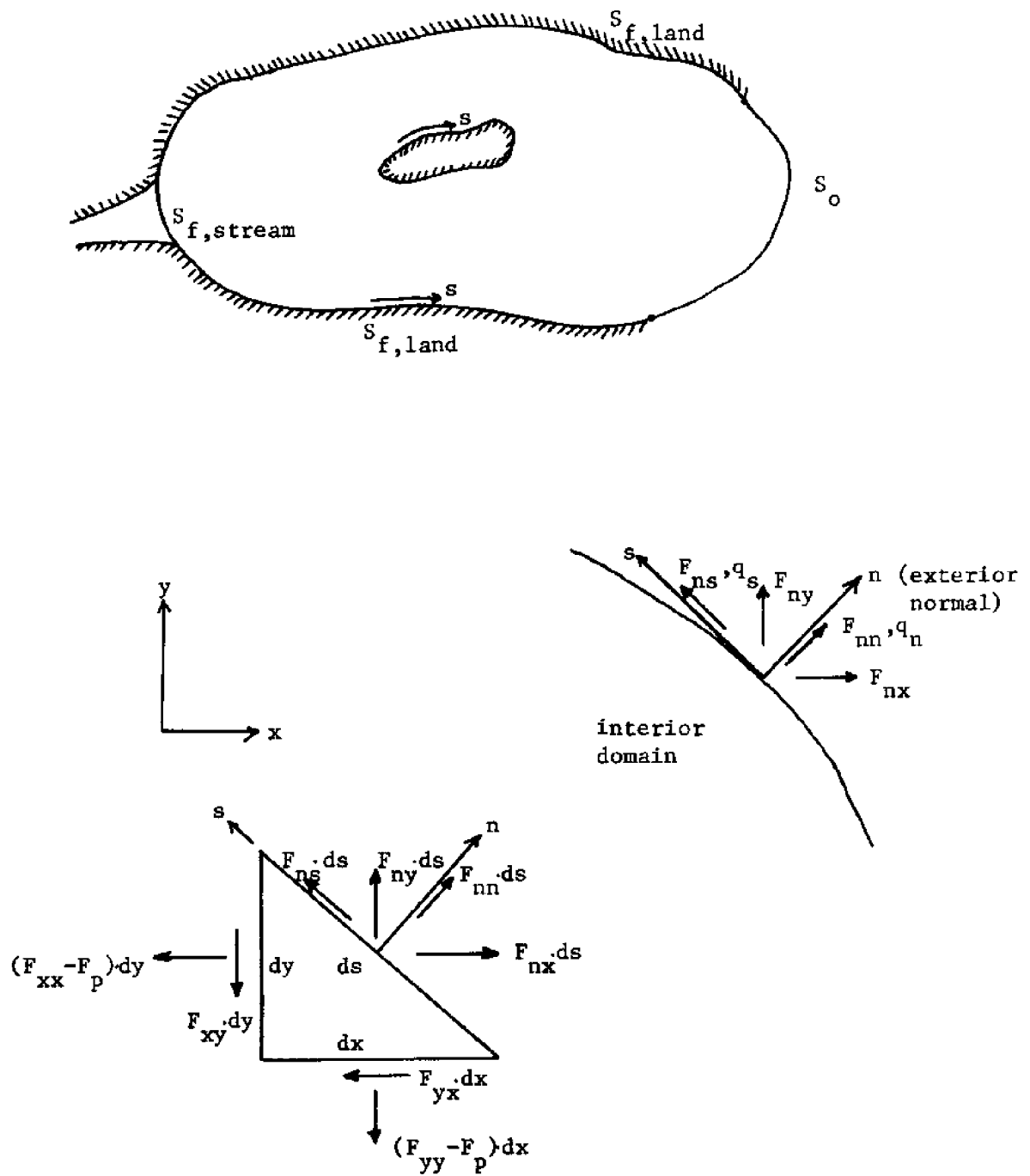


Figure 2. Boundary notation.

boundary force measures to the local reference frame defined by the exterior normal, n , and the tangential direction, s , where $n \rightarrow s$ has the same sense as $x \rightarrow y$.

Mass flux is a vector quantity and its components transform according to

$$\begin{aligned} q_n &= \int_{-h}^{\eta} \rho u_n dz = \alpha_{nx} q_x + \alpha_{ny} q_y \\ q_s &= \int_{-h}^{\eta} \rho u_s dz = -\alpha_{ny} q_x + \alpha_{nx} q_y \end{aligned} \quad (16)$$

$$\alpha_{nx} = \cos(n, x) \quad \alpha_{ny} = \cos(n, y)$$

Consistent with interpreting the momentum flux due to nonuniform velocity distribution through the depth as equivalent internal force resultants, we write

$$\begin{aligned} F_{nx} &= \alpha_{nx} (F_{xx} - F_p) + \alpha_{ny} F_{yx} \\ F_{ny} &= \alpha_{nx} F_{xy} + \alpha_{ny} (F_{yy} - F_p) \end{aligned} \quad (17)$$

and then transform according to (16), obtaining

$$\begin{aligned} F_{nn} &= -F_p + F_{nn}^e \\ F_{ns} &= F_{ns}^e \\ F_{nn}^e &= \alpha_{nx}^2 F_{xx} + \alpha_{ny}^2 F_{yy} + 2\alpha_{nx}\alpha_{ny} F_{xy} \\ F_{ns}^e &= (\alpha_{nx}^2 - \alpha_{ny}^2) F_{xy} + \alpha_{nx}\alpha_{ny} (F_{yy} - F_{xx}) \end{aligned} \quad (18)$$

On a land boundary (assuming no tidal flats), the flux components are prescribed.

$$q_n = q_s = 0 \quad \text{on } S_{f, \text{land}} \quad (19)$$

On an ocean boundary, the normal and tangential boundary forces are prescribed.

$$\begin{aligned} F_{nn} &= \bar{F}_{nn} \\ F_{ns} &= \bar{F}_{ns} \end{aligned} \quad \text{on } S_o \quad (20)$$

On flux boundaries other than land such as at river entrances the normal flux is specified equal to the river mass flow.

$$\begin{aligned} q_n &= \bar{q}_{\text{river}} \\ q_s &= 0 \end{aligned} \quad \text{on } S_{\text{river}} \quad (21)$$

When the eddy viscosities are neglected, $F^e = 0$, and we cannot prescribe the tangential flux or tangential boundary force. The boundary conditions reduce to

$$q_n = \bar{q}_n \quad \text{on } S_f \quad (22)$$

and

$$F_{nn} = \bar{F} \quad \text{on } S_o \quad (23)$$

In the present model application, equation (23) with $\bar{F}_{nn} = -F_p$ is used although eddy viscosities are assumed non zero in the interior.

CHAPTER 3

VARIATIONAL STATEMENT

The governing equations are (8) and the appropriate boundary conditions. In what follows, we apply Galerkin's method [14] to establish the variational statements which are the basis for the finite element method.

Let ΔH , Δq_x , Δq_y represent weighting functions. We weight the continuity equation with respect to ΔH , the momentum equations with respect to Δq , integrate over the domain, and require the residuals to vanish. We also weight the force boundary conditions on S_o . The resulting expressions are

$$\iint_A \{ (\rho_o H)_{,t} + q_{x,x} + q_{y,y} - q_I \} \Delta H dA = 0 \quad (24)$$

and

$$\begin{aligned} \iint_A \{ q_{x,t} - \frac{\partial}{\partial x} (F_{xx} - F_p) - \frac{\partial}{\partial y} F_{yx} - B_x \} \Delta q_x dA &= 0 \\ \iint_A \{ q_{y,t} - \frac{\partial}{\partial x} F_{xy} - \frac{\partial}{\partial y} (F_{yy} - F_p) - B_y \} \Delta q_y dA &= 0 \end{aligned} \quad (25)$$

$$\int_{S_o} \{ -\bar{F}_{nx} + \alpha_{nx} (F_{xx} - F_p) + \alpha_{ny} F_{yx} \} \Delta q_x dS = 0$$

$$\int_{S_o} \{ -\bar{F}_{ny} + \alpha_{nx} F_{xy} + \alpha_{ny} (F_{yy} - F_p) \} \Delta q_y dS = 0$$

Here we have included the Coriolis and nonlinear terms in B.

$$B_x = B_x^* + f q_y - \frac{\partial}{\partial x} (\bar{u} q_x) - \frac{\partial}{\partial y} (\bar{u} q_y) \quad (26)$$

$$B_y = B_y^* - f q_x - \frac{\partial}{\partial x} (\bar{v} q_x) - \frac{\partial}{\partial y} (\bar{v} q_y)$$

Applying Gauss's theorem to eliminate the derivatives of the force terms in the momentum equations and combining with the boundary equations leads to the desired form:

$$\begin{aligned} & \iint_A \{ (q_{x,t} - B_x) \Delta q_x + (F_{xx} - F_p) (\Delta q_x)_{,x} + F_{yx} (\Delta q_x)_{,y} \} dA \\ & - \int_{S_o} \bar{F}_{nx} \Delta q_x dS = 0 \\ & \iint_A \{ (q_{y,t} - B_y) \Delta q_y + F_{xy} (\Delta q_y)_{,x} + (F_{yy} - F_p) (\Delta q_y)_{,y} \} dA \\ & - \int_{S_o} \bar{F}_{ny} \Delta q_y dS = 0 \end{aligned} \quad (27)$$

We have required the flux weighting functions to vanish on S_f ,

$$\Delta q_x = \Delta q_y = 0 \quad \text{on } S_f \quad (28)$$

and consequently the boundary integrals on S_f drop out of (27).

CHAPTER 4

FINITE ELEMENT MODEL

The continuity equation (24) and modified momentum equations (27,28) are the starting point for the finite element method. We visualize the domain to consist of subdomains (elements) and take as variables the values of q_x , q_y , H at the points (nodes) defining the discretization. This is illustrated in Figure 3. The distribution of a dependent variable over an elemental domain is expressed in terms of the values of the variable at nodes contained in the element domain and interpolation functions. In this way, the equations are transformed to a set of algebraic equations relating the discrete variables. In the present formulation the simplest elements, viz. triangular with linear interpolation functions, were chosen. However, more complex elements and expansion functions will be implemented in future modeling.

We define the following notation:

q_{xi} , q_{yi} , H_i = values at node i

$\tilde{q}_x^{(e)}$, $\tilde{q}_y^{(e)}$, $\tilde{H}^{(e)}$ are matrices containing the nodal variables

for an element

(29)

N = number of nodes

$\tilde{Q} = \{q_{x1}, q_{y1}, q_{x2}, \dots, q_{yN}\}$ = system flux matrix (2N nodal values)

$\tilde{H} = \{H_1, H_2, \dots, H_N\}$ = system elevation matrix (N nodal values)

For example, $\tilde{H}^{(e)} = \{H_{n1}, H_{n2}, H_{n3}\}$ for the triangular element shown in Figure 3. The expansions are written as

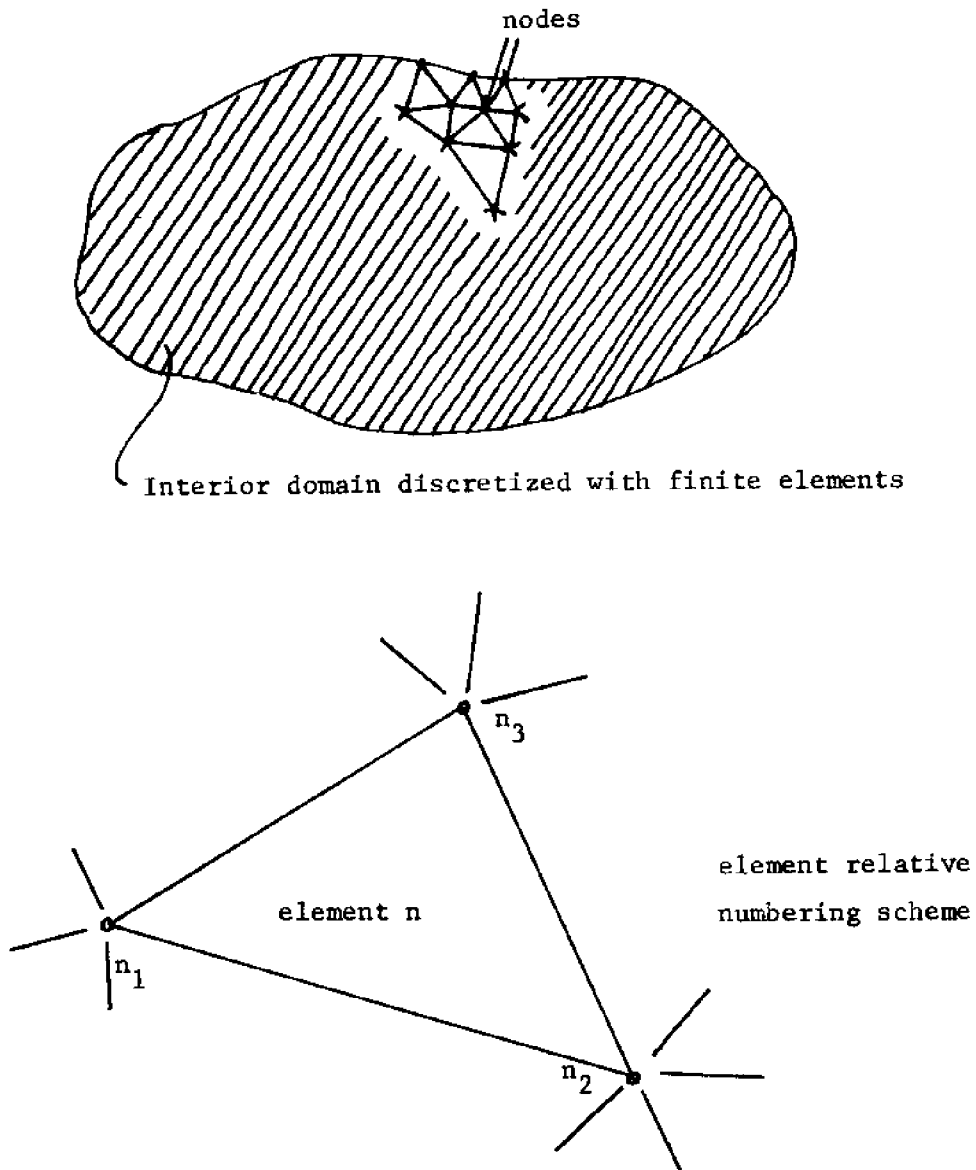


Figure 3. Finite element geometric discretization.
 n_1 , n_2 , n_3 are the actual node numbers
for the nodes in the domain of element n .

$$\begin{aligned}
 q_x &= \tilde{\Phi} q_x^{(e)} \\
 q_y &= \tilde{\Phi} q_y^{(e)} \\
 H &= \tilde{\Phi} H^{(e)}
 \end{aligned}
 \tag{30}$$

where $\tilde{\Phi}$ is a row matrix. We are considering 3 variables per node. One can generalize the approach and allow for a variable number of unknowns per node, i.e., different expansions for flux and elevation, but we prefer to work with the simplest scheme.

In the Galerkin method, one takes the weighting functions identical to the coordinate functions. Since the finite element method employs local functions, the weighting function for a particular nodal variable is finite (non-zero) only for those elements incident on the node. Rather than treat individual nodes, it is more convenient to evaluate element residuals and then superimpose the element contributions at the nodes.

Taking the complete set of weighting functions for an element as

$$\begin{aligned}
 \Delta q_x &= \tilde{\Phi} \Delta q_x^{(e)} \\
 \Delta q_y &= \tilde{\Phi} \Delta q_y^{(e)} \\
 \Delta H &= \tilde{\Phi} \Delta H^{(e)}
 \end{aligned}
 \tag{31}$$

and substituting in (24), (27) results in the following element residuals:

$$\begin{aligned}
 R|_{el} &= (\Delta \tilde{q}_x^{(e)})^T (\tilde{M}^{(e)} \frac{\partial \tilde{q}_x^{(e)}}{\partial t} + \tilde{p}_x^{(e)}) \\
 &+ (\Delta \tilde{q}_y^{(e)})^T (\tilde{M}^{(e)} \frac{\partial \tilde{q}_y^{(e)}}{\partial t} + \tilde{p}_y^{(e)}) \\
 &+ (\Delta \tilde{H}^{(e)})^T (\tilde{M}^{(e)} \frac{\partial \tilde{H}^{(e)}}{\partial t} + \tilde{p}_h^{(e)})
 \end{aligned} \tag{32}$$

where

$$\begin{aligned}
 \tilde{M}^{(e)} &= \iint_{A^{(e)}} \tilde{\phi}^T \tilde{\phi} dA \\
 \tilde{p}_x^{(e)} &= \iint_{A^{(e)}} [-\tilde{\phi}^T B_x + \tilde{\phi}_{,x}^T (F_{xx} - F_p) + \tilde{\phi}_{,y}^T F_{xy}] dA \\
 &\quad - \int_{S_o} \tilde{\phi}^T \tilde{F}_{nx} dS \\
 \tilde{p}_y^{(e)} &= \iint_{A^{(e)}} [-\tilde{\phi}^T B_y + \tilde{\phi}_{,x}^T F_{xy} + \tilde{\phi}_{,y}^T (F_{yy} - F_p)] dA \\
 &\quad - \int_{S_o} \tilde{\phi}^T \tilde{F}_{ny} dS \\
 \tilde{p}_h^{(e)} &= \frac{1}{\rho_o} \iint_{A^{(e)}} \tilde{\phi}^T (q_{x,x} + q_{y,y} - q_I) dA
 \end{aligned} \tag{33}$$

The forces and flux derivatives in (33) are evaluated using (30) and the force expressions (10), (14), (26).

The total residual must vanish for arbitrary Δq_{xi} , Δq_{yi} , ΔH_i ($i = 1, 2, \dots, N$). Then,

$$R|_{\text{total}} = \sum_{\text{elements}} R|_{\text{el}} = 0 \quad (34)$$

for arbitrary ΔQ , ΔH .

We write the expanded form of (34) as

$$R|_{\text{total}} = (\Delta Q)^T \left(\tilde{M} \frac{\partial}{\partial t} \tilde{Q} + \tilde{P} \right) + (\Delta H)^T \left(\tilde{M}_h \frac{\partial}{\partial t} \tilde{H} + \tilde{P}_h \right) \quad (35)$$

and it follows that

$$\begin{aligned} \tilde{M} \dot{\tilde{Q}} + \tilde{P} &= 0 \\ \tilde{M}_h \dot{\tilde{H}} + \tilde{P}_h &= 0 \end{aligned} \quad (36)$$

Finally, we introduce the boundary conditions by modifying the rows and columns of \tilde{M} corresponding to the prescribed variables and incorporating the prescribed terms in \tilde{P} . To minimize notation proliferation, we assume (36) represent the final constrained equations.

CHAPTER 5

NUMERICAL INTEGRATION SCHEMES

Efficient stable numerical integration schemes are essential since a typical problem will involve several hundred node points and integrations over at least one tidal cycle. Complex multi-step methods, although more accurate, require considerably more computation time and storage. Therefore, we have concentrated in this study on investigating the stability and accuracy of relatively simple implicit schemes.

Explicit stability criteria for finite element formulations such as (36) have not yet been developed. The difficulty is due to the arbitrariness of the coefficient matrices (i.e., the elements are confined to a zone adjacent to the diagonal but their magnitudes may be irregular) and also the skew symmetry of the Coriolis and surface elevation terms. One generally has to resort to approximate stability measures based on norms. We make no attempt here to resolve this problem since our primary objective is to evaluate the performance of various schemes.

The simplest scheme is the trapezoidal rule. Its one dimensional form is

$$\begin{aligned} \frac{dy}{dt} &= f(y,t) \\ y_{n+1} - y_n &= \frac{\Delta t}{2} (f_{n+1} + f_n) + E\Delta t \\ E &= \frac{1}{12}(\Delta t)^2 \left| \frac{d^2 f}{dt^2} \right|_{\xi} \quad t_n < \xi < t_{n+1} \end{aligned} \tag{37}$$

Iteration is required since the forcing terms in (36) are non-linear. We include a relaxation factor to accelerate convergence and evaluate the terms in the following order:

$$M_h (H^* - H_n) = \frac{\Delta t}{2} (P_{h,n+1}^{j-1} + P_{h,n})$$

$$H_{n+1}^j = \theta_h H^* + (1 - \theta_h) H_{n+1}^{j-1}$$

and

$$P_{n+1}^{j-1} = P(H_{n+1}^j, Q_{n+1}^{j-1}, t_{n+1}) \quad (38)$$

$$M(Q^* - Q_n) = \frac{\Delta t}{2} (P_{n+1}^{j-1} + P_n)$$

$$Q_{n+1}^j = \theta_Q Q^* + (1 - \theta_Q) Q_{n+1}^{j-1}$$

The mass matrices are factored initially and the iteration and time stepping consists of successive forward and backward substitutions. Convergence is defined by the percentage change in the Euclidian norms for the surface elevation and mass flux vectors.

$$\left(\frac{\sum_{i=1}^N (H_{n+1}^{j+1} - H_{n+1}^j)_i^2}{\sum_{i=1}^N (H_{n+1}^{j+1})_i^2} \right)^{1/2} \leq \epsilon_h$$

(39)

$$\left(\frac{\sum_{i=1}^{2N} (Q_{n+1}^{j+1} - Q_{n+1}^j)_i^2}{\sum_{i=1}^{2N} (Q_{n+1}^{j+1})_i^2} \right)^{1/2} \leq \epsilon_Q$$

where N is the total number of nodes, and ϵ_h, ϵ_Q are the specified tolerances.

The second method examined is the third order predictor-corrector iterative scheme,

$$\frac{dy}{dt} = f(y, t)$$

Predictor:

$$f_{n+1}^1 = 3f_n - 3f_{n-1} + f_{n-2}$$

Corrector:

(40)

$$y^* - y_n = \frac{\Delta t}{12}(5f_{n+1}^{j-1} + 8f_n - f_{n-1}) + E \Delta t$$

$$y_{n+1}^j = \theta y^* + (1 - \theta) y_{n+1}^{j-1}$$

$$E = \frac{1}{12}(\Delta t)^3 \left| \frac{d^3 f}{dt^3} \right|_{\xi} \quad t_n < \xi < t_{n+1}$$

This scheme is not self-starting and requires more storage than the trapezoidal rule. However, it is more accurate and usually converges faster. Equations (39) are again taken as the convergence criteria.

The predictor-corrector scheme (40) is coupled with the following version of the fourth order Runge-Kutta method,

$$\frac{dy}{dt} = f(y, t)$$

$$k_1 = \Delta t \cdot f(y_n, t_n)$$

$$k_2 = \Delta t \cdot f(y_n + 0.4k_1, t_n + 0.4\Delta t)$$

$$k_3 = \Delta t \cdot f(y_n + 0.296978k_1 + 0.158760k_2, t_n + 0.455737\Delta t) \quad (41)$$

$$k_4 = \Delta t \cdot f(y_n + 0.218100k_1 - 3.050965k_2 + 3.832864k_3, t_n + \Delta t)$$

$$y_{n+1} = y_n + 0.174760k_1 - 0.551481k_2 + 1.205535k_3 + 0.171185k_4$$

$$E = O(\Delta t^4)$$

This scheme has the lowest bound on the error for this family of Runge-Kutta methods [15].

The solution of a given problem begins with an optional number of integration steps using the Runge-Kutta method, (minimum three time steps) and then shifts to the predictor-corrector method. At any time step it is possible to change back to the Runge-Kutta method to take advantage of its better accuracy. This flexible formulation also makes it very easy to increase or decrease the time increment, Δt , if so desired.

CHAPTER 6

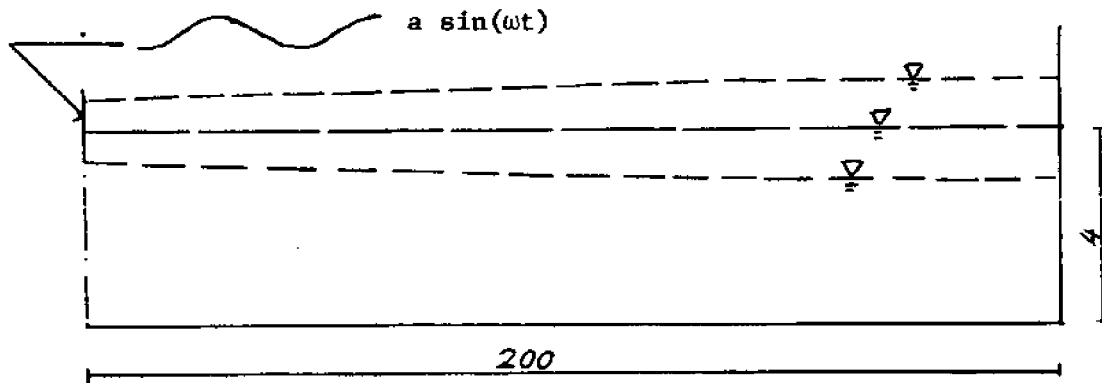
MODEL COMPARISONS AND RESULTS

The objective of this study is to develop a general numerical model for the prediction of 2-dimensional hydrodynamic circulation in waterbodies which are well-mixed through the water column.

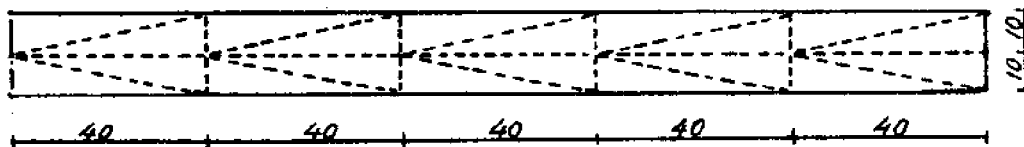
Several example problems for which analytical solutions are readily obtainable were solved with the finite element numerical model. These examples demonstrate how the model performs in situations of varying geometry and also show the effect of eddy diffusivity on damping short "noise" waves generated by the numerical scheme due to truncation and round-off errors. A circulation analysis for Massachusetts Bay was carried out.

The initial numerical solutions with the trapezoidal rule required an average of 7 iterations per time step to obtain comparable results. Since the higher accuracy Runge-Kutta method only requires 4 evaluations of the integrand per time step, this was found unsatisfactory. Convergence with the trapezoidal rule can be accelerated by extrapolating the integrand at the start of each new time step. However, this necessitates more storage and the computational effort is now of the same order as the predictor-corrector method. Therefore, subsequent efforts were concentrated on the fourth order Runge-Kutta and third order predictor-corrector methods.

In the first example, the forced standing wave in a rectangular channel without friction or coriolis effect was modeled as shown in Figure 4. The analytical solution is



a. Channel section



b. Plane view showing arrangement of elements.
(lengths in meters).

Figure 4. Sketch of rectangular channel.

TABLE 1

Comparison of analytical and numerical solution.

Rectangular channel. Initial velocities given by analytical solution. Runge-Kutta method. $\Delta t = 2.5$ sec.

SURFACE HEIGHTS				VELOCITIES		
numerical	analytical	difference	time	numerical	analytical	difference
-1.0000	-1.0000	-	$3T/4$	0.0003	0	0.0003
-1.0217	-1.0210	0.0017		0.0002	0	0.0002
-1.0378	-1.0374	0.0004		0.0003	0	0.0003
-1.0491	-1.0492	0.0001		0.0003	0	0.0003
-1.0565	-1.0563	0.0002		0.0004	0	0.0004
-1.5900	-1.0586	0.0004		0.0001	0	0.0001
0.0000	0	-	T	0.5443	0.5440	0.0003
0.0000	0	0.0000		0.4382	0.4382	0.0000
0.0001	0	0.0001		0.3305	0.3303	0.0002
0.0001	0	0.0001		0.2213	0.2211	0.0002
0.0001	0	0.0001		0.1108	0.1108	0.0000
0.0001	0	0.0001		0.0000	0	0.0000

$$\eta = \frac{a}{\cos \omega \frac{L}{\sqrt{gh}}} \cos\left\{\omega \frac{L}{\sqrt{gh}} \left(\frac{x}{L} - 1\right)\right\} \sin \omega t \quad (42)$$

$$u = - \frac{a \sqrt{gh}}{h \cos \omega \frac{L}{\sqrt{gh}}} \sin\left\{\omega \frac{L}{\sqrt{gh}} \left(\frac{x}{L} - 1\right)\right\} \cos \omega t$$

where the forcing function at the open end, $x = 0$, is

$$\eta_{x=0} = a \sin \omega t$$

and L , h are the channel length and depth. The numerical model was started with the velocity distribution defined by (42) for $t = 0$. For $t > 0$, $\eta = a \sin \omega t$ was prescribed at the 3 open end nodes and the y velocities were set to zero along the boundaries. A comparison of the numerical and analytical results is listed in Table 1. The agreement is very good as expected.

In a "real" situation, one usually does not know the initial velocity field. One possible approach is to start the model with all surface elevations and velocities set to zero (or some other estimated values). The second example demonstrates this type of start up for the rectangular channel. The exact solution was obtained with the method of characteristics. The results with the Runge-Kutta scheme for this problem follow the exact solution closely. However, the predictor-corrector results exhibit an instability characterized by the growth of short waves as demonstrated in Figure 5. This phenomenon was attributed to less accuracy of the scheme. The problem was resolved by introducing some eddy viscosity ($\epsilon_x = \epsilon_y = 2\epsilon_{xy} = 10 \text{ m}^2/\text{sec}$) and again good agreement between analytical and numerical solutions

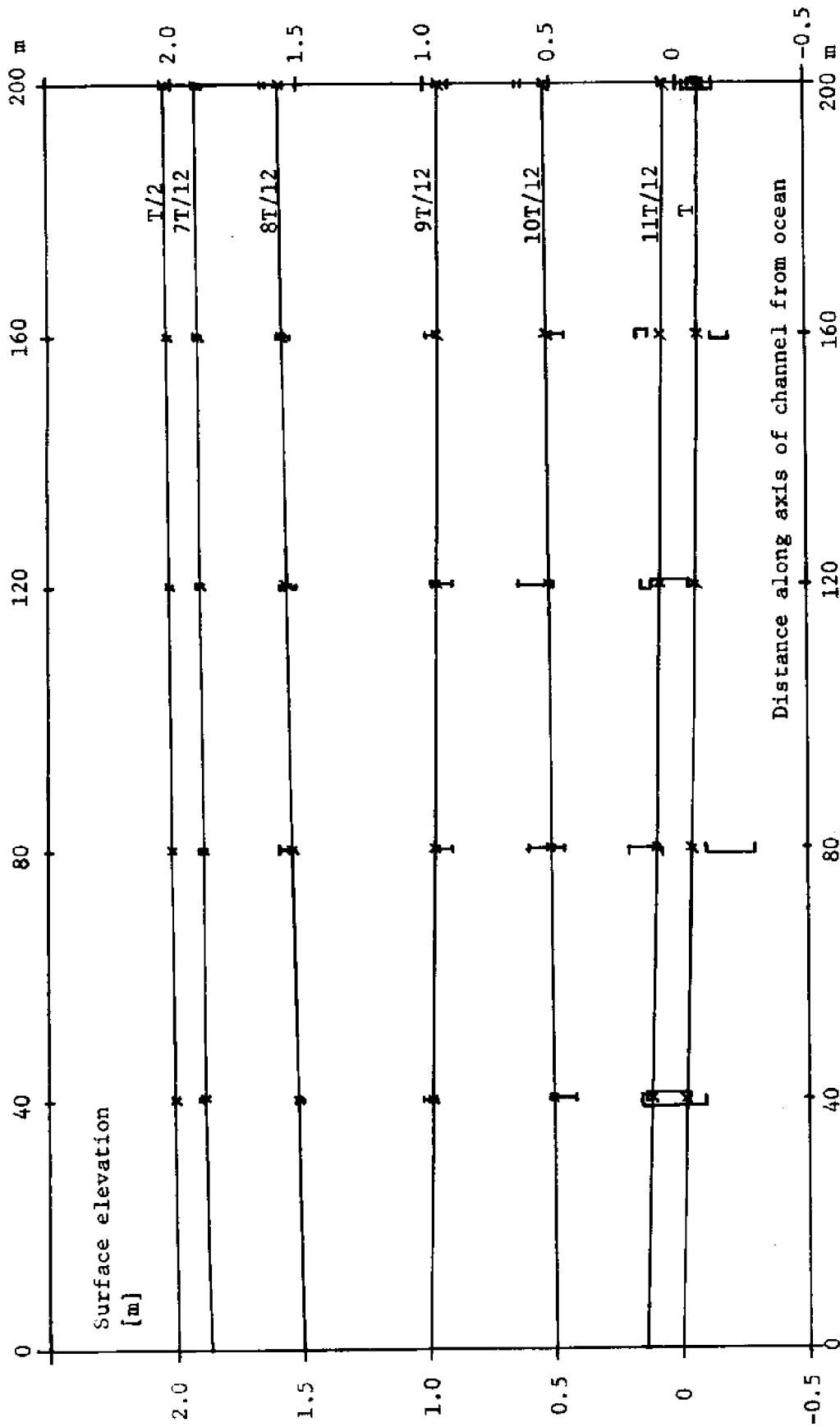


Figure 5. Tidal excitation of one dimensional rectangular channel starting from rest.
 Comparison of analytical and numerical solutions with and without eddy diffusivity.
 Integration by predictor-corrector method. $\Delta t = 2.5$ sec. Period $T = 600$ sec.
 — exact solution.
 x numerical solution without eddy diffusivity, (value range of 3 cross sectional nodes).
 x numerical solution with eddy diffusivity, $\epsilon_x = \epsilon_y = 2\epsilon_{xy} = 10 \text{ m}^2/\text{sec}$.

was obtained. For the same time increments, the predictor-corrector method requires approximately 25% less time than the Runge Kutta scheme.

The 2-dimensional Courant-Friedricks-Lewy stability criterion for explicit differencing of the wave equation is

$$\Delta t \leq \frac{\delta}{\sqrt{2} c} \quad (43)$$

where δ is the grid size and c is the wave velocity. For the rectangular channel we have

$$c = \sqrt{gh} = \sqrt{9.81 \cdot 4} = 626 \text{ m/sec.}$$

so that $10 \text{ m} \leq \delta \leq 40 \text{ m} \rightarrow 1.13 \text{ sec} \leq \Delta t_c \leq 4.5 \text{ sec.}$

The results plotted in Figure 5 were obtained with $\Delta t = 2.5 \text{ sec.}$ When Δt was increased to 5 sec., gradual instability was observed.

An analytical solution in infinite series for the harmonic forcing of a rectangular basin with a slot has recently been derived by Briggs and Madsen [17]. Figure 6 shows their results for a constant depth (36.6 m) model representative of Massachusetts Bay. The model geometry and corresponding finite element layout is shown in Figure 7. The numerically computed surface elevations and current velocities, Figures 8 and 9, compare favorably with the analytical. One explanation for the small discrepancies may be found in the treatment of the ocean boundary condition. In the numerical model the height is prescribed exactly equal to $1.31 \text{ m} \cdot (1 - \cos \omega t)$ across the slot, whereas the analytical solution only satisfies this at four discrete points. The numerical results were obtained with the Runge-Kutta method without bottom friction, eddy viscosity or Coriolis effect. The C-F-L criterion

----- contour lines, (high tide).
velocity, (high water slack).

velocity scale
0 0.5 m/sec

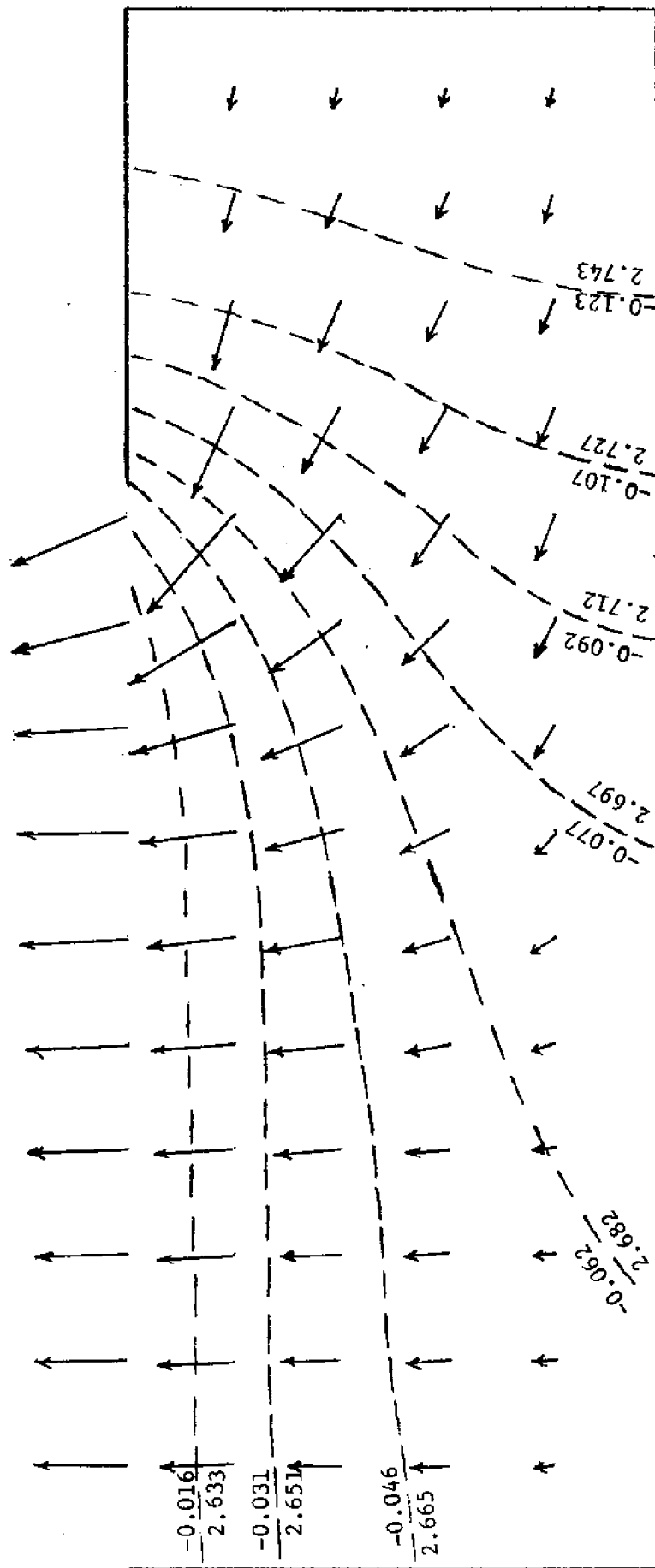


Fig. 6 Rectangular model of Massachusetts Bay.
Analytical solution for surface elevations and currents.
On each contour line the tidal range in meters is indicated.

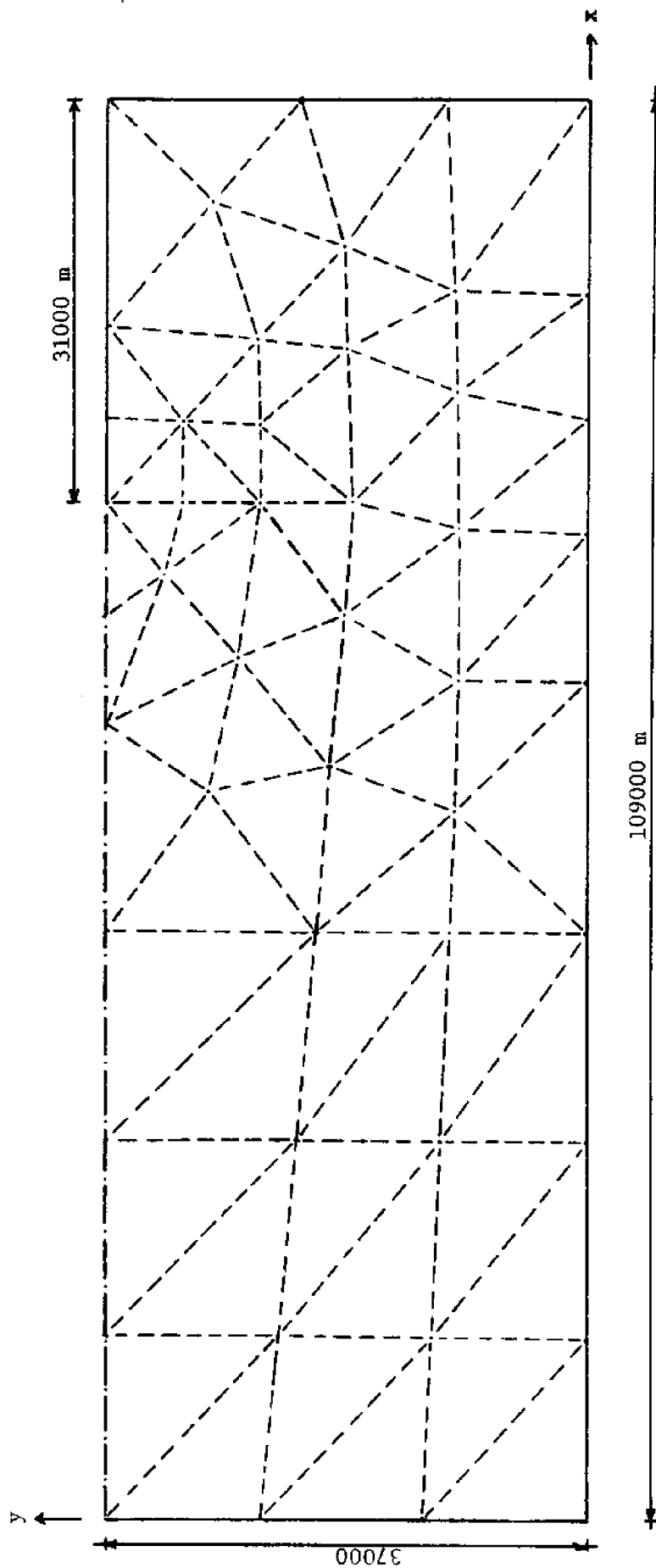


Fig. 7. Rectangular model of Massachusetts Bay.
 Dimensions and element layout. Constant depth = 36.6 m.
 71 elements and 48 nodes.

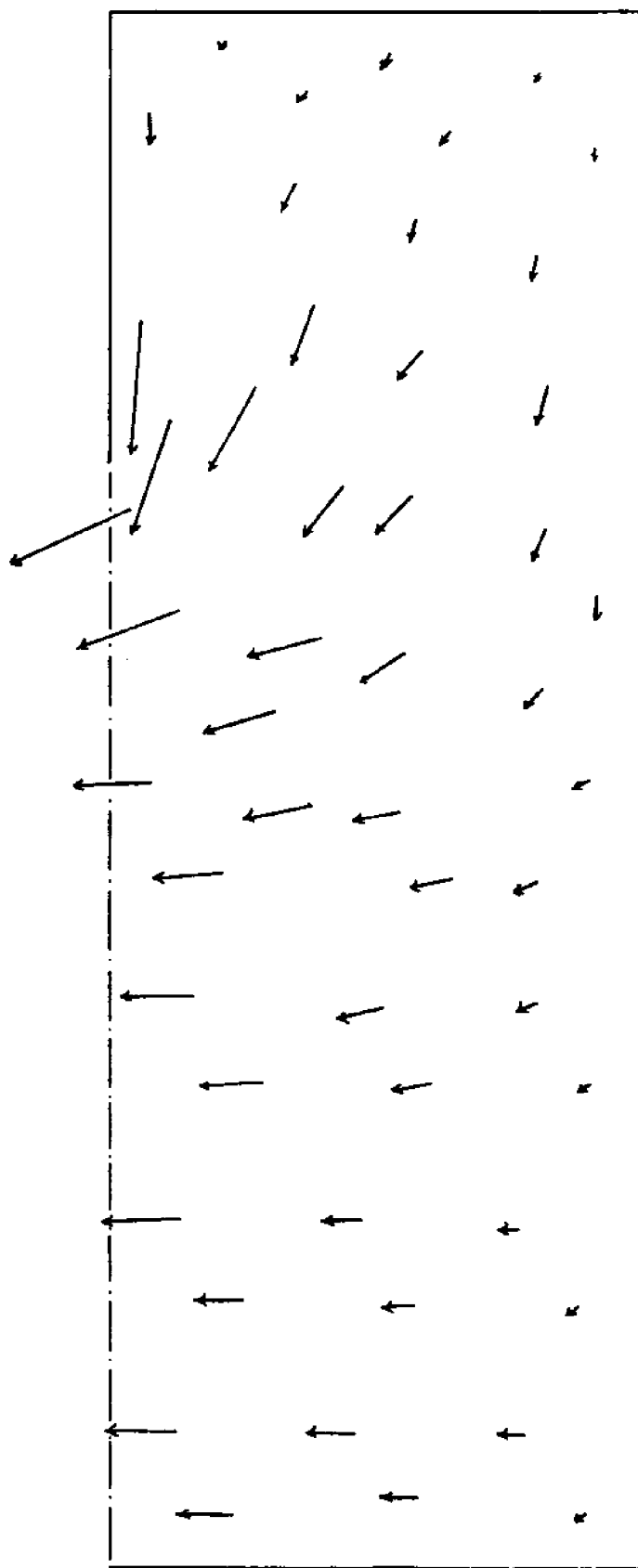



Fig 9. Rectangular model of Massachusetts Bay.

Finite element solution. Runge-Kutta method, $\Delta t = 200$ sec.
Tidal current velocities after 80000 sec., 1.75 tidal period.

velocity scale  0.2 m/sec

is

$$c = \sqrt{9.81 \cdot 36.6} = 18.9 \text{ m/sec}$$

$$t_c = \frac{\delta}{\sqrt{2c}} = \frac{5700}{1.41 \cdot 18.9} = 214 \text{ sec}$$

and a $t = 200 \text{ sec}$ was selected.

Lastly the tidal and winddriven circulation in Massachusetts Bay was computed. The geographic boundaries and the finite element grid are shown in figure 10. Since very little actual data is available, a model yielding only the gross circulation is appropriate at this time. A fairly coarse grid of 74 elements and 53 nodes was laid out reflecting somewhat the varying bottom topography. The tidal ranges for the two shore nodes at the extremities of the ocean boundary were obtained from tide tables [18] and the tide level was assumed to vary smoothly in between. The Coriolis parameter was determined for a latitude of 42°N , $f = 0.973 \cdot 10^{-4} \text{ sec}^{-1}$. No attempts were made to model lateral inflows at this stage.

An initial solution for pure tidal motion with a small constant value of C_f was carefully examined in order to estimate new improved C_f 's for each element, so that the tidal ranges and lag times at the shore points more closely match available tide table data. In estimating C_f , a strong correlation with local depth was assumed. The final solution for which surface contour lines at high and low tide are shown on Figures 11-12 had C_f varying between $0.0025 \rightarrow 0.0011$. However, to really tune the model, current records at several points are desirable.

The calculated tidal water velocities are shown in Figures 13-14 and typical time histories of surface elevations and velocities are plotted in Figures 15-16.

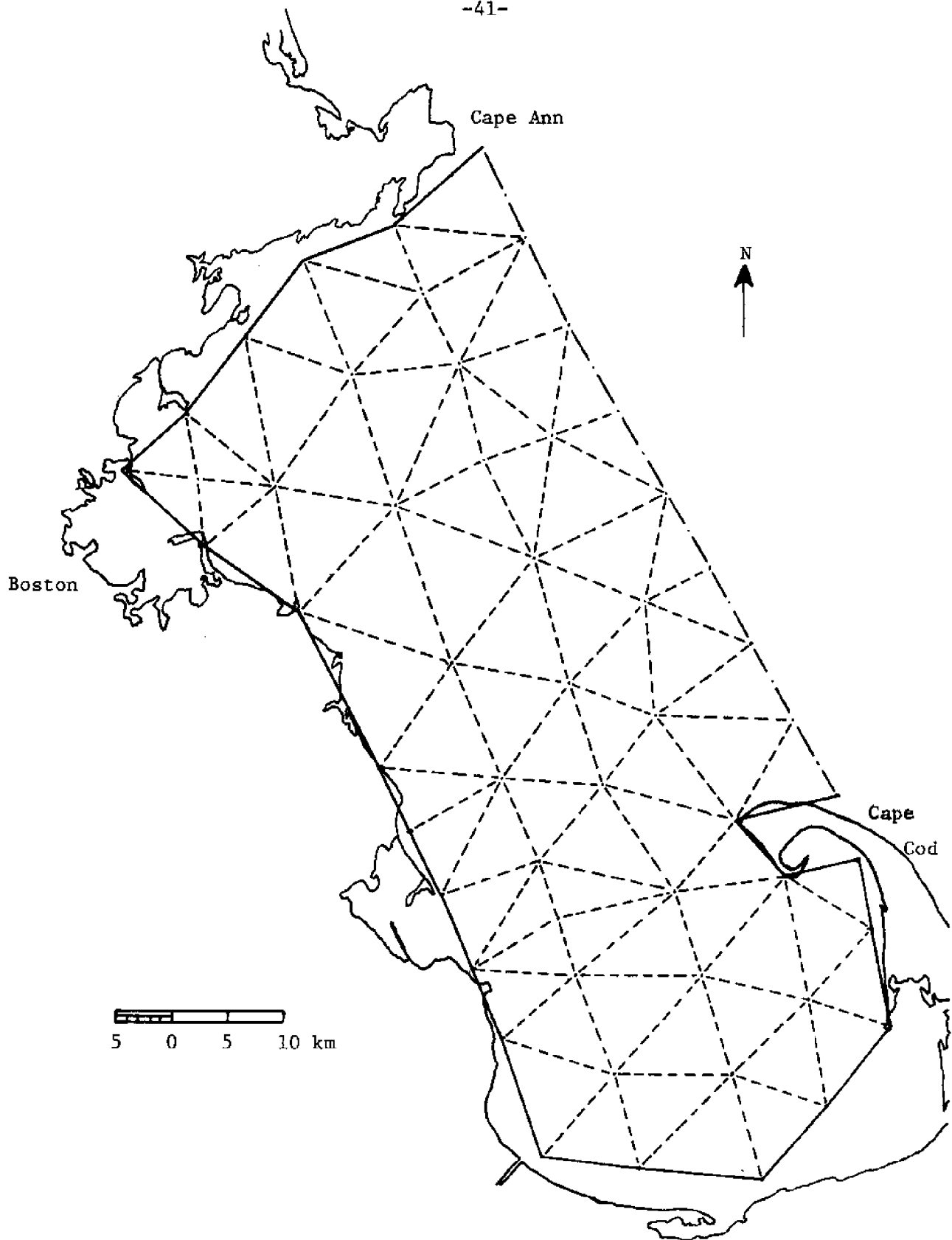


Fig. 10. Massachusetts Bay. Geographical boundaries and finite element grid.

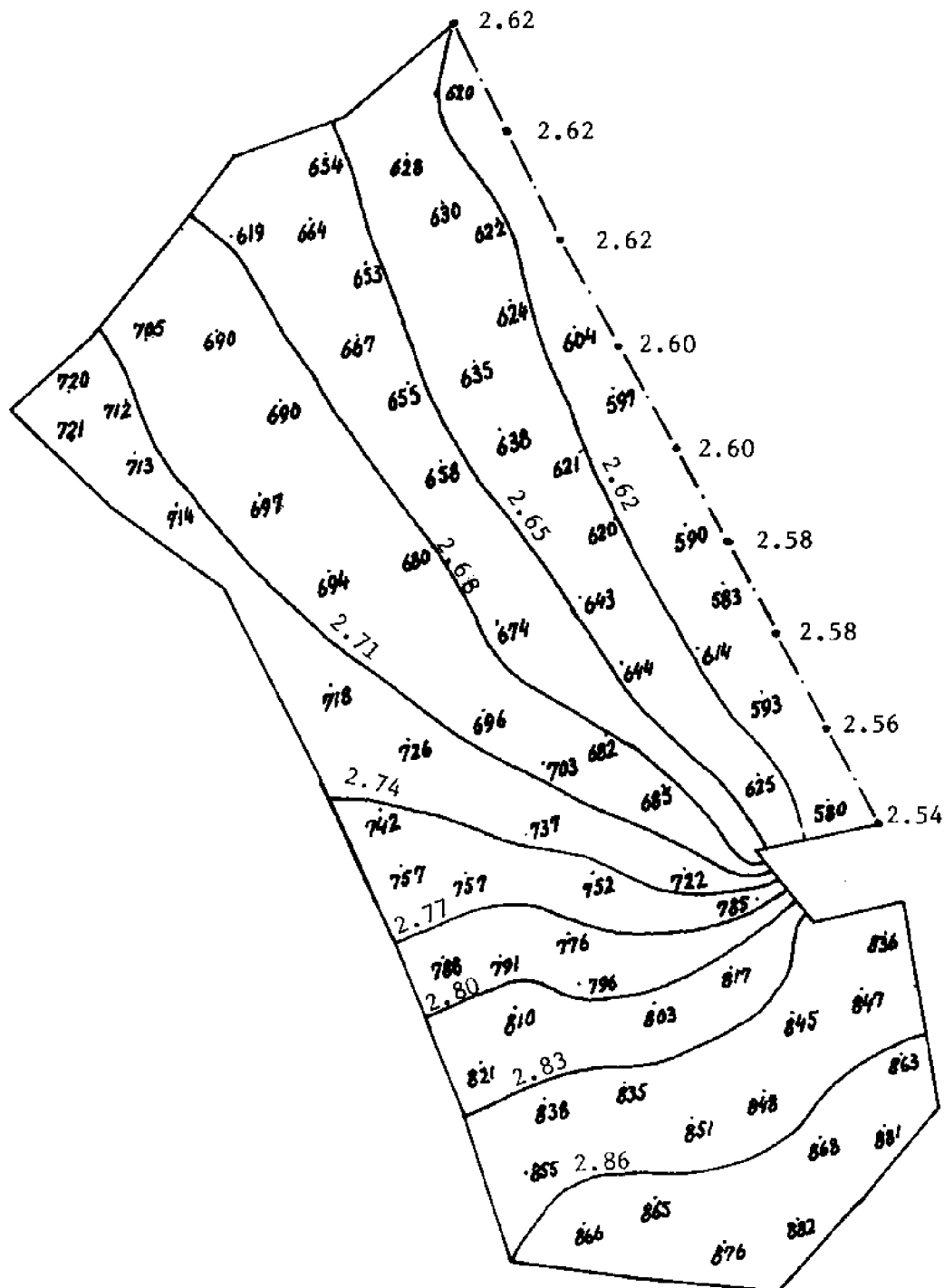


Fig. 11. Surface contour lines after 68000 sec. (1.5 tidal cycle).
The elevations are given in meters above MLW. Note that only
decimals are shown for centroidal elevations.

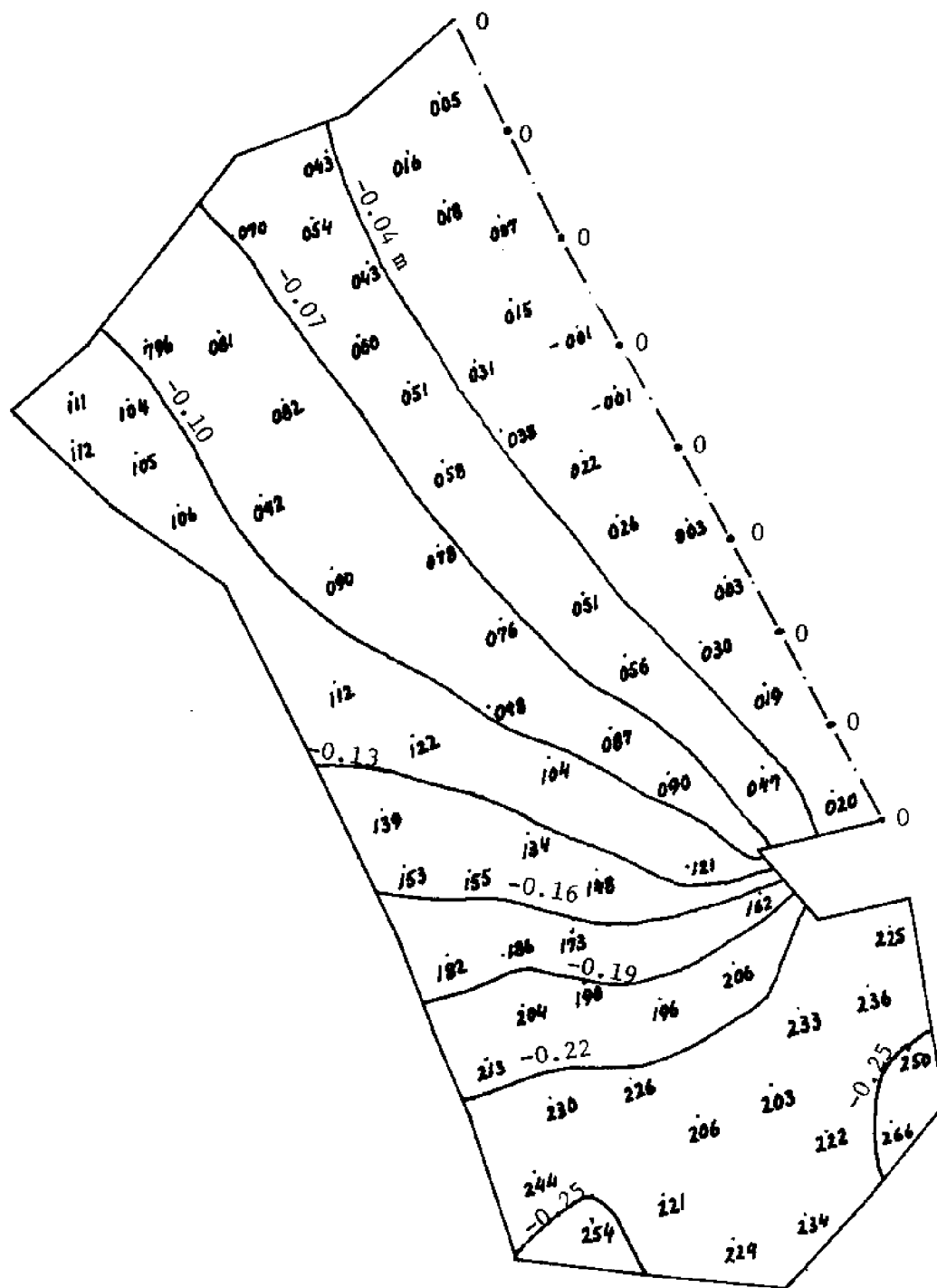


Fig. 12. Surface contour lines after 90000 sec (2 tidal cycles).
Centroidal elevations are given in mm below MLW.

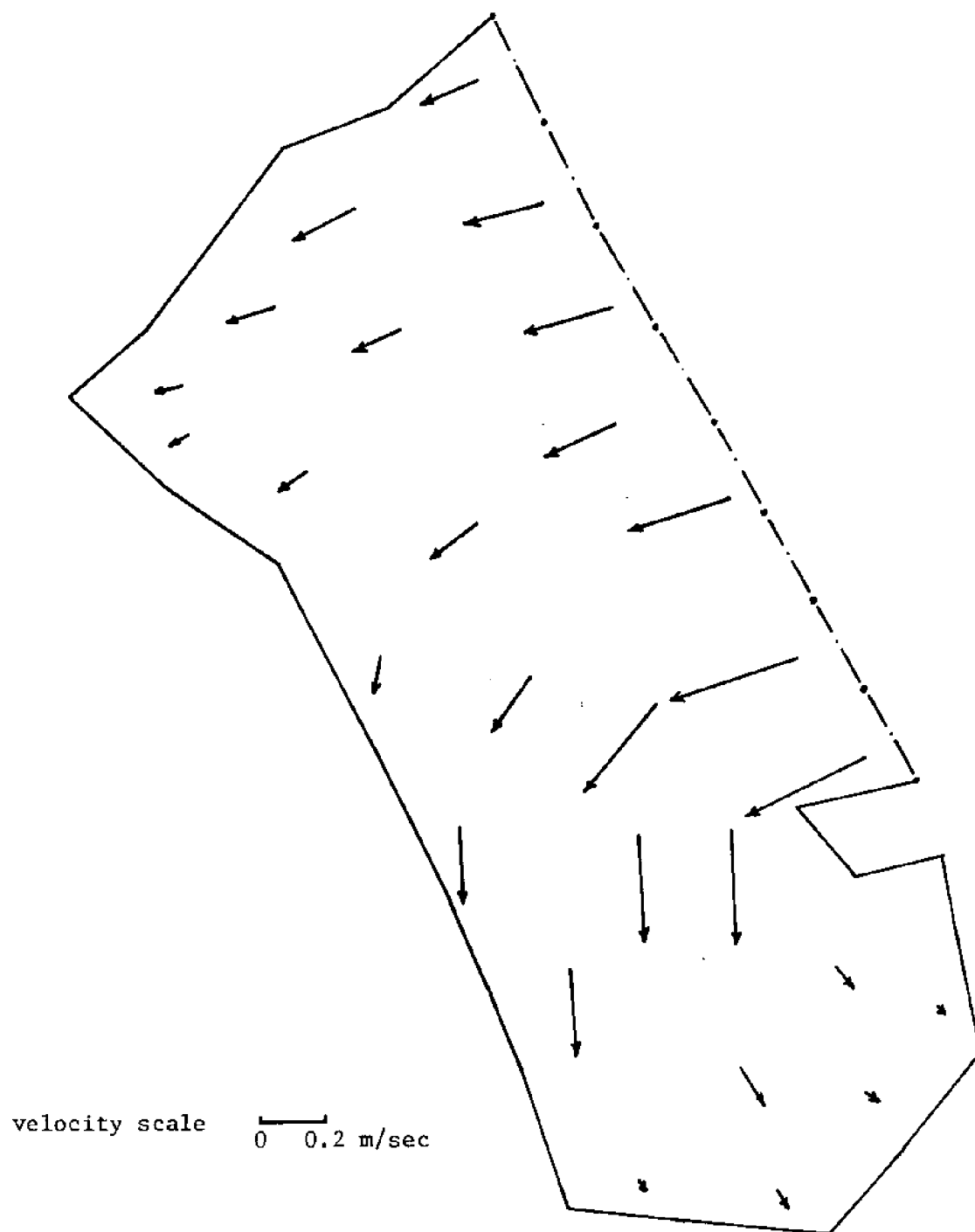


Fig. 13. Computed currents after 56000 sec. (1.25 tidal cycle).
Flooding Tide.

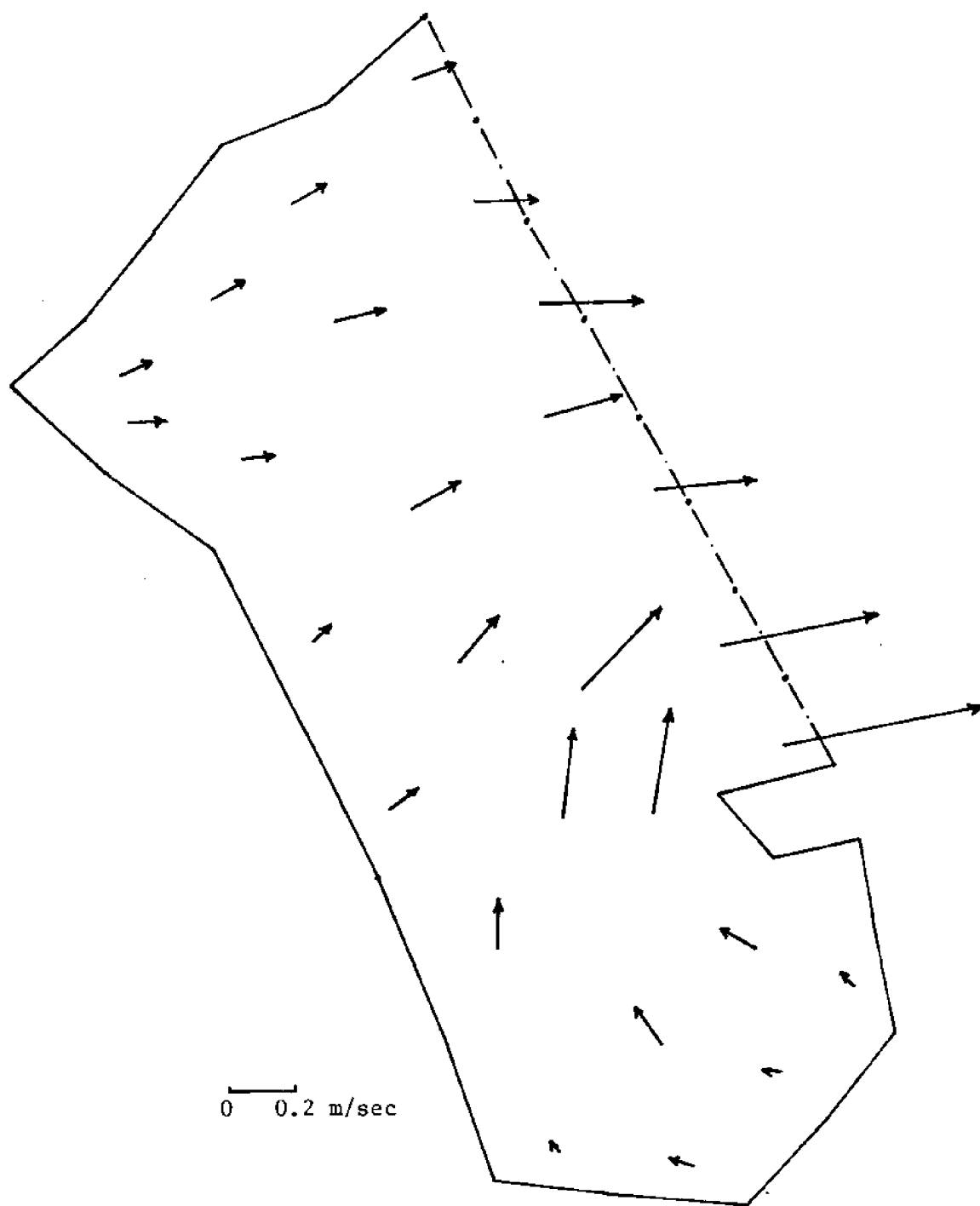
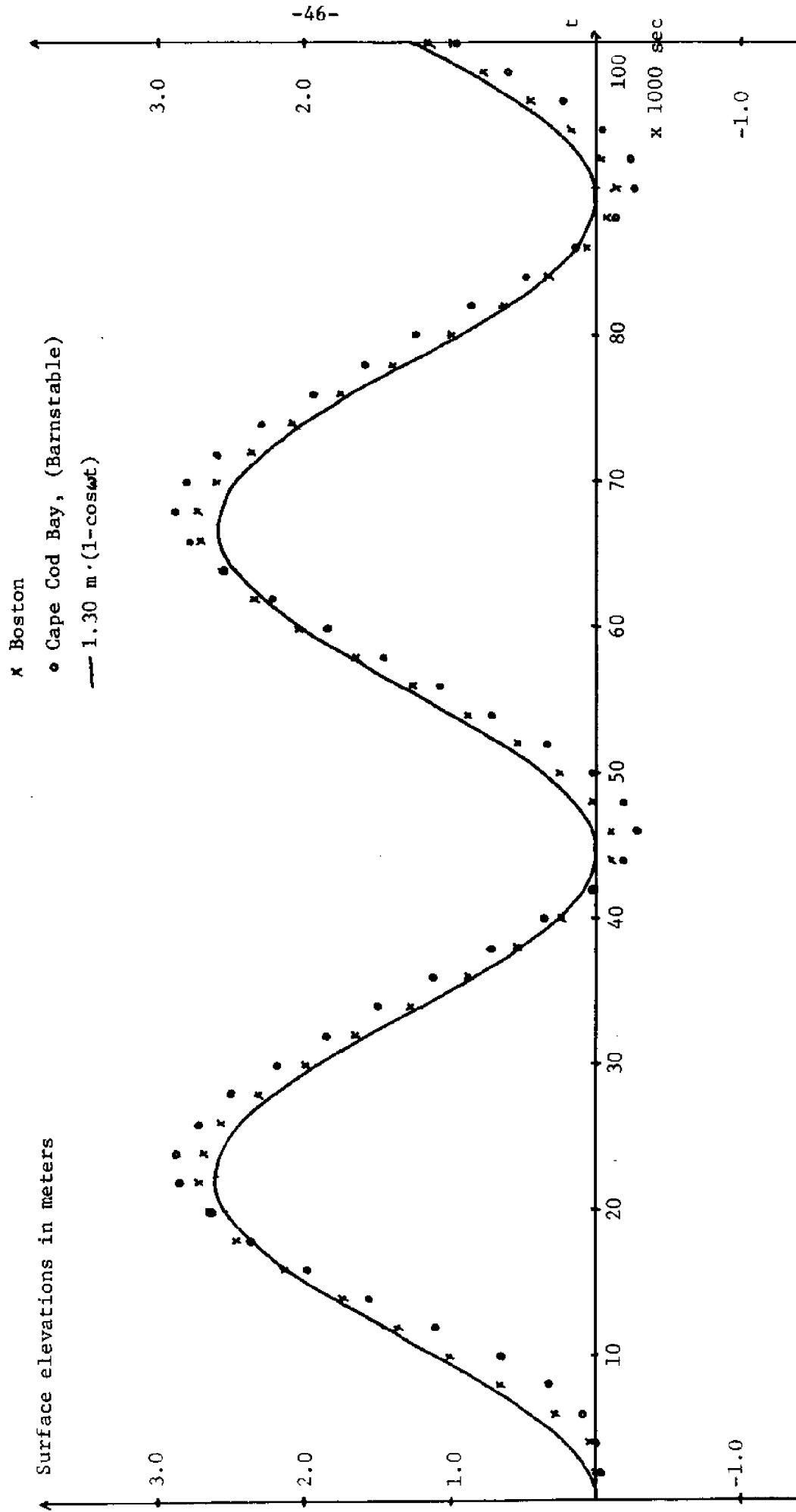


Fig. 14. Computed currents after 78000 sec. (1.75 tidal cycle).
Ebbing tide.

Fig. 15. Time history of computed elevations at Boston and in Cape Cod Bay.



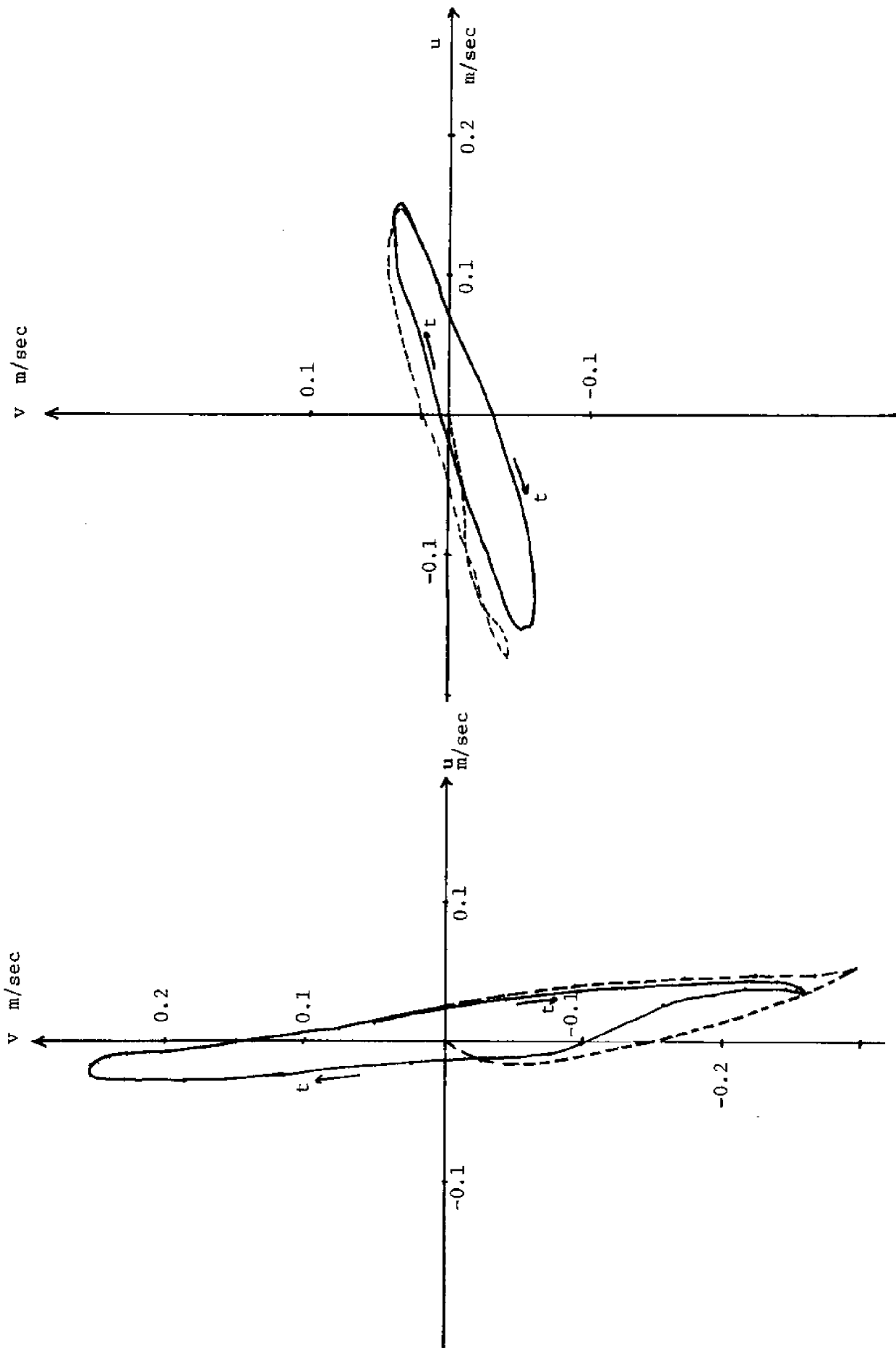


Fig. 16. Time history of computed currents. a) Center of Cape Cod Bay. b) 15 km East of Boston.

The results were obtained using the Runge-Kutta integration scheme neglecting convective terms and eddy diffusion in the momentum equations. The CFL criterion is

$$\Delta t_c \leq \frac{\delta}{\sqrt{2} c} \approx \frac{6000}{\sqrt{2} 19} = 223 \text{ sec.}$$

and a $\Delta t = 200$ sec was selected. The predictor-corrector scheme was applied to the same problem but exhibited gradual instability after one tidal cycle (44600 sec). When Δt was reduced to 150 sec, comparable results were obtained for more than 2 tidal cycles. However, 5% more computing time was required.

Several cases of wind forcing were also investigated. Massachusetts Bay is characterized by a low Rossby number (about 0.1), small surface elevation change compared to the mean depth, and minor effect of bottom friction. Therefore, it is reasonable to assume the response of the system is linear. This is very important since it allows one to use superposition which reduces the computational effort considerably.

To verify the "permissability" of superposition, two wind situations without tidal motion were executed until steady state was essentially achieved. The 10m wind velocity, U_{10} , was 10 m/sec which produces a surface shear stress of approximately 1 dyn/cm^2 according to the relationship given by Wu [19]:

$$\tau^s = \frac{1}{2} \rho_{\text{air}} C \cdot U_{10}^2$$

$$C = 0.5 \cdot 10^{-3} \cdot U_{10}^{1/2} \quad 1 < U_{10} < 15 \text{ m/sec.}$$

This is a frequently measured surface stress in the area.

The steady-state current field for wind from North and South-West are shown in Figures 17, 18. As a preliminary test of linear behavior, a situation with wind from South was also computed yielding numerical values of velocities and surface elevations within 1% of the North wind case.

Figures 19, 20 show Calcomp plots of a superposition of velocities produced by wind from SW alone and pure tidal motion, whereas Figures 21, 22 show the same velocity fields but computed simultaneously. The validity of a linear system assumption as a first approximation is clearly demonstrated.

The limited experience acquired so far has demonstrated that the finite element discretization approach is a reliable and efficient method for fluid flow problems with complex boundaries. Of the two integration schemes tested, the Runge-Kutta method seems to be universally applicable whereas the predictor-corrector scheme is prone to exhibit instability. If the forcing terms are sufficiently complicated to estimate, the savings in iterations may give the latter scheme a computational advantage, even if a smaller time step must be used. This might, for instance, be the case when the convective terms must be retained. Also the improved stability through the smoothing effect of adding diffusive terms needs further examination.

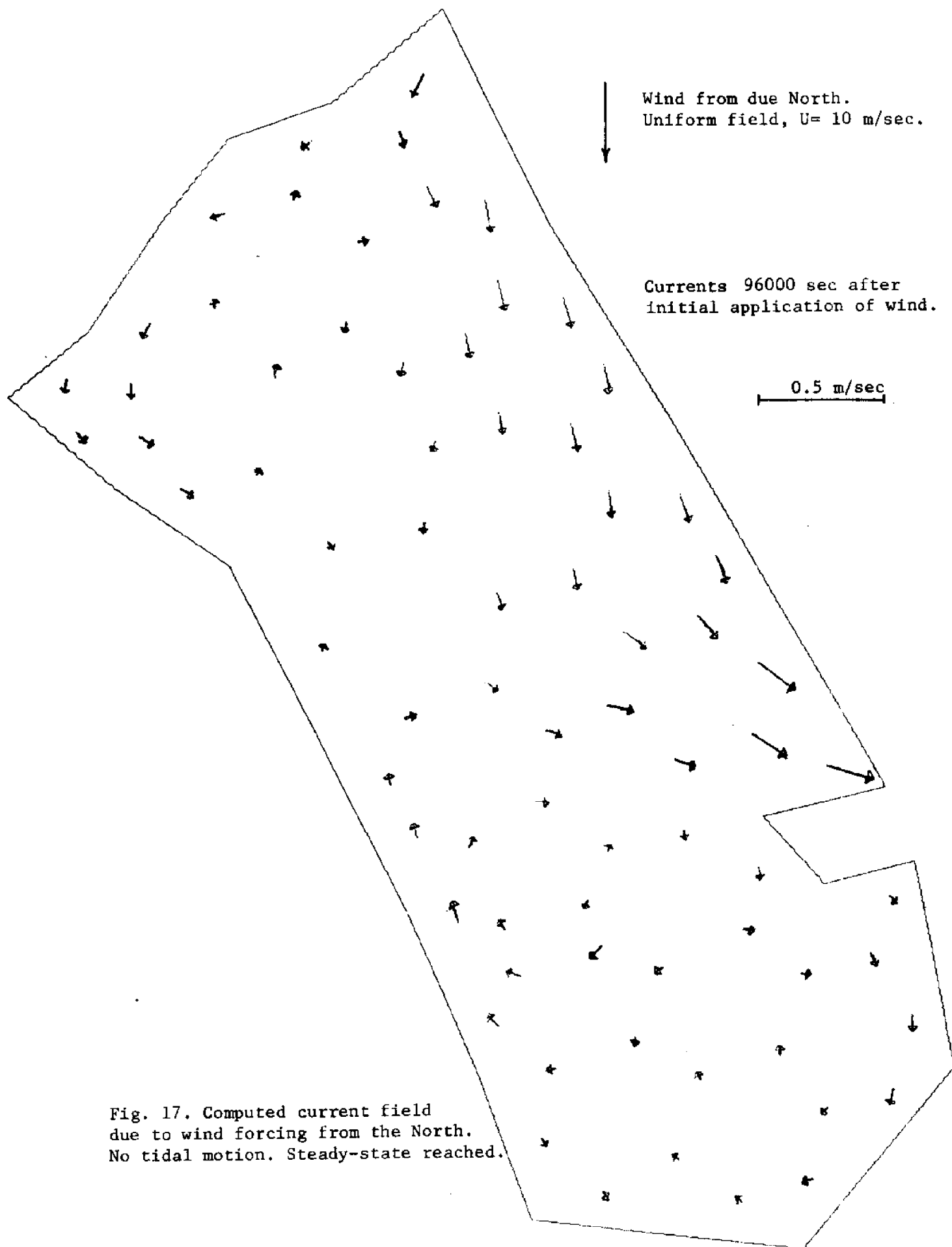


Fig. 17. Computed current field
due to wind forcing from the North.
No tidal motion. Steady-state reached.

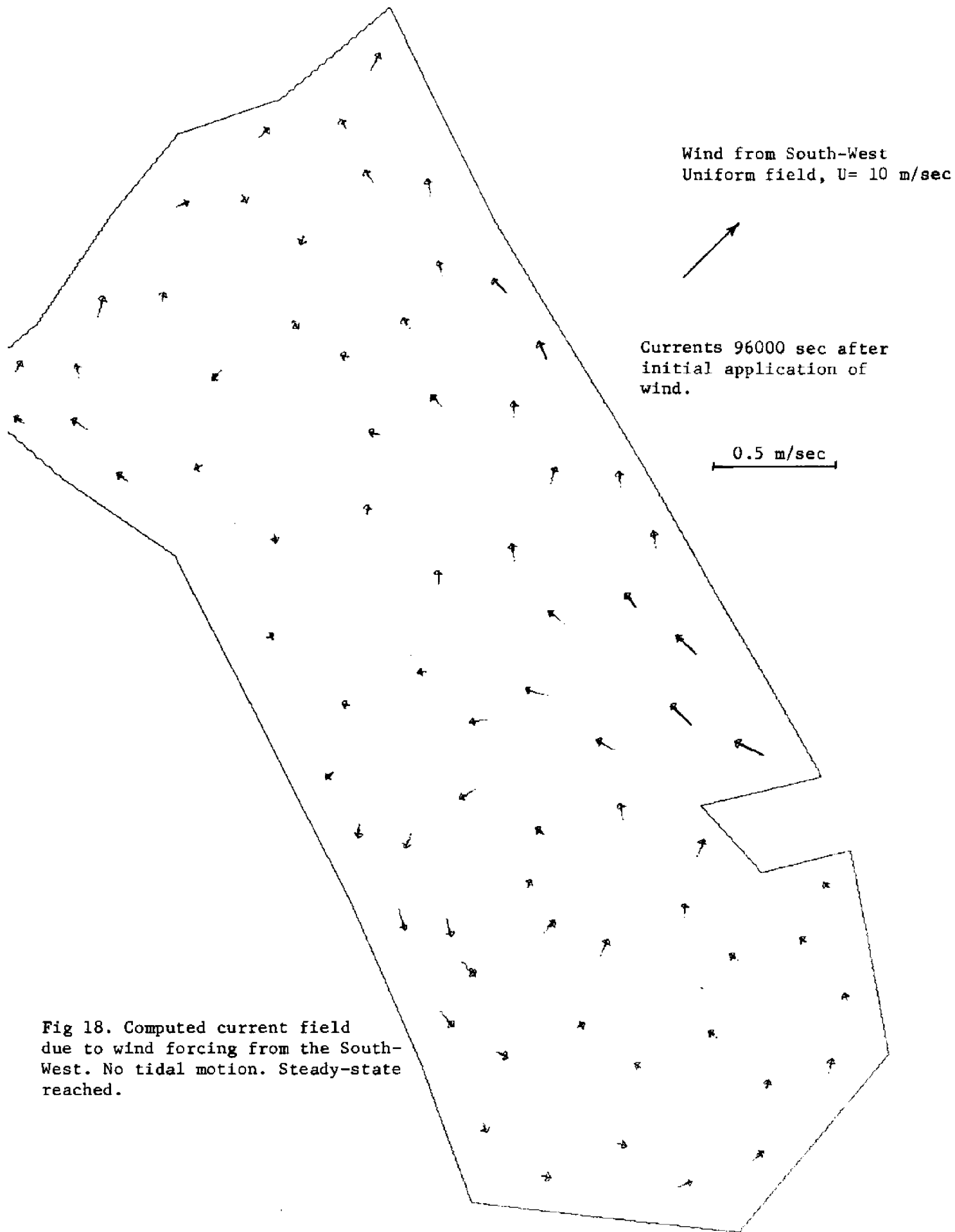


Fig 18. Computed current field due to wind forcing from the South-West. No tidal motion. Steady-state reached.

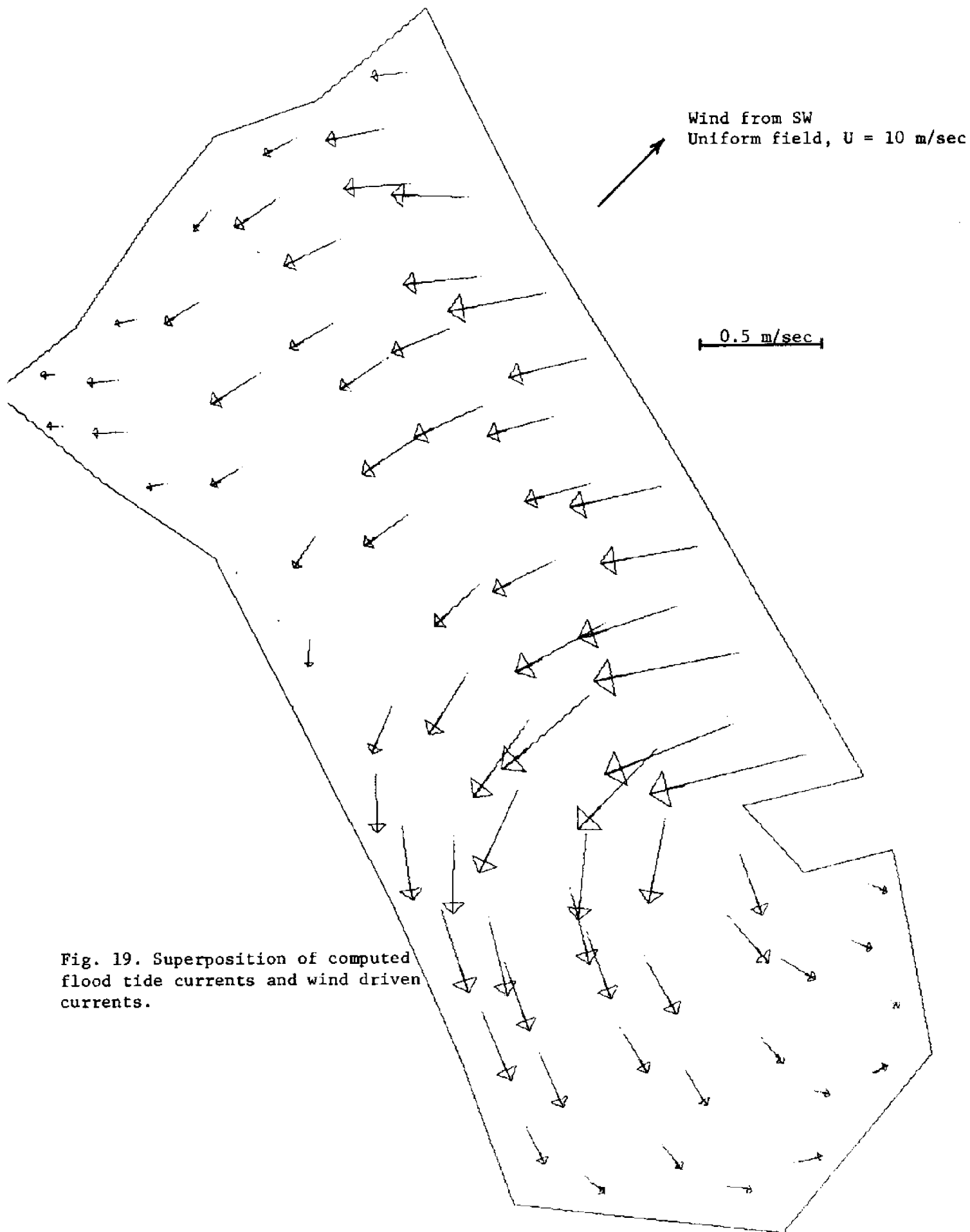


Fig. 19. Superposition of computed flood tide currents and wind driven currents.

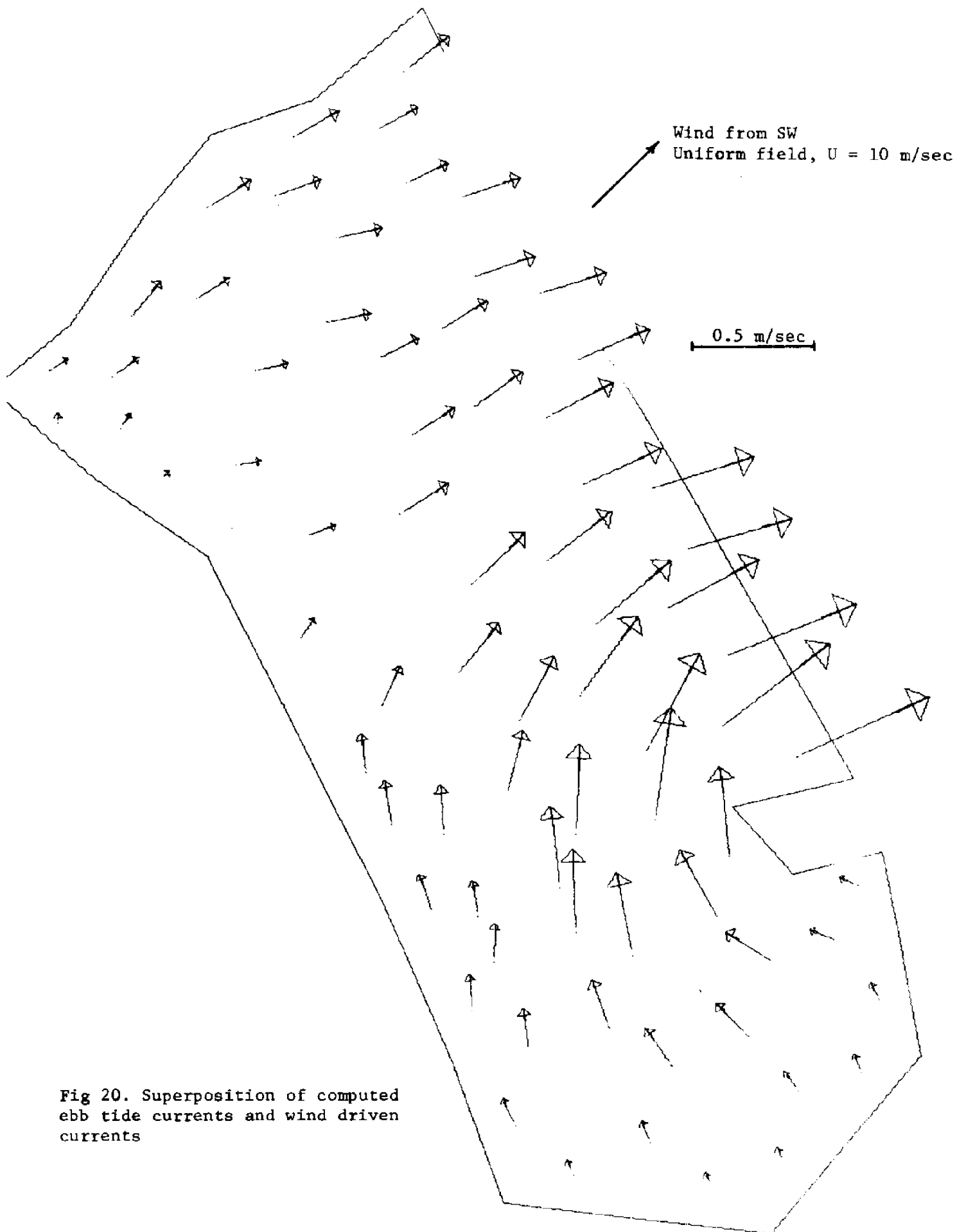


Fig 20. Superposition of computed ebb tide currents and wind driven currents

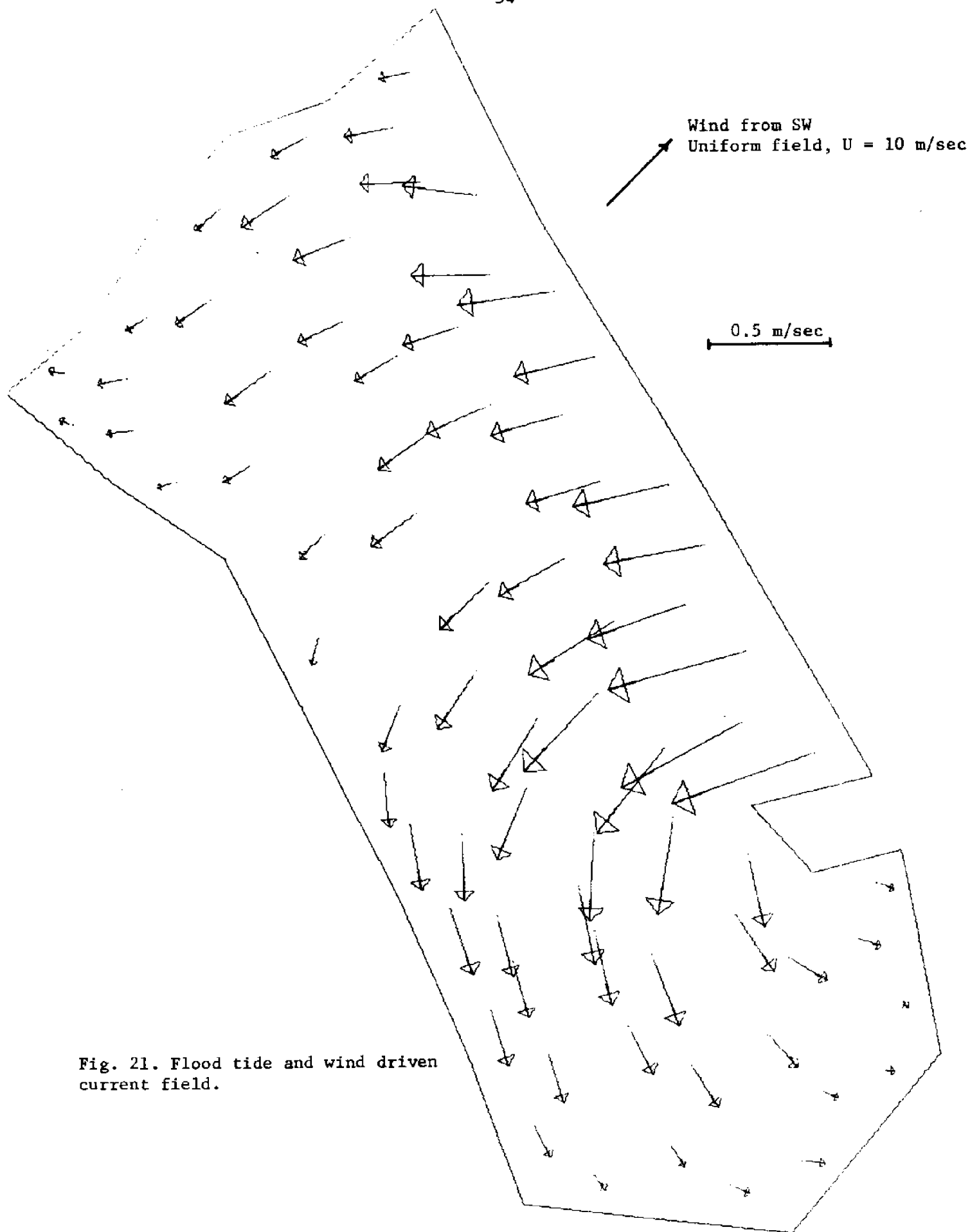


Fig. 21. Flood tide and wind driven current field.

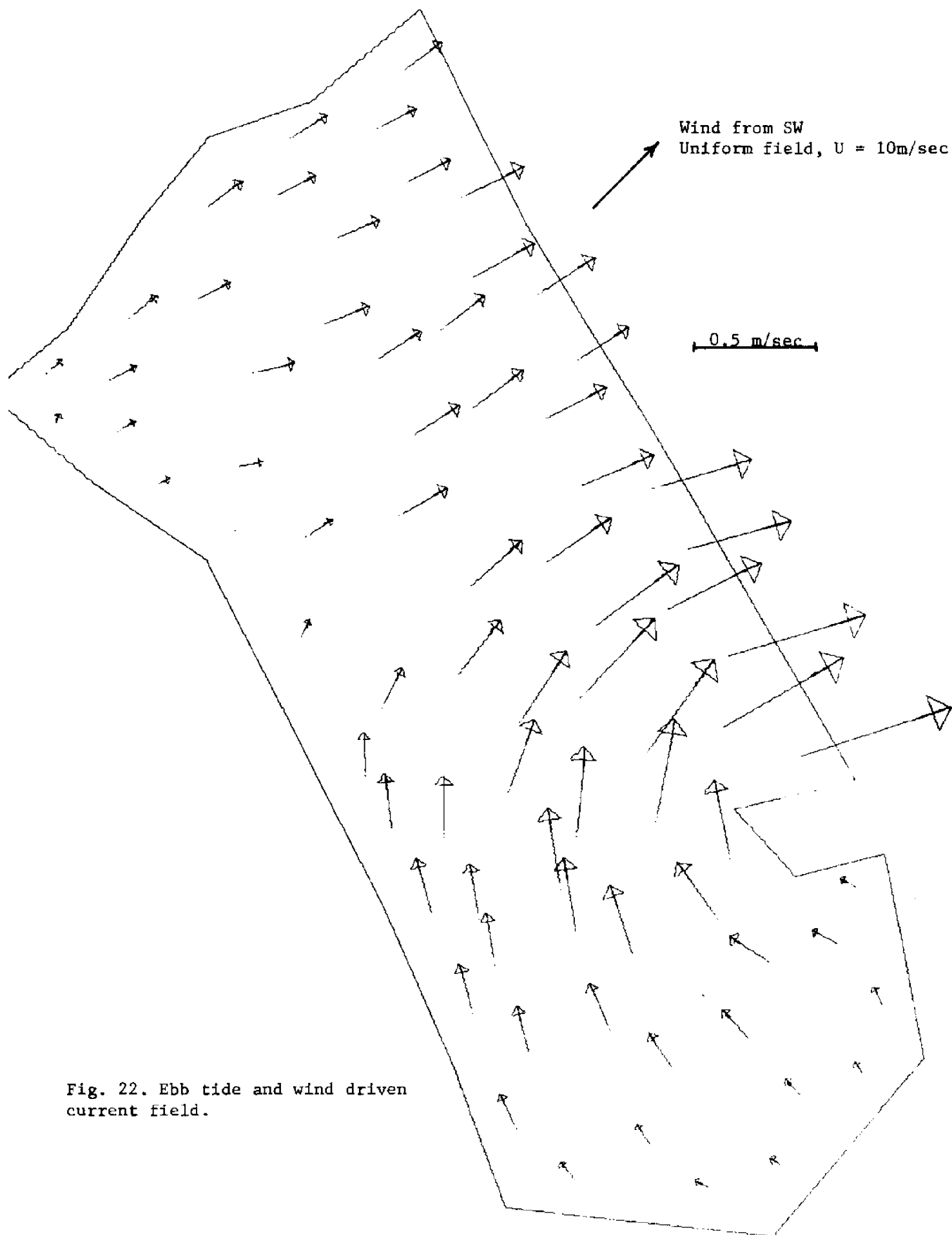


Fig. 22. Ebb tide and wind driven current field.

REFERENCES

1. Reid, R.O. and B.R. Bodine: "Numerical Model for Storm Surges in Galveston Bay", Journal of the Waterways and Harbors Division, ASCE, Vol. 94, No. WW1, 1968
2. "Estuarine Modeling: An Assessment", Water Pollution Control Research Series, Water Quality Office, Environmental Protection Agency, Feb., 1971
3. Leendertse, J.J.: "A Water Quality Model for Well-Mixed Estuaries and Coastal Seas, Vol. I, Principles of Computation", Memorandum RM-6230-RC, The Rand Corporation, Santa Monica, California, Feb., 1970
4. Masch, F.D. and N.J. Shankar: "Mathematical Simulation of Two-Dimensional Horizontal Convective-Dispersion in Well-Mixed Estuaries", Int. Assoc. for Hydraulic Research, 1971
5. Brady, D.K. and J.C. Geyer: "Development of a General Computer Model for Simulating Thermal Discharges in Three Dimensions", Edison Electric Institute Publication No. 72-902, Feb., 1972
6. Pearce, B.R.: "Numerical Calculation of the Response of Coastal Waters to Storm Systems", TR 12, Coastal and Oceanographic Engineering Lab., University of Florida, August, 1972
7. Abbott, M.B., Damsgaard, A. and G. S. Rodenhuis: "System 21, Jupiter", Journal of Hydraulic Research, Vol. 11, No. 1, 1973
8. Martin, H.C.: "Finite Element Analysis of Fluid Flows", Proc. 2nd Conf. Matrix Meth. Str. Mech., AFFDL TR68-50, Wright-Patterson AFB, Ohio, 1969
9. Tong, P.: "The Finite Element Method for Fluid Flow", Recent Advances in Matrix Methods of Structural Analysis and Design", R. Gallagher et al (Editors) U. of Alabama Press, 1971
10. Proceedings, 14th Conf. on Great Lakes Research, Int. Assoc. for Great Lake Research, 1971
11. Loziuk, L., Anderson, J. and T. Belytschko: "Hydrothermal Analysis by Finite Element Method", J. Hyd. Div., ASCE, Vol. 98, No. HY11, November, 1972
12. Davis, J.M., Ph.D. Thesis, University College of Swansea, Sept., 1972
13. Guymon, G.: "Finite Element Solution for General Fluid Motion", J. Hyd. Div., ASCE, Vol. 99, No. HY 6, June, 1973

14. Finlayson, B.A. and L. E. Scriven: "The Method of Weighted Residuals and its Relation to Certain Variational Principles for the Analysis of Transport Processes," Chemical Engineering Science, Vol. 20, 1965
15. Ralston, A.: "A First Course in Numerical Analysis", McGraw Hill, 1965
16. Richtmyer, R.D. and K.W. Morton: "Difference Methods for Initial-Value Problems", Interscience (Wiley), Second Edition, 1967
17. Briggs, D. and O. Madsen, Department of Civil Engineering, M.I.T., Private communication
18. U.S. Department of Commerce, NOAA, Tide Tables, East Coast of North and South America, 1973
19. Wu, J.: "Wind Stress and Surface Roughness at Air-Sea Interface", J. Geoph. Res., V. 74, No. 2, Jan., 1969

MATHEMATICAL MODELS OF THE MASSACHUSETTS BAY

PART II

ANALYTICAL MODELS FOR ONE- AND TWO-
LAYER SYSTEMS IN RECTANGULAR BASINS

BY

DOUGLAS A. BRIGGS

AND

OLE S. MADSEN

RALPH M. PARSONS LABORATORY

FOR WATER RESOURCES AND HYDRODYNAMICS

Department of Civil Engineering

Massachusetts Institute of Technology

Prepared with the Support of

Sea Grant Office
National Oceanographic and Atmospheric Administration
Department of Commerce
Washington, D.C.

MATHEMATICAL MODELS OF THE MASSACHUSETTS BAY

ABSTRACT - PART II

ANALYTICAL MODELS FOR ONE- AND TWO- LAYER SYSTEMS IN RECTANGULAR BASINS

BY

DOUGLAS A. BRIGGS

AND

OLE S. MADSEN

A need for qualitative information concerning the hydrodynamics of Massachusetts Bay has been seen from recent oceanographic measurements and current studies in the Bay area. In response to this, two analytical models have been derived for a simple rectangular configuration which can be applied to the geometry of Massachusetts Bay. A one layer model has been developed to simulate the conditions found during the winter season when the water column is well mixed. A two layer model represents the stratified case generally observed, with the presence of a strong thermocline, during the summer.

Both models are derived from the linearized long wave equations in two dimensions and analytical solutions are obtained by neglecting Coriolis force, bottom friction, and wind stress. The models are depth averaged and the geometry of the Bay is represented by a rectangle. The boundary conditions are specified as zero normal velocity along the walls and a constant surface slope across the opening connecting Massachusetts Bay to the ocean.

The results of the two models indicate that the surface elevations at high tide are fairly insensitive of the assumed conditions (one or two layer model). However, for the two layer model, relatively large interfacial waves are predicted as well as velocities which at some locations in the upper layer, are directed shoreward on the ebbing tide, rather than seaward. Comparison of available field observations with these results verify, qualitatively, that these conditions do exist and shows that if a model capable of predicting velocities in the Bay is desired, it must incorporate the conditions corresponding to a two layer flow.

PART II

ACKNOWLEDGEMENTS

This study constitutes a part of a series of investigations in a major environmental research program on the "Sea Environment in Massachusetts Bay and Adjacent Waters". This program consists of theoretical and field investigations and is under the administrative and technical direction of Dr. Arthur T. Ippen, Institute Professor, Department of Civil Engineering and of Dr. Erik L. Mollo-Christensen, Professor, Department of Meteorology as co-principal investigators. Support of the program is provided in part by the Sea Grant Office of NOAA, Department of Commerce, Washington, D.C. through Grant No. NG-43-72, in part by the Henry L. and Grace Doherty Charitable Foundation, Inc., and in part by the Department of Natural Resources, Commonwealth of Massachusetts through Project No. DMR-73-1. The project which is the subject of this report was conducted by staff members of the Ralph M. Parsons Laboratory for Water Resources and Hydrodynamics and was administered under Project No. DSR 80344 and DSR 81100 at M.I.T.

This report was prepared by Mr. Douglas A. Briggs, Research Assistant, and Dr. Ole S. Madsen, Assistant Professor of Civil Engineering and formed the subject of a thesis for the M.S. degree, which Dr. Madsen supervised. His advice and guidance is hereby gratefully acknowledged.

Many staff members at the Laboratory were involved in the field observations utilized for comparison with the results of the two models developed in this report. The assistance of the following is sincerely acknowledged in this connection: Dr. Bryan R. Pearce, Research Associate, George C. Christodoulou, Ms. Sheila Frankel, Mr. William F. Leimkuhler, Mr. Edward F. McCaffrey, Mr. Robert F. Paquette, and Mr. John D. Wang. Appreciation is expressed here, also, to Ms. Stephanie M. Demeris for her excellent typing of this manuscript.

TABLE OF CONTENTS

	<u>Page</u>
TITLE PAGE	1
ABSTRACT	2
ACKNOWLEDGEMENTS	3
TABLE OF CONTENTS	4
LIST OF FIGURES	6
LIST OF TABLES	8
LIST OF SYMBOLS	9
CHAPTER I INTRODUCTION	11
CHAPTER II THEORY AND DERIVATION OF THE ONE AND TWO LAYER MODELS	14
2.1 Linear Long Waves	14
2.2 One Layer Model	15
2.3 Two Layer Model	23
CHAPTER III RESULTS OF THE ONE LAYER MODEL	36
3.1 Computational Aspects	36
3.1.1 Mathematical Simulation of the Ocean Boundary	36
3.1.2 Number of Terms Required in the Determination of η	49
3.2 Data Available for Comparison	49
3.3 Discussion of the Model Results	50
CHAPTER IV RESULTS OF THE TWO LAYER MODEL	54
4.1 Computational Considerations	54
4.1.1 Results of the Two Layer Model	54
4.1.2 Model Sensitivity	63

	<u>Page</u>
4.2 Available Data for Comparison	69
4.3 Discussion of the Model Results	77
CHAPTER V CONCLUDING REMARKS	84
BIBLIOGRAPHY	87
APPENDIX A LISTING OF THE PROGRAM USED FOR COMPUTATIONS PRESENTED IN CHAPTER IV	88

LIST OF FIGURES

<u>Figure</u>	<u>Title</u>	<u>Page</u>
1-A	Massachusetts Bay, Depth Contours in Feet	12
2-A	One Layer Model, Coordinate System and Nomenclature	16
2-B	Geometry of Massachusetts Bay for the One and Two Layered Models	19
2-C	Two Layer Model, Coordinate System and Nomenclature	24
3-A	Massachusetts Bay, Observed Differences in Tidal Amplitude at High Tide	38
3-B	One Layer Model of Massachusetts Bay, One Increment Channel	41
3-C	One Layer Model of Massachusetts Bay, with Stellwagen Bank Closed	44
3-D	One Layer Model of Massachusetts Bay, Four Increment Channel	46
3-E	Numerical Model of Massachusetts Bay	48
4-A	Two Layer Model of Massachusetts Bay at High Tide. $h_1 = 100.0$ Ft., $h_2 = 20.0$ Ft.	58
4-B	Two Layer Model of Massachusetts Bay. Velocities at Maximum Ebb. $h_1 = 100.0$ Ft., $h_2 = 20.0$ Ft.	60
4-C	Two Layer Model of Massachusetts Bay at High Tide. $h_1 = 80.0$ Ft., $h_2 = 40.0$ Ft.	62
4-D	Two Layer Model of Massachusetts Bay. Velocities at Maximum Ebb. $h_1 = 80.0$ Ft., $h_2 = 40.0$ Ft.	64
4-E	Velocity Variations as a Function of h_1 and h_2	68

<u>Figure</u>	<u>Title</u>	<u>Page</u>
4-F	C.T.D. Cast Taken in Massachusetts Bay	71
4-G	Current Drogue Study in Massachusetts Bay. July 27, 1972	76
4-H	Current Drogue Study in Massachusetts Bay. July 31, 1972	78
4-I	Two Layer Model of Massachusetts Bay. Velocities at Maximum Ebb. $h_1 = 100.0$ Ft., $h_2 = 20.0$ Ft.	82

LIST OF TABLES

<u>Table</u>	<u>Title</u>	<u>Page</u>
4-1	Sensitivity of B_0 to the Choice of Interfacial Amplitude	65
4-2	Observed Spatial Variation in Depth of Interface below the Surface	73

LIST OF SYMBOLS

A_o	Constant governing the surface profile
B_o	Constant governing the interfacial profile
A_n	Constants evaluated at integer values of n
B_n	Constants evaluated at integer values of n
C_f	Bottom shear stress coefficient
f	Coriolis acceleration
g	Acceleration of gravity
h	Average depth of the Bay
h_1	Depth of layer one (lower layer)
h_2	Depth of layer two (upper layer)
H	Surface wave height
H_1	Interfacial wave height
k	Wave number
L	Surface wave length
L_1	Interfacial wave length
m	Wave number
N	Value where m_{n_2} becomes imaginary
t	Time
T	Tidal period of 12.4 hours
u	Depth averaged velocity in the x-direction
u_1	Depth averaged velocity in layer one, x-direction
u_2	Depth averaged velocity in layer two, x-direction
U	Depth averaged velocity

U_1	Depth averaged velocity in layer one
U_2	Depth averaged velocity in layer two
v	Depth averaged velocity in the y-direction
v_1	Depth averaged velocity in layer one, y-direction
v_2	Depth averaged velocity in layer two, y-direction
V	Total volume of fluid above mean sea level
V_1	Volume of fluid in layer one above the mean interfacial level
V_2	Volume of fluid in layer two above mean sea level
x_0	Length of the Bay geometry, x-direction
x_1	Boundary of the channel opening
x_2	Boundary of the channel opening
y_0	Width of the Bay geometry, y-direction
η	Surface amplitude
η_1	Interfacial amplitude (layer one)
η_2	Surface amplitude (layer two)
λ	Linearized bottom friction term
ρ_1	Density, layer one
ρ_2	Density, layer two
τ_b	Bottom shear stress
τ_i	Interfacial shear stress
τ_s	Surface or wind stress
ϕ	Latitude
ω	$\frac{2\pi}{T}$
ω_e	Angular velocity of the earth

CHAPTER I

INTRODUCTION

Massachusetts Bay, as seen in Figure 1-A, lies at the eastern edge of Massachusetts and is surrounded by land on three sides. The average depth of the Bay is approximately 120 feet with the ocean boundary between the tip of Cape Ann and the tip of Cape Cod, a distance of the order 41.0 nautical miles. Located on the northwest is Boston Harbor through which three rivers, the Charles, the Chelsea, and the Mystic, flow into the Bay. In addition, the Cape Cod Canal exerts an effect on the Bay circulation by allowing an exchange with Buzzards Bay to the southwest.

The results of current observations and other oceanographic measurements recently taken in Massachusetts Bay have shown the occurrence of some interesting and unusual conditions. Field data concerning the vertical structure of temperature, salinity, and density suggests that a rather pronounced stratification exists during the summer months. Drogue studies during periods of pronounced stratification exhibited some rather peculiar phenomena. Thus, it was found that shallow drogues during ebbing tide proceeded towards the shore rather than seaward, as expected. Although the well mixed situation, encountered during the winter season, is of interest and will be considered, it is the stratified case that is of primary concern since it is this situation that exhibits the most unusual condition.

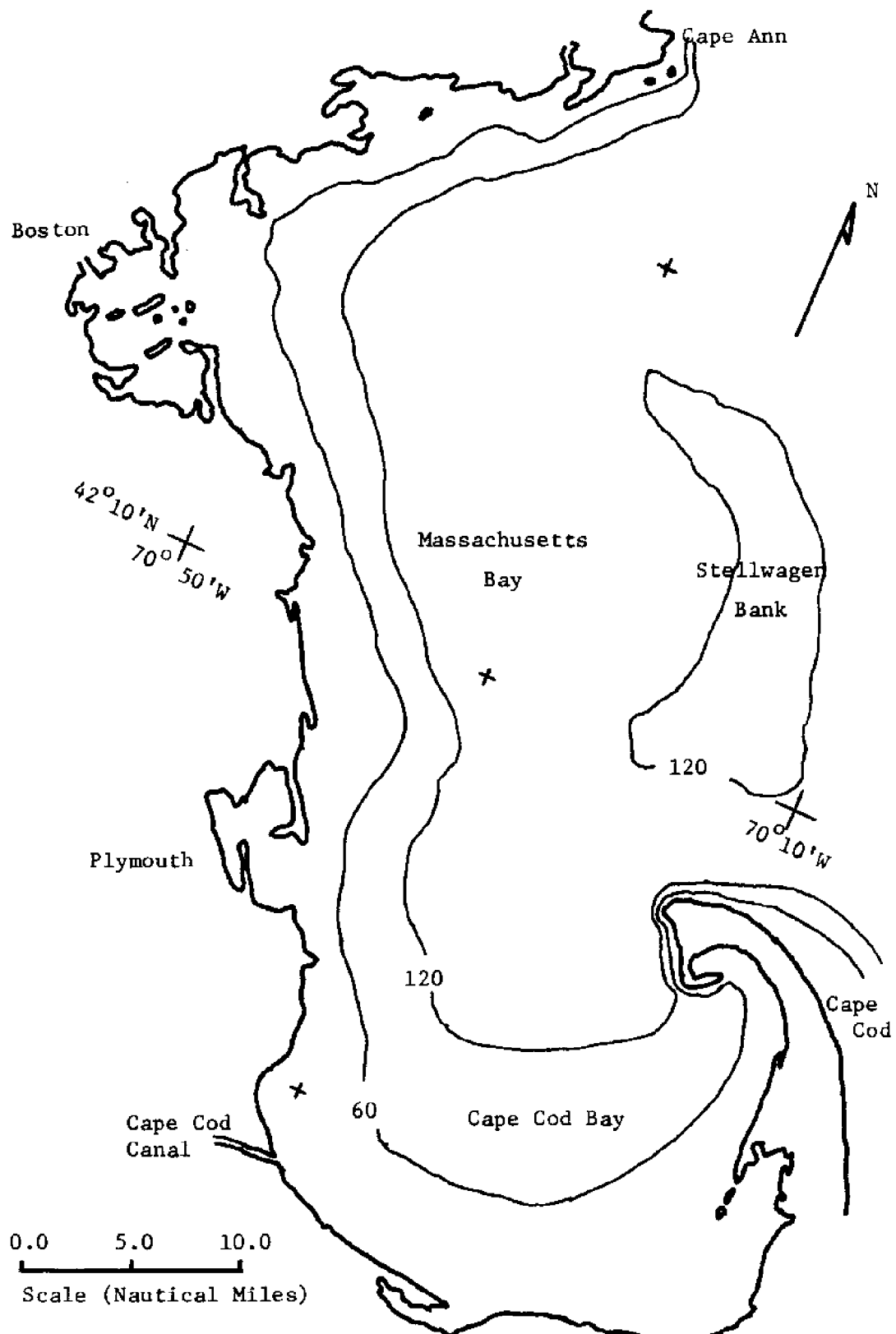


Figure 1-A: Massachusetts Bay, Depth Contours in Feet

Thus it was felt that a simple model predicting the hydrodynamics of Massachusetts Bay, shown in Figure 1-A, could lead to source insight into the Bay circulation and possibly explain some of the unusual field observations. Consequently, the theoretical development of two analytical models, a one layer model representing the well mixed case and a two layer model representing the stratified case, was undertaken in an attempt to explain some of these conditions. The primary quality of the desired model was that it be simple, such that an analytical solution could be obtained and readily evaluated. This was attained by the simplifying assumption of a depth averaged rectangular configuration for the Bay area. Further, by linearizing the governing equations neglecting Coriolis force, bottom friction, and wind stress, a simple analytical solution was obtained, which qualitatively explains some of the observed phenomena.

The models predict currents and amplitudes for the entire area of Massachusetts Bay. Results of the model show a difference in the predicted current pattern, suggesting the necessity of including, in a more sophisticated model, the effects of stratification if an accurate prediction of the current field is desired. By comparing the results of the two layer model with field observations, it is demonstrated that such occurrences as relatively large interfacial waves and currents flowing toward the boundaries in the upper layer during an ebbing tide are qualitatively explained by the simple two layer model presented here.

CHAPTER II

THEORY AND DERIVATION OF THE ONE AND TWO LAYERED MODELS

2.1 Linear Long Waves

Two dimensional long wave propagation has, in the past decade, received considerable attention from both analytical and numerical modelers as the system of equations describes a physical situation of considerable interest to the coastal engineer. Able to predict the hydrodynamics associated with storm surge and tidal-wave propagation, models utilizing long wave theory have provided engineers and related practitioners with the ability to predict tidal currents and elevations in estuaries and coastal areas.

The long wave equations describe flow in the nearly horizontal direction, with the implication that the pressure distribution is hydrostatic and that the vertical accelerations are negligible. Due to the fact that even numerical solutions of the non-linear equations are rather difficult to obtain, the present models will be restricted to the linearized equations of motion in two dimensions. The equations, which are vertically averaged, neglect convective accelerations and allow a simplistic approach in their application to Massachusetts Bay.

Derivation of the one and two layered models are quite similar in nature and both include, in the governing equations, Coriolis force and frictional forces.

However, in order to preserve simplicity, we neglect the influence of the Coriolis force as well as bottom and interfacial

friction in the application of the two models.

2.2 One Layered Model

The dynamic equations for the one layered model can be derived through the application of the Navier-Stokes equations for incompressible fluids. The equations of continuity can be derived by summing the mass flux through a control volume. Representation of the coordinate system and nomenclature for the one layered model is found in Figure 2-A. In linearized form, assuming constant depth and vertically averaged velocities, the governing momentum equations for tidal wave propagation, including bottom friction and Coriolis force, become in the x and y directions respectively:

$$g \frac{\partial \eta}{\partial x} + \frac{\partial u}{\partial t} - \frac{1}{2} C_f U \frac{1}{h} u - 2\omega_e (\sin \phi) v = 0 \quad (2.1A)$$

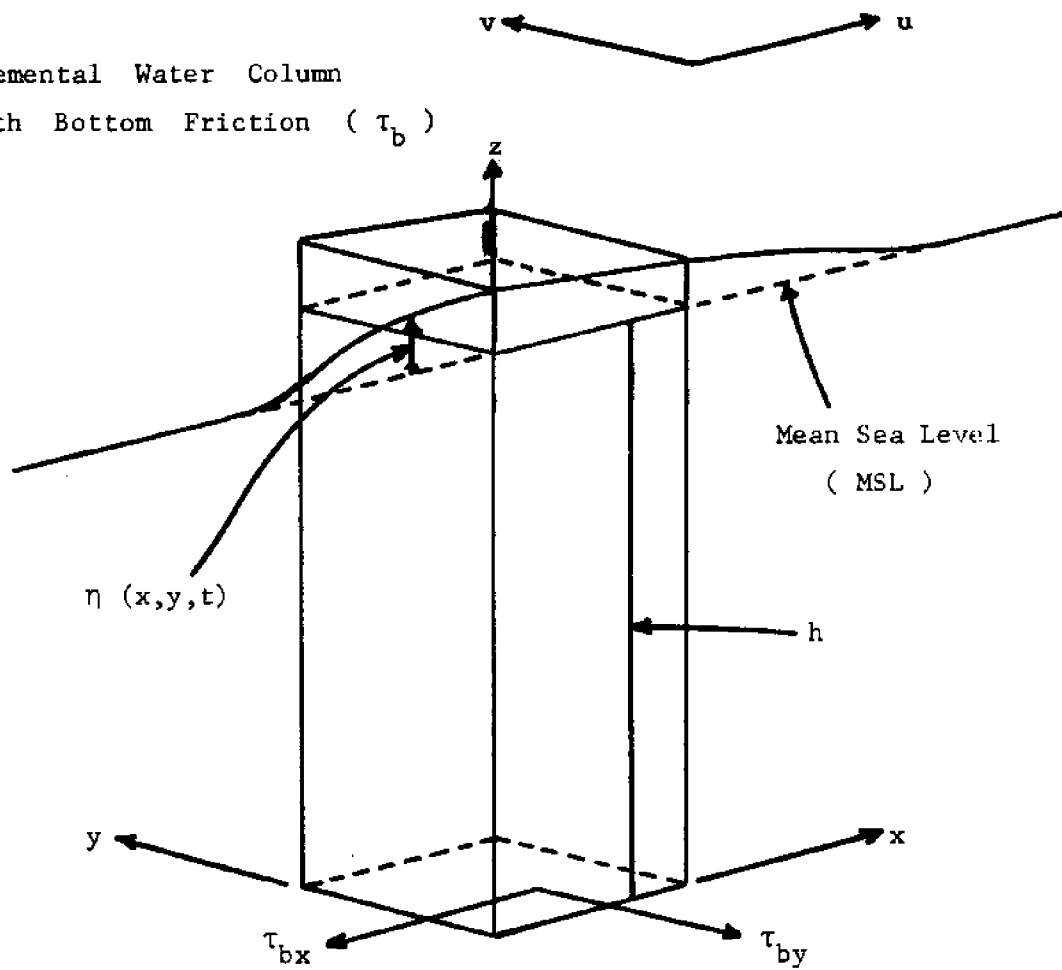
$$g \frac{\partial \eta}{\partial y} + \frac{\partial v}{\partial t} - \frac{1}{2} C_f U \frac{1}{h} v + 2\omega_e (\sin \phi) u = 0 \quad (2.1B)$$

where u and v are respectively components of the water velocity in the x and y directions, t is time, g is acceleration due to gravity, η is the surface elevation relative to mean sea level, C_f is the local shear-stress coefficient, $U = \sqrt{u^2 + v^2}$, h is the depth, ω_e is the angular velocity of the earth, and ϕ is the latitude. The linearized form of the continuity equation is:

$$\frac{\partial \eta}{\partial t} + \frac{\partial(hu)}{\partial x} + \frac{\partial(hv)}{\partial y} = 0 \quad (2.2)$$

Assuming periodic motion, where $\omega = \frac{2\pi}{T}$ and T equals the tidal period of 12.4 hours;

Elemental Water Column
With Bottom Friction (τ_b)



One Layer Model

Coordinate System and Nomenclature

Figure 2-A

$$(u,v) = \text{Real} \{ (u,v) e^{i\omega t} \} \quad (2.3A)$$

$$\eta = \text{Real} \{ \eta e^{i\omega t} \} \quad (2.3B)$$

it can be shown after linearization of the friction term by letting

$\lambda = \frac{1}{2} C_f U \frac{1}{h}$ and by setting $f = 2 \omega_e (\sin \phi)$ that:

$$g \frac{\partial \eta}{\partial x} + i\omega u - \lambda u - f v = 0 \quad (2.4A)$$

$$g \frac{\partial \eta}{\partial y} + i\omega v - \lambda v + f u = 0 \quad (2.4B)$$

Equation (2.4B) can be solved for v which is then introduced into Equation (2.4A) giving u in the form:

$$u = - \frac{g}{i\omega - \lambda + \frac{f^2}{i\omega - \lambda}} \frac{\partial \eta}{\partial x} - \frac{f g}{(i\omega - \lambda)^2 + f^2} \frac{\partial \eta}{\partial y} \quad (2.5A)$$

By the same manner solving for u in Equation (2.4A) v can be obtained as:

$$v = - \frac{g}{i\omega - \lambda + \frac{f^2}{i\omega - \lambda}} \frac{\partial \eta}{\partial y} + \frac{f g}{(i\omega - \lambda)^2 + f^2} \frac{\partial \eta}{\partial x} \quad (2.5B)$$

Differentiating equation Equation (2.5A) with respect to x and Equation (2.5B) with respect to y and multiplying both by h allows substitution of the $\frac{\partial(hu)}{\partial x}$ and $\frac{\partial(hv)}{\partial y}$ terms in Equation (2.2). The continuity equation now becomes:

$$\frac{\partial \eta}{\partial t} - \frac{gh}{i\omega - \lambda + \frac{f^2}{i\omega - \lambda}} \left(\frac{\partial^2 \eta}{\partial x^2} + \frac{\partial^2 \eta}{\partial y^2} \right) = 0 \quad (2.6)$$

By letting $\frac{\partial \eta}{\partial t} = i\omega\eta$ the governing equation for η in the one layer model becomes in final form:

$$\frac{\partial^2 \eta}{\partial x^2} + \frac{\partial^2 \eta}{\partial y^2} + \frac{\omega^2}{gh} \left(1 + i \frac{\lambda}{\omega} - \frac{(f/\omega)^2}{1 + i \frac{\lambda}{\omega}} \right) \eta = 0 \quad (2.7)$$

The special case of no bottom friction, $\lambda = 0$, and no Coriolis force, $f = 0$, leads to:

$$\frac{\partial^2 \eta}{\partial x^2} + \frac{\partial^2 \eta}{\partial y^2} + \frac{\omega^2}{gh} \eta = 0 \quad (2.8)$$

It is clear from (2.5A), (2.5B) and (2.7) that a non-zero bottom shear stress will introduce a phase difference between u , v and $\frac{\partial \eta}{\partial x}$ and $\frac{\partial \eta}{\partial y}$. The magnitude of the term $\frac{\lambda}{\omega}$ may be estimated, from an assumption of $C_f \approx 0.005$, $h = 120$ ft, and $U \approx 1$ ft/sec, to be $\frac{1}{8}$ which indicates that it is reasonable to neglect this term.

It is worth noting in the governing equation, the importance of Coriolis effect on Massachusetts Bay where the mid-latitude is approximately 42°N . The Coriolis term in Equation (2.7) is of the order 0.45 since $(\frac{f}{\omega})^2 \approx \sin^2 42^\circ$, and obviously neglecting f is a relatively poor assumption. However, by retaining Coriolis, the boundary conditions become complicated and difficult to solve and since the purpose of the study is to develop a simple qualitative model, f is set equal to zero.

Now that the simplified governing equation has been developed for the one layered model, the various conditions must be imposed on the boundaries to specify the particular problem. As shown in

Figure 2-B, a simple geometry has been assumed with effectively impermeable walls on all sides except at $y = y_0$ between x_1 and x_2 where there is an opening representing the ocean boundary between Massachusetts Bay and the Gulf of Maine.

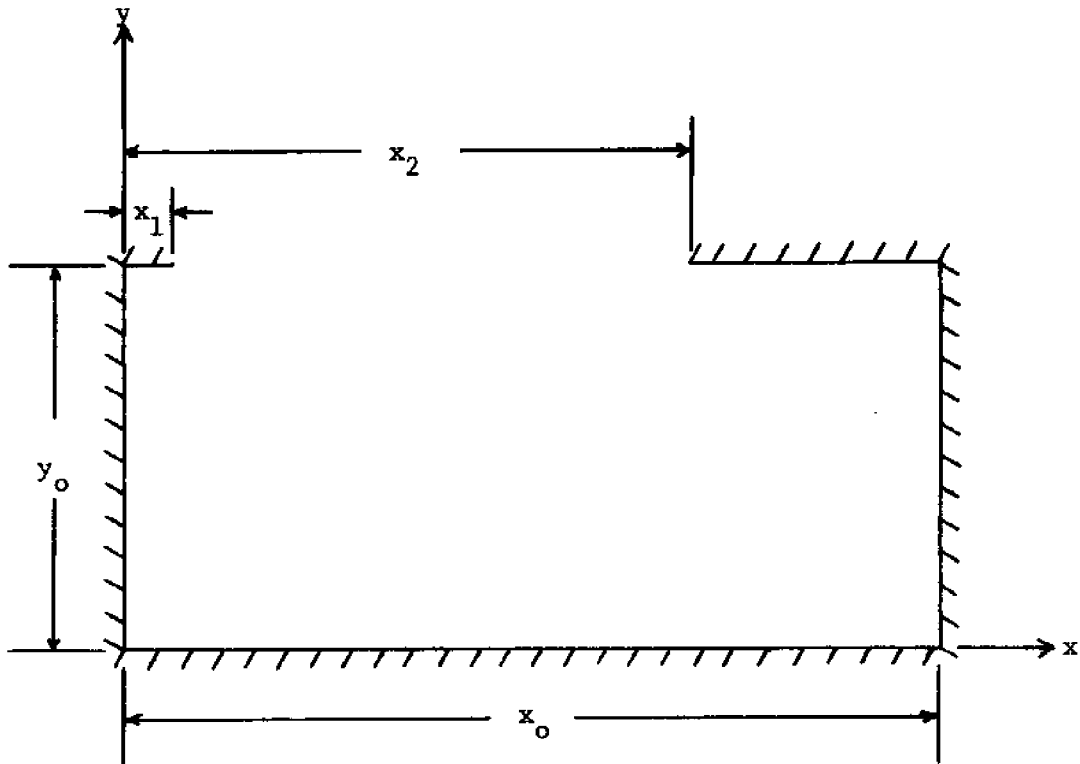


Figure 2-B: Geometry of Massachusetts Bay For The One and Two Layered Models.

Consequently the velocities can be specified along the walls such that $u = 0$ at $x = 0$ and x_0 for all y and that $v = 0$ at $y = 0$ for all x and at $y = y_0$ for $0 < x < x_1$, $x_2 < x < x_0$. Neglecting Coriolis effects it is seen that $u = 0$ corresponds to $\frac{\partial \eta}{\partial x} = 0$ from Equation (2.5A) and that $v = 0$ corresponds to $\frac{\partial \eta}{\partial y} = 0$ from Equation (2.5B). Consequently the boundary conditions may be summarized as:

$$\text{At } x = 0 \quad \frac{\partial \eta}{\partial x} = 0 \quad (2.9A)$$

$$\text{At } x = x_0 \quad \frac{\partial \eta}{\partial x} = 0 \quad (2.9B)$$

$$\text{At } y = 0 \quad \frac{\partial \eta}{\partial y} = 0 \quad (2.9C)$$

$$\text{At } y = y_0 \quad \frac{\partial \eta}{\partial y} = 0 \quad \begin{array}{l} 0 \leq x \leq x_1 \\ x_2 \leq x \leq x_0 \end{array} \quad (2.9D)$$

If the width of the opening between x_2 and x_1 is small it may be assumed that $\frac{\partial \eta}{\partial y}$ or v is constant over the entire opening. A gross conservation of mass consideration then gives, with V being the volume of fluid in the bay above mean sea level:

$$V = \int dx \int \eta dy$$

$\frac{\partial V}{\partial t}$ = rate of change of volume within the bay must be equal to the inflow through the opening. This can be written as:

$$\frac{\partial V}{\partial t} = -v(x_2 - x_1)h \quad \text{at } y = y_0 \quad (2.10)$$

From Equation (2.5B), assuming no friction and no Coriolis effect, it can be shown that:

$$\frac{\partial \eta}{\partial y} = \frac{i\omega}{g} \frac{1}{(x_2 - x_1)h} \frac{\partial \Psi}{\partial t} \quad (2.11)$$

Assuming that the tidal motion within the bay is periodic where $\Psi = \Psi e^{i\omega t}$ or $\frac{\partial \Psi}{\partial t} = i\omega \Psi$ the last boundary condition can be determined:

$$\text{At } y = y_0 \quad \frac{\partial \eta}{\partial y} = - \frac{\omega^2}{gh} \frac{1}{x_2 - x_1} \Psi \quad x_1 \leq x \leq x_2 \quad (2.12)$$

The solution can be expected to be determined except for a constant since only derivatives are prescribed as boundary conditions. This constant is determined from considerations of the amplitude of the tidal motion at some point in the bay.

The boundary conditions specified in (2.9A) and (2.9B) suggest an x-dependence in the solution of η such that $\eta = \cos k_n x$. It is apparent that $\frac{\partial \eta}{\partial x} = 0$ at $x = 0$ and also at $x = x_0$ if $k_n x_0 = n\pi$ for $n = 0, 1, 2, \dots$. Thus k_n will take the form:

$$k_n = \frac{n\pi}{x_0} \quad (2.13)$$

The boundary condition in (2.9C) suggests a dependency in y such that $\eta = \cos m_n y$. As a result $\frac{\partial \eta}{\partial y} = 0$ at $y = 0$ and consequently a solution of the following form will be sought:

$$\eta = e^{i\omega t} \sum_{n=0}^{\infty} A_n \cos k_n x \cos m_n y \quad (2.14)$$

The solution must satisfy the governing equation (2.8), and by substituting the general solution (2.14) into (2.8) m_n can be solved in terms of k_n :

$$m_n = \sqrt{\frac{\omega^2}{gh} - k_n^2} \quad n = 0, 1, 2, \dots \quad (2.15)$$

For the particular case of Massachusetts Bay $h \approx 120$ feet and $x_0 = 59$. NM (nautical miles) and it can be shown that m_n is imaginary for $n > 0$. Since we are seeking only that portion of the solution which is real and by the fact that $\cos i \alpha = \cosh \alpha$ the general solution may be written as:

$$\eta = e^{i\omega t} \left\{ A_0 \cos m_0 y + \sum_{n=1}^{\infty} A_n \cos k_n x \cosh m_n y \right\} \quad (2.16)$$

where m_0 is evaluated for $n = 0$ in Equation (2.15). The constants A_n must be determined from the remaining boundary conditions specified at $y = y_0$.

Evaluating the volume of water in the bay, V , it can be shown that only the term corresponding to $n = 0$ contributes to the volume since integration of the terms for $n > 0$ from $x = 0$ to x_0 give zero by virtue of the boundary conditions. Hence:

$$V = \frac{1}{m_0} A_0 x_0 \sin m_0 y_0 \quad (2.17)$$

which determines the boundary condition, stated in (2.12), to be satisfied at $y = y_0$.

The y derivative of the solution given by Equation (2.16) can now be matched at $y = y_0$ with the boundary conditions given in (2.9D) and (2.12) with V from (2.17). Through a Fourier expansion the coefficients A_n can be determined leading to the final form of the general solution:

$$\eta = A_0 e^{i\omega t} \left\{ \cos m_0 y - \sum_{n=1}^{\infty} \frac{2m_0 \sin m_0 y_0 (\sin k_n x_2 - \sin k_n x_1)}{m_n k_n (x_2 - x_1)} \cdot \frac{\cosh m_n y}{\sinh m_n y_0} \cos k_n x \right\} \quad (2.18)$$

where A_0 can be evaluated once the elevation η at some point in the Bay is known.

2.3 Two Layered Model

Derivation of the two layered analytical model is similar to the one layered one although discrete differences appear with the introduction of the second layer. The dynamic equations are again formulated in two dimensions by the application of the Navier-Stokes equations and the continuity relationships through a mass balance. The model is able to predict water surface and interface profiles and velocities in both layers.

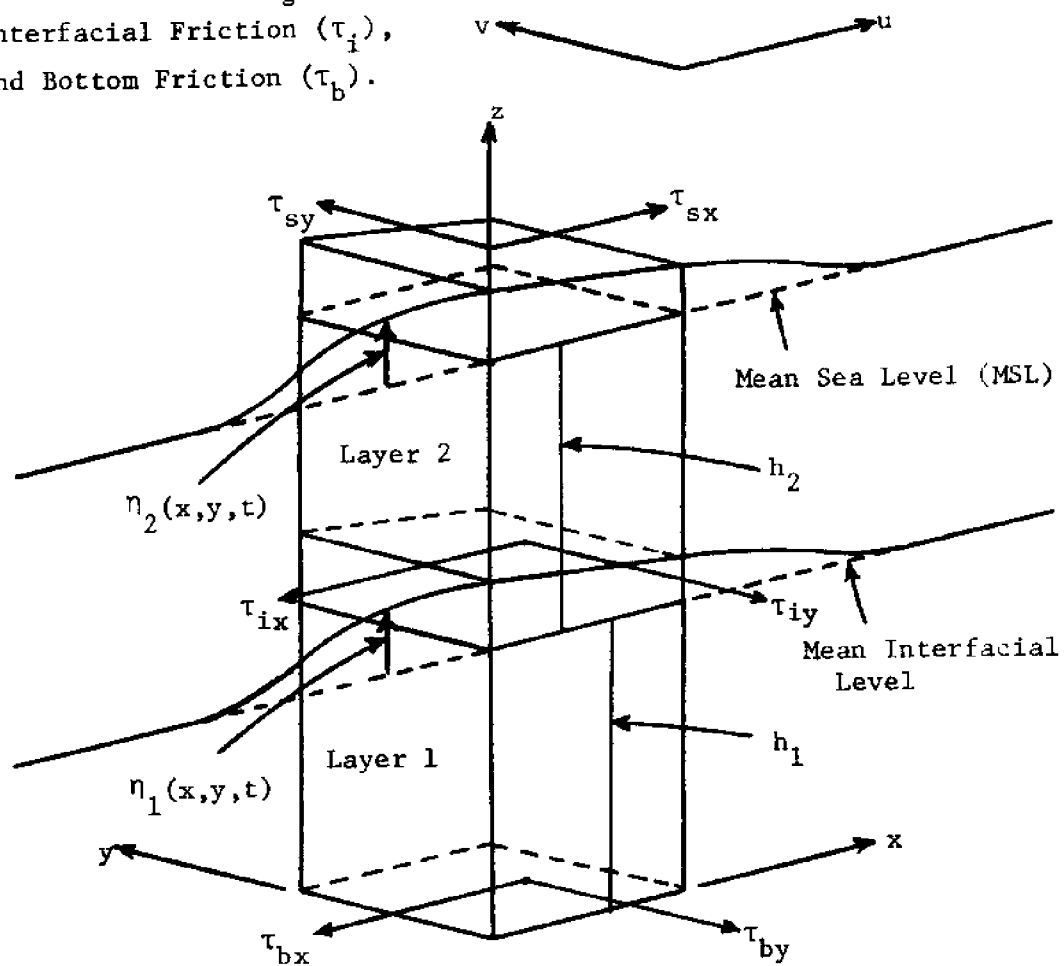
Representation of the coordinate system for the two layered model is shown in Figure 2-C. The lower layer is specified as layer one and the upper layer as layer two with the subscripts 1 and 2, respectively. With this the dynamic equations, in linear form, for the two layered model become:

Layer 1, x-direction

$$\frac{\partial u_1}{\partial t} + \frac{\rho_2}{\rho_1} g \frac{\partial \eta_2}{\partial x} + \frac{\rho_1 - \rho_2}{\rho_1} g \frac{\partial \eta_1}{\partial x} - \frac{1}{2} C_f u_1 \frac{1}{h_1} u_1 + \frac{\tau_{ix}}{\rho_1 h_1} =$$

$$2\omega_e (\sin \phi) v_1 = 0 \quad (2.19A)$$

Elemental Water Column With
 Surface Friction (τ_s),
 Interfacial Friction (τ_i),
 and Bottom Friction (τ_b).



Two Layer Model

Coordinate System and Nomenclature

Figure 2-C

Layer 1, y-direction

$$\frac{\partial v_1}{\partial t} + \frac{\rho_2}{\rho_1} g \frac{\partial \eta_2}{\partial y} + \frac{\rho_1 - \rho_2}{\rho_1} g \frac{\partial \eta_1}{\partial y} - \frac{1}{2} C_f U_1 \frac{1}{h_1} v_1 + \frac{\tau_{iy}}{\rho_1 h_1} + 2\omega_e (\sin \phi) u_1 = 0 \quad (2.19B)$$

Layer 2, x-direction

$$\frac{\partial u_2}{\partial t} + g \frac{\partial \eta_2}{\partial x} - \frac{\tau_{ix}}{\rho_2 h_2} + \frac{\tau_{sx}}{\rho_2 h_2} - 2\omega_e (\sin \phi) v_2 = 0 \quad (2.19C)$$

Layer 2, y-direction

$$\frac{\partial v_2}{\partial t} + g \frac{\partial \eta_2}{\partial x} - \frac{\tau_{iy}}{\rho_2 h_2} + \frac{\tau_{sy}}{\rho_2 h_2} + 2\omega_e (\sin \phi) u_2 = 0 \quad (2.19D)$$

where ρ is the density, τ_{ix} and τ_{iy} are the interfacial friction terms, and τ_s indicates a surface wind shear stress. The remaining terms were defined in the one layer model and remain the same. The conservation of mass equations are similar to those in the previous model and when linearized take the form:

Layer 1

$$\frac{\partial \eta_1}{\partial t} + \frac{\partial(h_1 u_1)}{\partial x} + \frac{\partial(h_1 v_1)}{\partial y} = 0 \quad (2.20A)$$

Layer 2

$$\frac{\partial \eta_2}{\partial t} + \frac{\partial(h_2 u_2)}{\partial x} + \frac{\partial(h_2 v_2)}{\partial y} - \frac{\partial \eta_1}{\partial t} = 0 \quad (2.20B)$$

The above continuity equations have assumed two immiscible fluids,

i.e., no exchange of mass across the interface. If a mass exchange between the two layers were considered the interfacial friction would be influenced by the associated momentum transfer across the interface. For a discussion of this reference is given in Pedersen (1972). The governing equations are the linearized form of those given by Grubert and Abbott (1972).

It is obvious that retaining the Coriolis and the frictional terms tends to make the governing equations quite lengthy and difficult to solve. Consequently, the bottom and interfacial friction terms, the Coriolis force, and surface shear stress will be set equal to zero in order to retain the simplicity that is desired in the model.

It is important to note the result of the steady state condition, as in the case of wind setup, where $\frac{\partial u}{\partial t}$ and $\frac{\partial v}{\partial t}$ are zero. It can be shown that if $\frac{\partial \eta_2}{\partial x}$ and $\frac{\partial \eta_2}{\partial y}$ do not equal zero then the momentum equations for layer one, given by (2.19A) and (2.19B), reduce to:

x-direction

$$\frac{\partial \eta_1}{\partial x} = - \frac{\rho_2}{\rho_1 - \rho_2} \frac{\partial \eta_2}{\partial x} \quad (2.21A)$$

y-direction

$$\frac{\partial \eta_1}{\partial y} = - \frac{\rho_2}{\rho_1 - \rho_2} \frac{\partial \eta_2}{\partial y} \quad (2.21B)$$

Obviously, if the densities of the two fluids are within a few percent of each other, the slope of the interface is far greater than that of the surface. In addition the slope of one is tilted in an opposite direction from the other.

In Massachusetts Bay the density of one layer is generally within 0.4 percent of the other. Since the two densities are so close together, an approximate form of the momentum equations for layer one could be obtained by replacing $\frac{\rho_2}{\rho_1}$ in η_2 by unity.

Again summing the tidal motion in the bay to be periodic we take:

$$(\eta_1, \eta_2, u_1, u_2, v_1, v_2) = \text{Real} (\eta_1, \eta_2, u_1, u_2, v_1, v_2) e^{i\omega t}$$

$$\left(\frac{\partial u_1}{\partial t}, \frac{\partial u_2}{\partial t}, \frac{\partial v_1}{\partial t}, \frac{\partial v_2}{\partial t} \right) = i\omega (u_1, u_2, v_1, v_2)$$

the governing equations can be derived for velocities and elevations.

Velocities in the upper layer, u_2 and v_2 , can be obtained directly from the momentum Equations (2.19C) and (2.19D)

$$u_2 = - \frac{g}{i\omega} \frac{\partial \eta_2}{\partial x} \quad (2.22A)$$

$$v_2 = - \frac{g}{i\omega} \frac{\partial \eta_2}{\partial y} \quad (2.22B)$$

By taking the derivative of u_2 with respect to x and the derivative of v_2 with respect to y , the $\frac{\partial(h_2 u_2)}{\partial x}$ and $\frac{\partial(h_2 v_2)}{\partial y}$ terms can be obtained and introduced into the continuity equation for layer two, (2.20B). In terms of η_2 the governing equation for the interface profile becomes:

$$\eta_1 = \eta_2 + \frac{gh_2}{\omega^2} \left(\frac{\partial^2 \eta_2}{\partial x^2} + \frac{\partial^2 \eta_2}{\partial y^2} \right) \quad (2.23)$$

The x and y derivatives of η_1 can now be introduced into Equations (2.19A) and (2.19B) respectively. By this the velocities in the lower layer are determined as:

$$u_1 = -\frac{g}{i\omega} \frac{\partial \eta_2}{\partial x} - \frac{g}{i\omega} \frac{\rho_1 - \rho_2}{\rho_1} \frac{gh_2}{\omega^2} \left(\frac{\partial^3 \eta_2}{\partial x^3} + \frac{\partial^3 \eta_2}{\partial x \partial y^2} \right) \quad (2.24A)$$

$$v_1 = -\frac{g}{i\omega} \frac{\partial \eta_2}{\partial y} - \frac{g}{i\omega} \frac{\rho_1 - \rho_2}{\rho_1} \frac{gh_2}{\omega^2} \left(\frac{\partial^3 \eta_2}{\partial x^2 \partial y} + \frac{\partial^3 \eta_2}{\partial y^3} \right) \quad (2.24B)$$

Now that the velocities in layer one have been derived, it only remains to determine the equation governing η_2 . It should be noted that the development of the governing equations has specified all velocities and η_1 in terms of η_2 . The surface profile, η_2 , can be determined in much the same manner in which η_1 was found, i.e., $\frac{\partial(h_1 u_1)}{\partial x}$ and $\frac{\partial(h_1 v_1)}{\partial y}$ can be derived from Equations (2.24A) and (2.24B) respectively and along the Equation (2.23) can be introduced into the Conservation of Mass equation for layer one, (2.20A). Consequently, the governing equation for η_2 takes the form:

$$\eta_2 + \frac{g(h_1 + h_2)}{\omega^2} \left(\frac{\partial^2 \eta_2}{\partial x^2} + \frac{\partial^2 \eta_2}{\partial y^2} \right) + \frac{gh_1}{\omega^2} \frac{gh_2}{\omega^2} \frac{\rho_1 - \rho_2}{\rho_1} \left(\frac{\partial^4 \eta_2}{\partial x^4} + \frac{2\partial^4 \eta_2}{\partial x^2 \partial y^2} + \frac{\partial^4 \eta_2}{\partial y^4} \right) = 0 \quad (2.25)$$

For the case $\rho_1 = \rho_2$ it should be noted that the above equation reduces to the linear long wave equation in two dimensions.

The same geometry used in the one layered model will be applied to the two layered situation. As shown in Figure 2-B, the Bay is assumed rectangular with impermeable boundaries except for the section between Cape Cod and Cape Ann which is open to the Gulf of Maine. The boundary conditions are formulated by specifying the velocities,

in both layers, equal to zero along the walls and can be summarized as:

$$u_1, u_2 = 0 \quad \text{at } x = 0 \text{ and } x_0 \quad (2.26A)$$

$$v_1, v_2 = 0 \quad \text{at } y = 0 \quad (2.26B)$$

This suggests a solution of the following form:

$$\eta_2 = i\omega t \sum_0^{\infty} A_n \cos k_n x \cos m_n y \quad (2.27)$$

where the constants A_n , k_n , and m_n must be determined for each n .

Applying now the boundary conditions in (2.26A) to the assumed solution for u_2 , given by Equations (2.22A) and (2.27), k_n can be derived in the following form:

$$k_n = \frac{n\pi}{x_0} \quad n = 0, 1, 2, \dots$$

which is the same as derived previously for the one layered case and will satisfy u_1 as given in Equation (2.24A).

The condition that v_2 is equal to zero at $y = 0$ can be applied to the solution for v_2 as given by Equations (2.22B) and (2.27). Combined with the expression for v_1 it is seen that both have a y dependence given by $\sin m_n y$ which vanishes at y equal to zero. Thus the assumed solution, as given by Equation (2.27), meets all the specified boundary conditions and seems promising as the general solution for η_2 .

Since k_n has been determined it now remains to find the

expression for m_n . Introducing the assumed solution for η_2 into the governing equation for the surface profile, Equation (2.25), yields an expression which can be reduced to the form $am_n^4 + bm_n^2 + c = 0$. As it is quadratic, the expression can be solved directly for m_n to the following point.

$$m_n^2 = -k_n^2 + \frac{1}{2} \frac{\omega^2}{gh_2} \frac{h_1+h_2}{h_1} \frac{\rho_1}{\rho_1-\rho_2} \left(1 \pm \sqrt{1 - 4 \frac{\rho_1-\rho_2}{\rho_1} \frac{h_1 h_2}{(h_1+h_2)^2}} \right)$$

The quantity $4 \frac{\rho_1-\rho_2}{\rho_1} \frac{h_1 h_2}{(h_1+h_2)^2} \leq \frac{\rho_1-\rho_2}{\rho_1}$ which will be far smaller than unity. Thus, the approximation can be made that $\sqrt{1-\epsilon}$ equals $1 - \frac{1}{2} \epsilon$. With this the final form of m_n is obtained as:

$$m_{n_1} = \sqrt{\frac{\omega^2}{g(h_1+h_2)} - k_n^2} \quad (2.29A)$$

$$m_{n_2} = \sqrt{\frac{\omega^2}{gh_2} \frac{\rho_1}{\rho_1-\rho_2} \frac{h_1+h_2}{h_1} - \frac{\omega^2}{g(h_1+h_2)} - k_n^2} \quad (2.29B)$$

where (2.29A) is seen to be identical to the result obtained for the one layer model, (2.15). Thus when the Bay dimensions are small compared to the tidal wave length it can be seen that m_{n_1} is imaginary except for $k_n = 0$. However, m_{n_2} will start out by being real if $\frac{\rho_1-\rho_2}{\rho_1}$ is sufficiently small, but at some $n = N$, m_{n_2} will also become imaginary. Hence, the solution may be written as:

$$\begin{aligned}
\eta_2 = e^{i\omega t} \{ & A_0 \cos m_{o1} y + \sum_{n=1}^{\infty} A_n \cos k_n x \cosh m_{n1} y \\
& + B_0 \cos m_{o2} y + \sum_{n=1}^{N-1} B_n \cos k_n x \cos m_{n2} y + \\
& \sum_{n=N}^{\infty} B_n \cos k_n x \cosh m_{n2} y \} \quad (2.30)
\end{aligned}$$

The solution for η_1 can now also be written in terms of A_n and B_n by the substitution of Equation (2.30) into Equation (2.23). From (2.30) and the similarity between (2.29A) and (2.15) it is obvious that the terms involving the constants A_n are similar to our one layer model, whereas the terms involving B_n express the influence of the two layered system.

As previously discussed, a gross conservation of mass consideration can be defined as:

$$\Psi = \int dy \int \eta dx$$

Applying this to the total water column and integrating from $x = 0$ to x_o and $y = 0$ to y_o yields the equation for the volume of fluid in the bay.

$$\Psi_{\text{total}} = \int dy \int \eta_2 dx = x_o \left[A_0 \frac{1}{m_{o1}} \sin(m_{o1} y_o) + B_0 \frac{1}{m_{o2}} \sin(m_{o2} y_o) \right] \quad (2.31A)$$

By the same method the volume, Ψ_1 , of the lower layer, can be determined since the solution to η_1 has been determined:

$$\begin{aligned} \Psi_1 = \int dy \int \eta_1 dx = x_o [A_o \frac{1}{m_{o1}} \sin(m_{o1} y_o) + B_o \frac{1}{m_{o2}} \sin(m_{o2} y_o)] \\ - x_o \frac{gh_2}{\omega^2} [A_o m_{o1} \sin(m_{o1} y_o) + B_o m_{o2} \sin(m_{o2} y_o)] \end{aligned} \quad (2.31B)$$

The change in volume within each layer, $\frac{\partial \Psi_1}{\partial t}$ and $\frac{\partial \Psi_2}{\partial t}$, is periodic and must be equal to the inflow through the opening. Consequently, as in the one layer model, the following can be written:

$$\frac{\partial \Psi_1}{\partial t} = -v_1 (x_2 - x_1) h_1 \quad \text{at } y = y_o \quad (2.32A)$$

$$\frac{\partial (\Psi_{total} - \Psi_1)}{\partial t} = -v_2 (x_2 - x_1) h_2 \quad \text{at } y = y_o \quad (2.32B)$$

Since v_2 is given by Equation (2.22B) it can be shown that, by substitution of v_2 into Equation (2.32B), $\frac{\partial \eta_2}{\partial y}$ will take the form:

$$\frac{\partial \eta_2}{\partial y} = - \frac{\omega^2}{gh_2 (x_2 - x_1)} (\Psi_{total} - \Psi_1) \quad (2.33)$$

By the fact that Ψ_1 and Ψ_{total} are given and since $\frac{\partial \eta_2}{\partial y}$ can be obtained from Equation (2.30) the above equation can be expressed completely in terms of A_n and B_n . Similarly, v_1 can be obtained by substitution of the solution for η_2 into Equation (2.24B) which when introduced into Equation (2.32A) also, by knowing Ψ_1 , gives an expression completely in A_n and B_n . These equations become:

Layer 1 (Bottom Layer)

$$\begin{aligned}
 & A_{001} \sin m_{01} y_0 - \sum_{n=1}^{\infty} A_{nm_{n1}} \cos k_n x \sinh m_{n1} y_0 + B_{002} \sin m_{02} y_0 \\
 & + \sum_{n=1}^{N-1} B_{nm_{n2}} \cos k_n x \sin m_{n2} y_0 - \sum_{n=N}^{\infty} B_{nm_{n2}} \cos k_n x \sinh m_{n2} y_0 \\
 & - \frac{\rho_1 - \rho_2}{\rho_1} \frac{gh_2}{\omega^2} \left[\sum_{n=1}^{\infty} - A_{nm_{n1}}^2 m_{n1} \cos k_n x \sinh m_{n1} y_0 \right. \\
 & + \sum_{n=1}^{\infty} A_{nm_{n1}}^3 \cos k_n x \sinh m_{n1} y_0 + \sum_{n=1}^{N-1} B_{nm_{n2}}^2 m_{n2} \cos k_n x \sin m_{n2} y_0 \\
 & - \sum_{n=N}^{\infty} B_{nm_{n2}}^2 m_{n2} \cos k_n x \sinh m_{n2} y_0 + \sum_{n=1}^{N-1} B_{nm_{n2}}^3 \cos k_n x \sin m_{n2} y_0 \\
 & \left. + \sum_{n=N}^{\infty} B_{nm_{n2}}^3 \cos k_n x \sinh m_{n2} y_0 \right] =
 \end{aligned}$$

$$\left\{ \begin{array}{ll} + \frac{\omega^2}{gh_1(x_2 - x_1)} v_1 & x_1 < x < x_2 \\ 0 & \text{elsewhere} \end{array} \right.$$

(2.34A)

Layer 2 (Top Layer)

$$A_o m_{o1} \sin m_{o1} y_o - \sum_{n=1}^{\infty} \frac{m_{n1}}{2} A_n \sinh m_{n1} y_o + B_o m_{o2} \sin m_{o2} y_o \\ + \sum_{n=1}^{N-1} \frac{m_{n2}}{2} B_n \sin m_{n2} y_o - \sum_{n=N}^{\infty} \frac{m_{n2}}{2} B_n \sinh m_{n2} y_o =$$

$$\left\{ \begin{array}{ll} \frac{\omega^2}{gh_2(x_2-x_1)} (V_{\text{total}} - V_1) & x_1 < x < x_2 \\ 0 & \text{elsewhere} \end{array} \right.$$

(2.34B)

Since the functions $\cos k_n x$ with $k_n = n\pi/x_o$ are orthogonal on the interval $x = 0, x_o$; each equation can be multiplied through by $\cos k_m x$ and integrated from 0 to x_o . By this method two equations, each with two unknowns, A_n and B_n , are obtained for each n .

Representatively, these take the form:

$$a_n A_n + b_n B_n = c_n A_o + d_n B_o \quad (2.35A)$$

$$a'_n A_n + b'_n B_n = c'_n A_o + d'_n B_o \quad (2.35B)$$

where the coefficients a_n , b_n , c_n , and d_n in both equations are known functions of n . Thus, in principle (2.35A) and (2.35B) could be solved to give the constants A_n and B_n as functions of n , A_o and B_o .

From the discussion following the derivation of (2.30) it is

clear that the constants A_0 and B_0 , although not independent, govern primarily the surface and interface elevations respectively. It should be noted that by letting B_0 equal to zero the solution for η_2 as given by Equation (2.30) approximates the form of the general solution for η in the one layer model.

The constants A_0 and B_0 must be specified by some type of field information, either elevations or velocities, at a known location. Specifying A_0 and B_0 allows the two equations to be solved for A_n and B_n which can then be introduced into the governing equation for η_2 . With this the remaining velocities or profiles can be determined through the appropriate governing equations.

CHAPTER III

RESULTS OF THE ONE LAYER MODEL

The one layer model represents the well mixed situation generally found in Massachusetts Bay during the winter months. Oceanographic data collected by the U. S. Department of the Interior (1959) shows that for the duration of the winter season the water column is fairly uniform in temperature and salinity because of the absence of a thermocline. As a result the Bay can be assumed of constant density with the one layer model being quite representative of the physical situation. The one layer model is consequently able to yield a simple prediction of the surface profile and currents due to the tidal action in the Bay for the winter season.

3.1 Computational Aspects

3.1.1 Mathematical Simulation of the Ocean Boundary

In the development of the general solution for the one layer model, as given by Equation (2.18), it was stated that to predict the surface profile and velocities the constant A_0 must be determined by field data. This field information which is required for the evaluation of A_0 can either be a tidal amplitude or current information specifying speed and direction for some known point in Massachusetts Bay. Since it is generally quite difficult to extract tidal current information from current meter records, a specified surface elevation will be used for the determination of A_0 . Specifically, the tidal range at Boston Light, located just outside Boston Harbor, has been

determined by the National Ocean Survey (1973) to be 9.0 feet with a corresponding tidal amplitude of 4.5 feet. This information was obtained from tide gauge records taken at Boston Light located on Little Brewster Island shown in Figure 3-A. With the geometry and coordinate system specified for the one layer model, Boston Light can be located at $x = 10.0$ NM, $y = 0.0$ NM.

Since the reference datum for the surface elevation in the one layer model is mean sea level (MSL) it will be the tidal amplitude with which we are concerned. Thus, using 4.5 feet for η at the x, y coordinates specified above, A_0 can be determined for a particular geometrical configuration from Equation (2.18). With the determination of this constant, the current field and surface profile for the entire Bay can be computed. It should be cautioned that A_0 is discrete for only one geometrical configuration. Changing the depth of the Bay or the width of the opening demands that A_0 be recalculated regardless of the fact that the same surface elevation is prescribed at the same location.

The constant A_0 actually determines the magnitude of the forcing function to be applied at the open boundary, across which the tidal amplitude is considered constant. In the one layer model the boundary conditions are so chosen that no interaction between the motion in the bay and that in the ocean is considered. This has implications where the exciting frequency is close to a resonant frequency. However, this plays a minor role in the case of tidal excitation of Mass Bay as will be discussed later (Section 3.3).

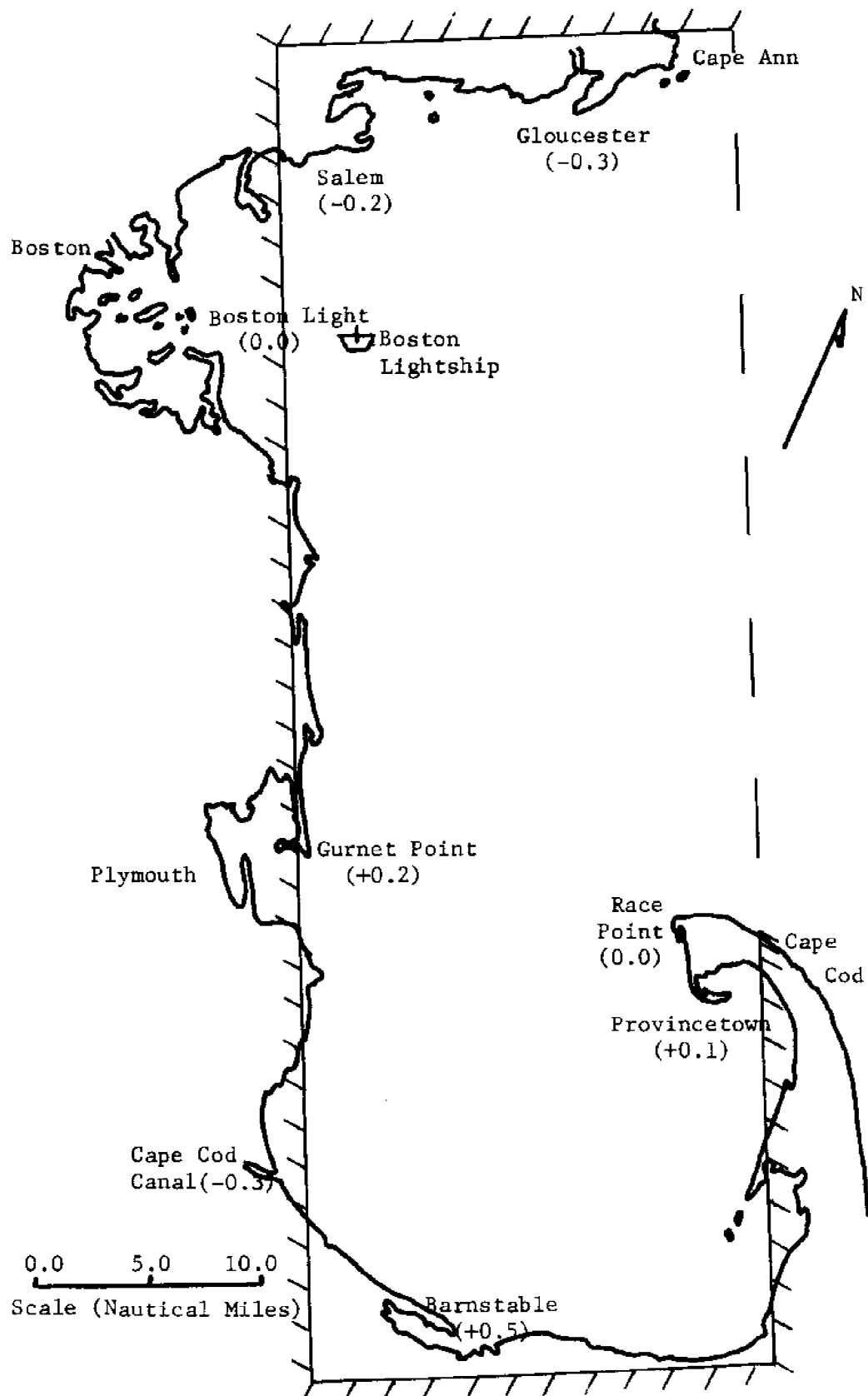


Figure 3-A: Massachusetts Bay; Observed Differences in Tidal Amplitude at High Tide, Measured in Feet. Reference Station-Boston Light.

Consequently, by specifying the tidal amplitude at $y = y_0$, the two dimensional bay appears to be driven by a wave with the magnitude a function of A_0 .

The boundary condition, specified at $y = y_0$ for $x_1 \leq x \leq x_2$, is given by Equation (2.12) and derived by considering the mass flux through the channel opening. An important assumption in determining this boundary condition is the assumption of $\frac{\partial \eta}{\partial y}$ or v being constant over the entire width of the opening. This assumption has previously been made by Ippen and Goda (1963) and would appear reasonable for narrow openings. It should be pointed out that the specified value of $\frac{\partial \eta}{\partial y}$ over the opening, as given by (2.12), is a function of A_0 . Since the value of A_0 is determined by matching the tidal amplitude at one point, it is not possible to satisfy the assumed condition of a constant tidal amplitude across the opening. However, the opening between x_1 and x_2 can be divided into increments and, since the governing equations are linear, the solution for η can be matched at the center of each increment. This method of solution will be discussed in detail later in this chapter.

The one layer analytical model for Massachusetts Bay was computed for a number of variations of the geometrical configuration presented in Figure 2-B. For the purposes of the model the bay is assumed rectangular with a length of 59.0 NM represented as x_0 and a width of 20.0 NM represented by y_0 . The width of the opening, given by $x_2 - x_1$ and representing the ocean boundary, is assumed to be 41.0 NM while the average depth in the Bay is equal to

approximately 120 feet.

Although a number of variations were introduced into the geometry in an attempt to simulate different conditions that could exist, only three variations will be discussed in this report. The first and most basic is the configuration presented in Figure 3-B which represents the geometry specified in the theoretical development of the one layer model. Initially, by setting η equal to 4.5 feet at Boston Light, the constant A_0 can be calculated. The surface profile and current field in Massachusetts Bay can then be computed with the results shown in Figure 3-B. Computed at time $t = 0$ from Equation (2.18), η is plotted in feet above mean sea level and corresponding to the amplitude at high tide. The surface elevation is seen to increase toward the southern or lower portion of the Bay. The speed and direction of the tidal current is given in knots during maximum ebb flow and is the result of plotting U where, as before,

$$U = \sqrt{u^2 + v^2}.$$

As can be seen by their governing equations, these velocities are functions of the surface slopes, $\frac{\partial \eta}{\partial x}$ and $\frac{\partial \eta}{\partial y}$, and they are consequently perpendicular to the co-tidal lines. Since the equations are periodic the surface profile attains a maximum slope at $t = \frac{T}{4} + n \frac{T}{2}$ for $n = 0, 1, 2, \dots$ with maximum velocities occurring simultaneously over the entire bay.

The model to this point has matched the surface elevation, η , with the boundary condition given by Equation (2.12) at only one point in the opening, i.e., $\frac{x_2 - x_1}{2}$. It is obvious from the results presented in Figure 3-B that the surface slope between x_1 and x_2

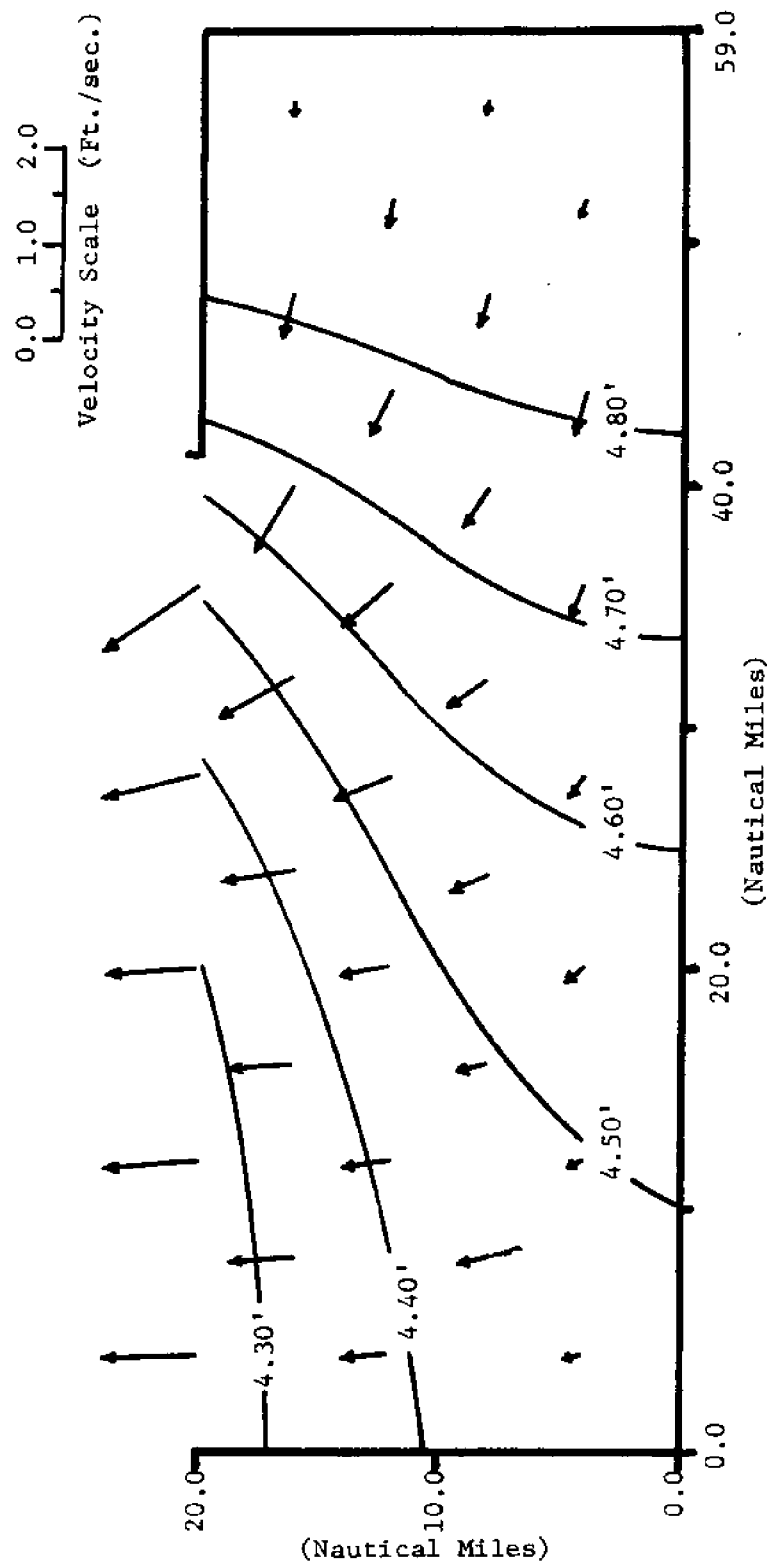


Figure 3-B: One Layer Model of Massachusetts Bay 1 Increment Channel. Surface Profile at High Tide in Feet Above MSL. Velocities at Maximum Ebb in Ft./sec.

does not equal zero and in fact the tidal amplitude varies of the order 0.40 feet across the opening. Although seemingly insignificant, this contradicts the physical assumption that η remains constant across the opening. As mentioned before, a method exists such that η can be matched at more than one point along $y = y_0$ between x_1 and x_2 . This is possible since the solution for η is obtained from a linear governing equation. Consequently, by dividing the opening into a number of sections the effect that one section exerts on the remaining sections can be computed. The surface elevation for the center point of each section can then be determined as the effects from the other sections are additive at that point. Computationally this requires, for n sections, the solution of n equations with n unknowns. This allows the surface elevation to be matched at n points across the opening therefore forcing the surface profile, at $y = y_0$, to better approximate the condition of η constant across the opening.

This method can be applied to the particular situation involving a partial constriction across the channel between x_1 and x_2 . In particular, this is introduced in an attempt to model the effect that Stellwagen Bank exerts on the tidal flow into Massachusetts Bay. From Figure 1-A it can be seen that Stellwagen Bank is a shoal area between Cape Ann and Cape Cod where the average depth of the Bank is approximately 90 feet, although in some areas depths of less than 60 feet occur. Since the possibility exists that the shoal could form a partial blockage to the tidal flux between the Gulf of Maine

and Massachusetts Bay, a method to model such an effect was introduced. This consisted of dividing the channel opening into two smaller channels separated by an impermeable constriction from $x = 16.5$ NM to $x = 29.0$ NM as shown in Figure 3-C. Representatively, the method of solution for this problem containing two channels, designated I and II, becomes:

$$a_I A_I + b_I B_{II} = C \quad (3.1A)$$

$$a_{II} A_I + b_{II} B_{II} = C \quad (3.1B)$$

where A_I and B_{II} are the values of the arbitrary constants for the two solutions obtained where one of the two openings is considered open and the other closed. a_I and b_I can be calculated and reflect the magnitude of the influence of A_I and B_{II} respectively at the center of one opening and a_{II} and b_{II} reflect the same influence for the second channel. C is the magnitude of the tidal amplitude that is to be matched at the center points of both channels. From this, Equations (3.1A) and (3.1B) can be solved for the two unknown constants A_I and B_{II} .

The surface profile for this variation of the one layer model is plotted in Figure 3-C. With an amplitude of 4.5 feet specified at Boston Light, an increase in the surface elevation of almost 0.20 feet occurs behind the assumed impermeable wall separating the two openings. This result casts some doubt on the validity of this particular model, which will be discussed later (Section 3.3), and velocities are therefore not shown.

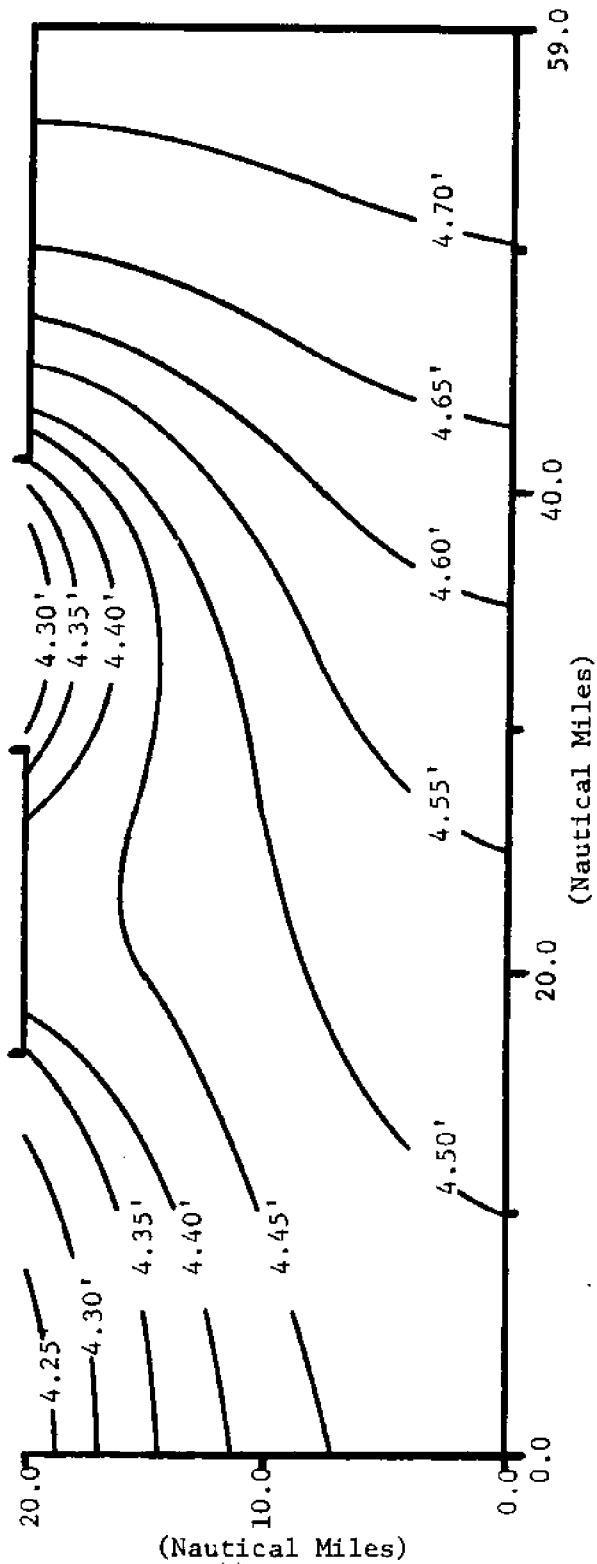


Figure 3-C: One Layer Model of Massachusetts Bay with Stellwagen Bank Closed.
Surface Profile at High Tide in Feet above MSL.

The third variation of the one layer model is similar to the model previously discussed with a full opening between $x_1 = 0.0$ NM and $x_2 = 41.0$ NM. Although the channel width is again 41.0 NM, the difference occurs in the treatment of the opening and the corresponding matched conditions. Here the channel is divided into four increments which, for reasons previously discussed, allows a better approximation of the boundary condition that η be constant across the opening, since a relatively flat surface profile, at $y = y_0$, is produced for each of the 10.25 NM increments. The method of solution discussed in the Stellwagen Bank model was employed and resulted in four equations and four unknowns with the matching point for η occurring in the center of each increment.

Results of this model are plotted in Figure 3-D and show the surface profile across the opening much more horizontal, and consequently more representative of our assumed boundary condition, than that given by the situation where η is matched at only one point. Obviously, dividing the channel into increments is advantageous since the boundary conditions are better satisfied. However, for a large number of channel increments, the solution becomes tedious to evaluate since the solution will consist of the summation of n infinite series where n is the number of channel subdivisions.

It should be noted that although the value of $\frac{\partial \eta}{\partial y}(v)$ is specified constant across each incremental opening, it was not imposed that $\frac{\partial \eta}{\partial y}$ be the same for all increments. The solution, however, clearly shows that $\frac{\partial \eta}{\partial y}(v)$ is essentially the same for all increments, except

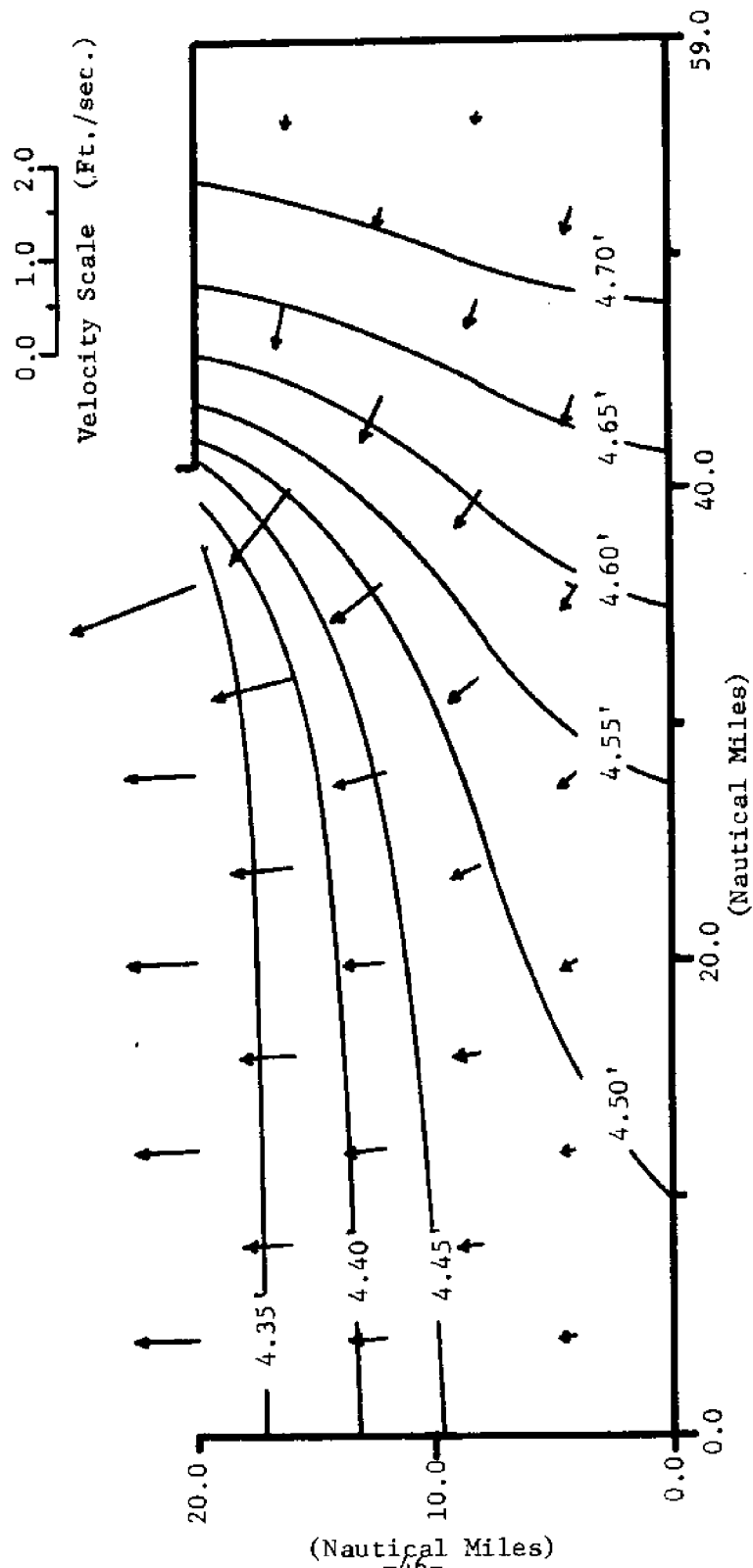


Figure 3-D: One Layer Model of Massachusetts Bay 4 Increment Channel. Surface Profile at High Tide in Feet above MSL. Velocities at Maximum Ebb in Ft./sec.

for a region close to the tip of Cape Cod, where deviations can be expected.

Alternate to an analytical solution, the hydrodynamic equations for the transient response of water bodies to tidal excitation can be solved by numerical methods. In particular, the finite element model has been applied to many problems in coastal and ocean engineering. Conner and Wang (1973) have recently applied such a model to the configuration of Massachusetts Bay. The model is restricted to vertically well mixed two dimensional flow and can incorporate both irregular geometry and variable depth. The numerical model employs triangular elements of varying dimensions and was first applied to a simple geometry identical to that for which results of the analytical model have been presented.

The surface profile and velocities are computed for the finite element model such that the results can be compared directly to the one layer analytical model. The numerical model is shown in Figure 3-E and neglects bottom friction, eddy viscosity, and Coriolis effects. Results for the numerical model compare favorably with those given by the analytical solution shown in Figures 3-B and 3-D. It can be seen that only small differences exist and these are partially explainable since the boundary conditions along the ocean opening are treated differently in the two models. The analytical model satisfies the boundary elevation criteria at discrete points (one for the case presented in Figure 3-B and four for the results given by Figure 3-D) whereas the numerical model satisfies the condition of constant

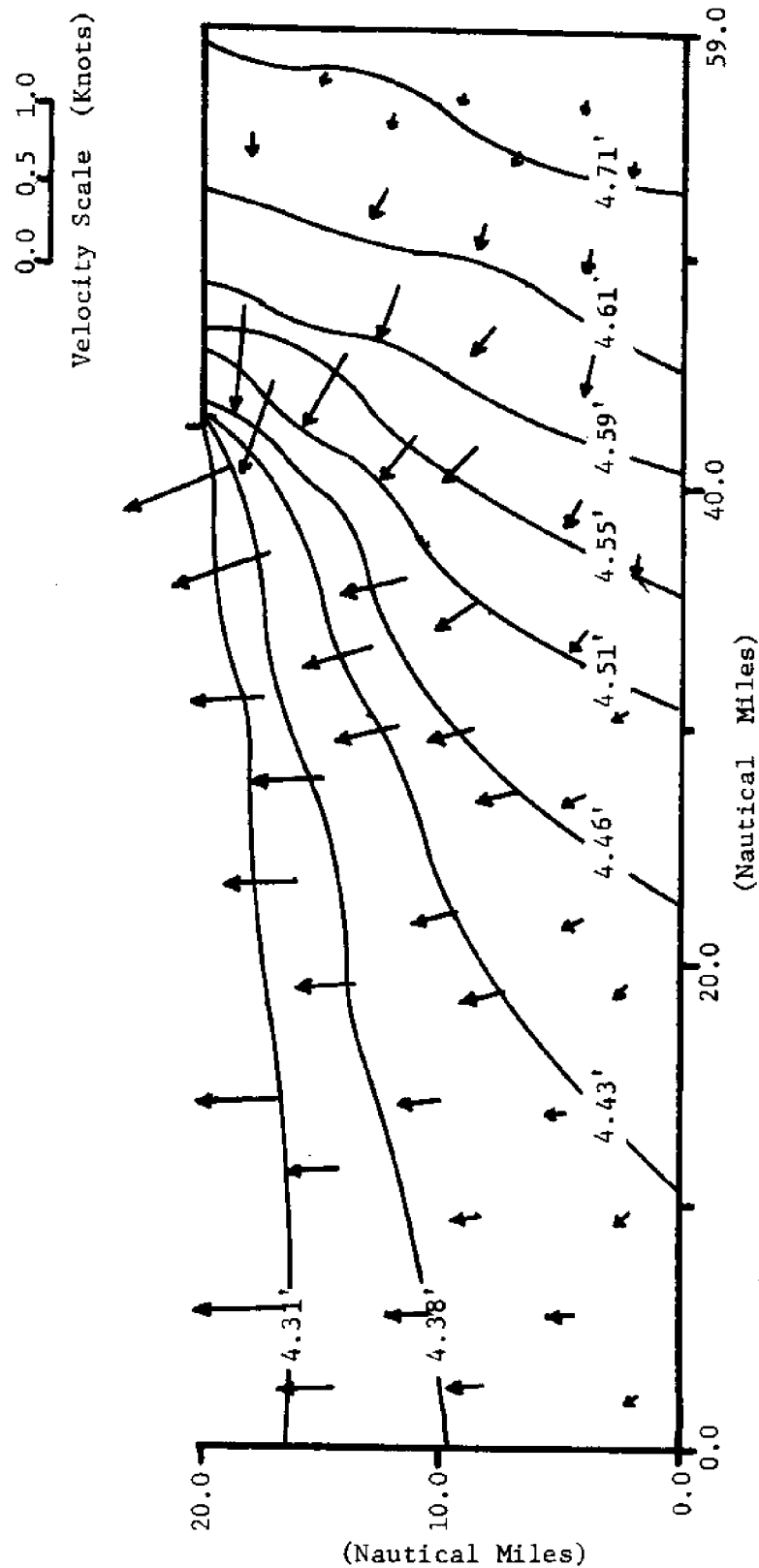


Figure 3-E: Numerical Model of Massachusetts Bay. Surface Profile at High Tide in Feet above MSL. Velocities at Maximum Ebb in Knots.

amplitude across the opening exactly. Comparison of the results of the analytical solution with those from the numerical model serve to demonstrate the close agreement between the two approaches and one of the reasons for developing the analytical one layer model was in fact to furnish Conner and Wang (1973) with a particular solution which could be used to test their numerical schemes.

3.1.2 Number of Terms Required in the Determination of η

The solution for η , given by Equation (2.18) and the solution for u and v , given respectively by Equations (2.5A) and (2.5B), were programmed on the Hewlett-Packard 2114B digital computer, allowing rapid computation of the surface profile and currents for the one layer model. It is important to note that the solution for η contains a summation for $n = 1$ to ∞ . A test for convergence of the summation and the number of terms required was of primary concern. Results clearly indicated that convergence was achieved by $n = 25$ although all computations for the one layer model were carried to $n = 100$.

3.2 Data Available for Comparison

Verification of the results of the one layer model, especially the predicted surface profiles, requires field information on the variation in tidal range over the Bay. Tide data taken by the National Ocean Survey (1973) in Massachusetts Bay has provided this information and has allowed the determination of the differences in tidal amplitude and surface slope. With Boston Light as the reference point, Figure 3-A shows the differences in tidal amplitude for selected locations around the Bay perimeter.

The information can be directly compared with the results of the one layer analytical model. The surface profile shown in Figures 3-B and 3-D, where the channel between x_1 and x_2 is completely open, produces some interesting facts when compared with field observations. Both models appear somewhat conservative in predicting the longitudinal slope from one end of the Bay to the other. Interestingly, the model with a one increment channel, shown in Figure 3-B, best approximates the surface slope computed from the tidal records in Cape Cod Bay. When comparing the surface elevation at specific locations, it can be seen that the four increment channel gives a close comparison at Race Point and Provincetown while the one increment case compares favorably at Gurnet Point and in the Gloucester Area.

Information on tidal currents around the Bay also allows a qualitative comparison of the model results with field data. Current observations taken by Butman (1971) confirm that velocities are of the same order of magnitude as those predicted by the model. However, these predicted results of velocities may be somewhat affected by the neglect of Coriolis force and the comparison can only be considered qualitative.

3.3 Discussion of the Model Results

The results of the one layer model for tidal amplitudes, when compared with available field information, are certainly acceptable for many situations, in spite of the many simplifying assumptions made in the development of the model and its application. Some of these assumptions will be discussed in the following.

One of the terms neglected during the development of the governing equations was the effect of friction on the tidal motion. As mentioned previously, the bottom shear stress, τ_b , creates a tidal phase lag from one part of the Bay to another. However, it can be seen from the National Ocean Survey Tide Tables (1973) that phase differences between the north and south end of Massachusetts Bay are small and, at high tide, average only about 10 minutes. Consequently, the neglect of friction seems appropriate for the physical situation considered.

Another important consideration is the possibility of resonant oscillations occurring as a result of the tidal forces. For an analysis of wave induced oscillations in harbors by Ippen and Goda (1963), the resonant characteristics of simple geometrical configurations has been determined. Applying their work on the frequency response of asymmetric harbors to the configuration assumed for Massachusetts Bay, where the tidal wave length is of the order 456.0 NM, since $L = T\sqrt{gh}$, the following can be concluded: (1) No resonant oscillations occur in Massachusetts Bay as a result of tidal excitation, since even the first resonant mode cannot be excited and (2) A wave length of less than 300 NM would be required to excite the first harmonic.

Figure 1-A shows that in the southern portion of Massachusetts Bay, more properly called Cape Cod Bay, gradual shoaling exists from approximately 13.0 NM offshore to the shoreline along the lower end of the Bay. The possibility exists that an additional increase in tidal range could occur in this area as the situation is quite analogous to a progressive two dimensional reflecting wave from a gently sloping

beach. That the tidal wave in the southern part of the Bay may be regarded approximately as a two dimensional standing wave in the x-direction is evident from the results given in, for example, Figure 3-D. This problem was treated by Doret and Madsen (1972) and using their results an increase in tidal amplitude, due to the shoaling at the lower end of the Bay, may be estimated to be of the order 0.06 ft., which is insignificant although giving a closer agreement between predicted and observed tidal amplitudes in this part of the Bay.

The variation simulating the effect of Stellwagen Bank on the tidal motion of Massachusetts Bay, although producing some interesting results, exhibits an increase in tidal amplitude behind the assumed barrier. Since the average depth of the shoal is only about 30 feet less than the average depth of the Bay, the effect of this increase in surface elevation will result in a considerable amount of volume exchange taking place over the shoal. This is not consistent with our assumption of an impermeable barrier, and consequently this model is discarded.

Certain known phenomena occurring in Massachusetts Bay contribute to some of the differences seen between the analytical results and field data. One of these is the body of water contained within the area surrounding Boston Harbor. This is a relatively shallow basin that most surely influences the hydrodynamics of the Bay, especially since it is the discharge point for three rivers in the Boston area. Additionally, the Cape Cod Canal, which forms an artery between Massachusetts Bay and Buzzards Bay 15 NM to the southwest, has a strong

effect on η as can be seen in Figure 3-A. A 0.5 foot discrepancy exists between the model results and the observed tidal height at the entrance to the Canal. Obviously, the fact that a phase lag of approximately 2.5 hours between the two Bays contributes to this discrepancy. These features should of course be simulated in a more sophisticated model.

In spite of the many assumptions involved, the one layer model seems quite representative of the physical situation observed in Massachusetts Bay as was seen from the results presented in Section 3.1.1. Comparison of the analytical results with tide data especially demonstrates the predictability of the model with a fully open channel between x_1 and x_2 . Although the surface profile given by the four increment channel in Figure 3-D better satisfies the imposed boundary conditions than that given by the one increment situation in Figure 3-B, the goodness of one variation over the other, when compared to field information, is difficult to assess. The tidal velocities given by the model are less reliable than the surface elevations but may produce an overview of the current field that can be expected in the Bay. Thus, keeping the desired simplicity of the model in mind, we conclude that results of the one layer model, with just one opening considered in its entirety, gives a reasonable description of the tidal motion in Massachusetts Bay.

CHAPTER IV

RESULTS OF THE TWO LAYER MODEL

The two layer analytical model, as mentioned previously, was developed in response to the physical characteristics encountered in Massachusetts Bay during the spring, summer, and fall. Oceanographic observations since 1925 at the Boston Lightship, as reported by the U. S. Department of the Interior (1959), show that the thermocline generally forms in May and overturns in September and October. Thus, stratification due to the variation in both temperature and salinity prevails for approximately six months out of the year.

Although the thermocline is quite variable in depth, historical data taken at Boston Lightship locates the average depth of the interface 30 feet below the surface. Water depth at the Lightship, which is approximately six nautical miles east of the entrance to Boston Harbor, is 100 feet at mean low water. (It should be noted that the Lightship, not to be confused with Boston Light, was moved to a new location on July 1, 1973. All references to Boston Lightship in this report are for its previous position of 42°20.4' N, 70°45.5' W).

4.1 Computational Considerations

4.1.1 Results of the Two Layer Model

The stratified case was developed as a simple model with the capability of determining velocities and elevations in both layers. Derivation of the governing equations for the stratified model parallels the theoretical development of the one layer model such

that the solutions for all velocities and the interface elevation η_1 are specified in terms of the surface elevation η_2 .

The general solution for η_2 , given by Equation (2.30), is a function of the constants A_n and B_n and it can be shown that A_0 essentially governs the surface profile while the motion of the interface is governed essentially by B_0 . By setting B_0 equal to zero, in Equation (2.30), η_2 takes the form:

$$\begin{aligned} \eta_2 = & A_0 \cos m_0 y + \sum_{n=1}^{\infty} A_n \cos k_n x \cosh m_{n1} y \\ & + \sum_{n=1}^{N-1} B_n \cos k_n x \cosh m_{n2} y + \sum_{n=N}^{\infty} B_n \cos k_n x \cosh m_{n2} y \end{aligned} \quad (4.1)$$

and it can be shown by calculation that the summation of the terms containing B_n for $n > 0$ is small compared to the summation of the terms containing A_n 's.

The solution for B_0 equal to zero shows that η_2 closely approximates the solution for η in the one layer model. Thus, we identify the constant A_0 as the one essentially governing the surface elevations whereas the value of the constant B_0 is reflected in the interface elevations.

The procedure for solving for the constants A_0 and B_0 contained in the general solution for η_2 , Equation (2.30), is discussed in Chapter II and is similar to the method for determining A_0 in the one layer model. For the stratified case, both a surface amplitude relative to mean sea level (MSL) and an interfacial amplitude

relative to the mean interfacial level must be specified at some point within the Bay. Alternatively, current velocities could be specified in each of the two layers although, as explained in the preceeding chapter, this data is often difficult to interpret from current records. With information on the surface and interface the two constants can be determined either through an iterative process or directly by rearrangement of the equations given representatively by (2.35A) and (2.35B).

Oceanographic data in the form of vertical profiles of temperature and salinity in Massachusetts Bay have been taken by various agencies and institutions. Unfortunately it is difficult to determine, with any degree of accuracy, the amplitude of the interface for a given location as the variation of temperature representing the thermocline is not discrete but varies rapidly in the vertical direction over a distance of as much as ten feet. As a result, unlike the information on the surface profile which is fairly well documented, the amplitude of the interface was specified arbitrarily at a certain location to allow for the determination of the two constants in Equation (2.30). Choosing the coordinates of $x = 10.0$ NM, $y = 5.0$ NM, the surface elevation, from the results of the one layer model, has been found to be of the order 4.5 feet. It is reasonable to assume that, for an h_2 of 20 feet, the amplitude of the interface is approximately $5/6$ the amplitude of the surface wave. Consequently, η_1 was chosen as 3.5 feet at this location.

With this information, the constants A_0 and B_0 can be computed for the two layer model. Through the solutions for the velocities and elevations given in the theoretical development, the surface and interfacial profiles and currents can be computed for Massachusetts Bay. The geometry of the stratified model is the same as that assumed for the one layer case where $x_1 = 0.0$ NM and $x_2 = 41.0$ NM. Results of the one layer model indicate that the fully open channel with no constrictions gave a fair representation of the physical situation and consequently only this configuration will be considered for the two layer model.

The solutions for the amplitude and velocities, as in the one layer model, contain summations for $n = 1$ to ∞ . Although convergence in this model was obtained by $n = 50$, the large number of computations required that the equations be solved on the IBM 370/155 computer located at M.I.T. A listing of this computer program, written in Fortran, can be found in Appendix A.

Results of the two layer analytical model can now be determined for a particular situation similar to that frequently found in Massachusetts Bay. Taken from actual field observations, the following parameters were first specified as input into the model. $h_1 = 100$ feet, $h_2 = 20$ feet, $\rho_1 = 1.02558$ g/cm³, $\rho_2 = 1.02250$ g/cm³. By additionally setting $\eta_1 = 3.5$ feet and $\eta_2 = 4.5$ feet at $x = 10.0$ NM, $y = 5.0$ NM, the interface and surface amplitudes can be computed by respectively Equations (2.23) and (2.30) with the resulting profiles shown in Figure 4-A. It can be seen that the surface profile is quite

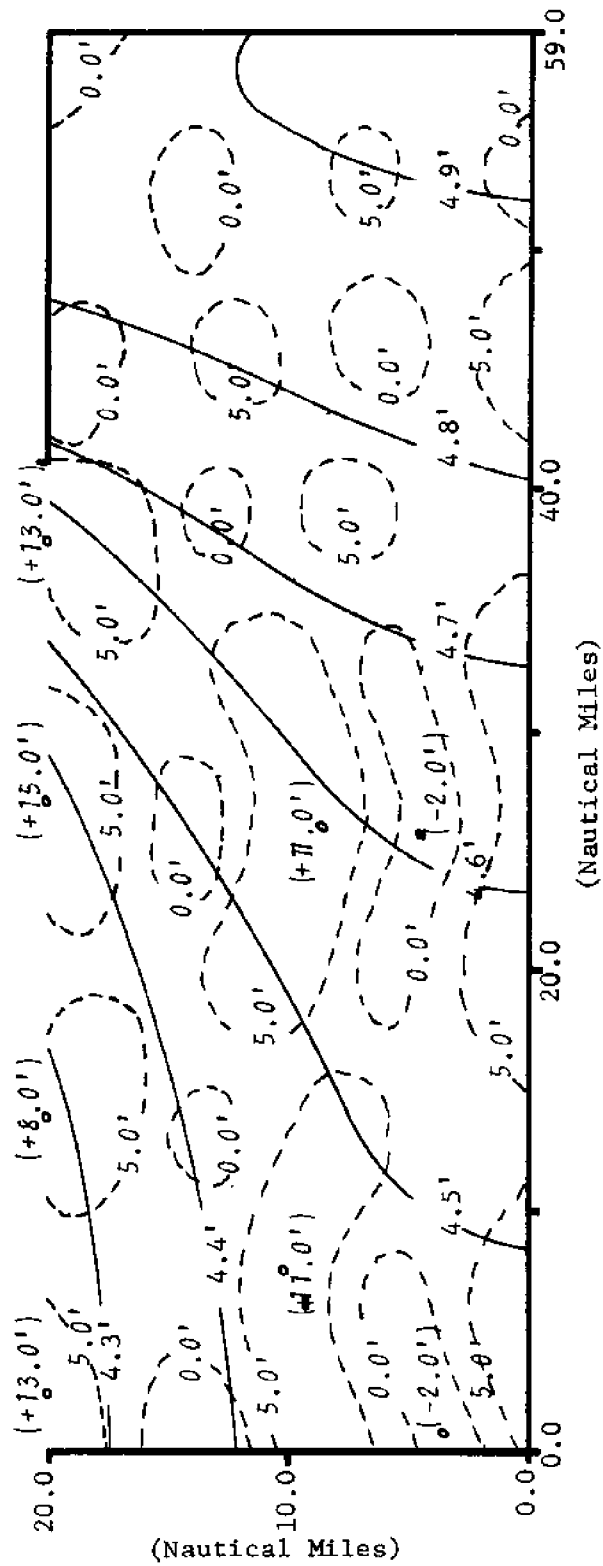


Figure 4-A: Two Layer Model of Massachusetts Bay at High Tide. Amplitudes Measured in Feet.

Surface Profile, η_2 ———
 Interfacial Profile, η_1 - - - - -
 $h_2 = 20.0 \text{ Ft.}, \rho_2 = 1.02250 \text{ g/cm}^3$
 $h_1 = 100.0 \text{ Ft.}, \rho_1 = 1.02558 \text{ g/cm}^3$

similar to that given by the one layer model (Figure 3-B) with the same geometrical configuration. Although the surface amplitude of 4.5 feet is specified at a slightly different location than in the one layer situation, the surface slope compares favorably with the model results and observational data previously presented. The surface profiles were smoothed slightly as small perturbations occurring in the contour lines were neglected.

From Figure 4-A it can be seen that the interfacial profile predicted for the two layer model exhibits some rather interesting and unusual results. Measured relative to the mean interfacial level, h_1 , this particular model shows the interface oscillating vertically from - 2.0 feet to + 15.0 feet with a wave length of the order 11.0 nautical miles. Since the solution for η_1 is periodic, the model resultingly predicts a standing wave which, at high tide, rises to within 10 feet of the free surface.

Velocities for this particular case are shown in Figure 4-B. The velocities are specified in terms of x and y derivatives of η_2 and consequently the surface profile determines the magnitude and direction of both U_1 and U_2 . By the nature of the equations for u_2 and v_2 , given respectively by Equations (2.22A) and (2.22B), the currents predicted in the upper layer are always perpendicular to the lines of constant surface amplitude with the velocity a function of the existing surface slope. The currents in the lower layer are specified as a function of both the first and third derivatives of η_2 . It will be noticed that the magnitude of U_1 is greater than that

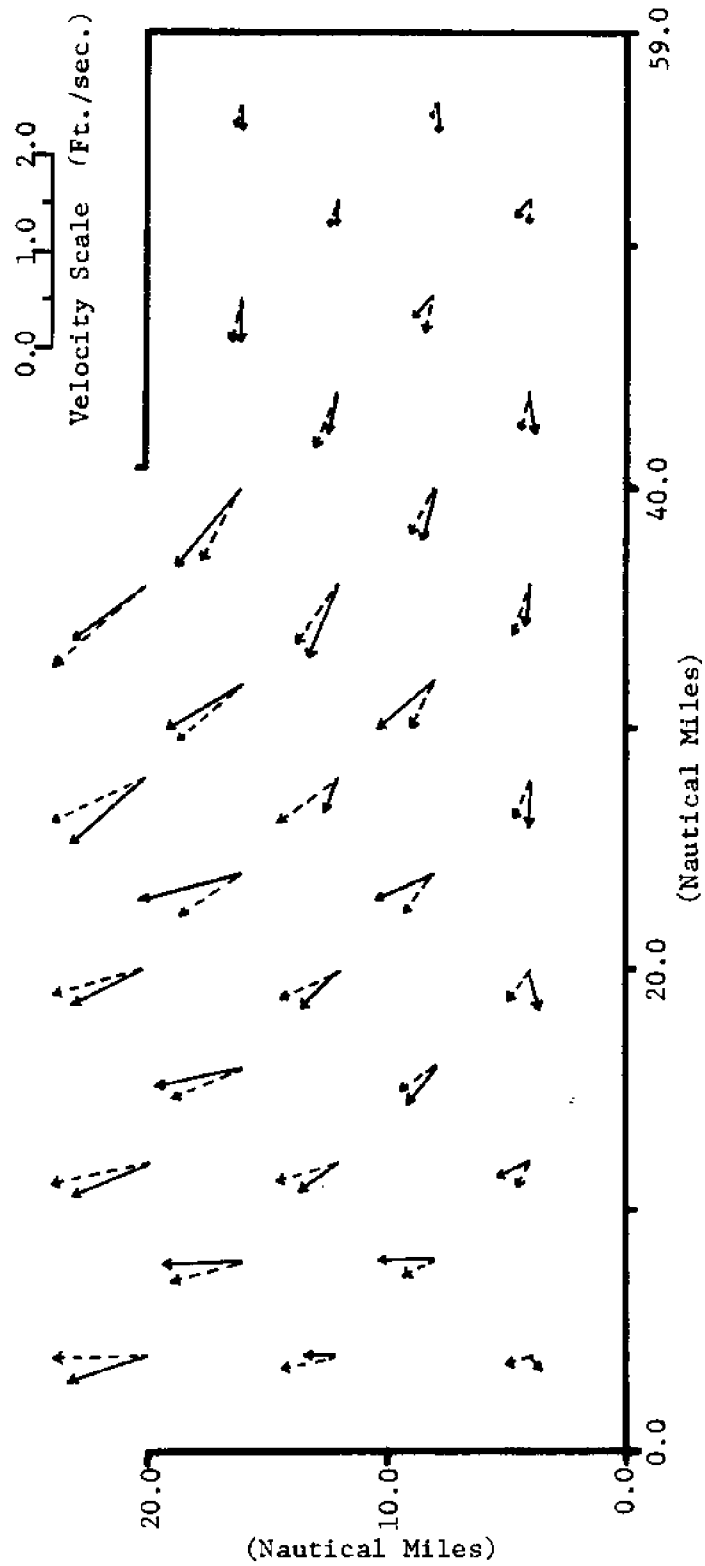


Figure 4-B: Two Layer Model of Massachusetts Bay.
Velocities at Maximum Ebb in Ft./sec.

U_2 (Upper Layer) ———

U_1 (Lower Layer) - - - - -

$h_2 = 20.0$ Ft., $\rho_2 = 1.02250 \text{ g/cm}^3$

$h_1 = 100.0$ Ft., $\rho_1 = 1.02558 \text{ g/cm}^3$

of U_2 at some positions in the model; at other locations the reverse is true. Of greater importance is the prediction that the directions of the currents in the two layers do not coincide.

The two layer analytical model was changed slightly and the amplitudes and velocities were computed for a second set of circumstances. The geometrical configuration remained the same; however, the difference in density between the two layers was increased slightly from the 0.3 per cent, given in the first set of results, to 0.5 per cent. The new densities were specified as $\rho_1 = 1.0050 \text{ g/cm}^3$ and $\rho_2 = 1.000 \text{ g/cm}^3$. In addition, the depth of the interface was increased by 20 feet such that $h_1 = 80.0$ feet and $h_2 = 40.0$ feet. The surface and the interfacial amplitudes were again specified at $x = 10.0 \text{ NM}$, $y = 5.0 \text{ NM}$ under the same set of assumptions as discussed earlier. Thus, again by setting $\eta_2 = 4.5$ feet it is reasonable to assume the amplitude of the interface as $(\frac{h_1}{h_1+h_2})\eta_2$ or 3.0 feet. For these conditions the stratified model was again solved for the area of Massachusetts Bay.

The surface and interfacial profiles for this model are shown in Figure 4-C. Obviously, much more activity exists here than in the previously discussed case. The surface profile, in this extreme case, reflects the influence of the interfacial waves. Close examination of the results of Figure 4-C as compared with Figure 3-B reveal the fact that the surface is lower, relatively, over an interfacial crest and higher over an interfacial trough. This serves to demonstrate the dependence of η_1 on η_2 as discussed in the theoretical

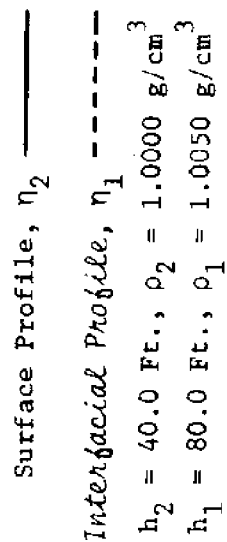


Figure 4-C: Two Layer Model of Massachusetts Bay at High Tide. Amplitudes Measured in Feet.

development of the two layer model. The interface exhibits some exceedingly large waves with a height of the order 50 feet and a wave length of approximately 24.0 NM.

The velocities in the upper and lower layer for this particular situation are given in Figure 4-D. Of primary importance in the results is the fact that, with large vertical displacements of the interface, currents in the two layers are quite variable and, at some positions, almost opposing each other. The currents in the vicinity of the boundaries are also unusual by the fact that, at some locations, on the ebbing (outgoing) tide, which is shown, they flow towards the walls and away from the channel opening in the upper layer. Resultingly, the interface and surface profiles and speed and direction of the currents are extremely variable and physically difficult to determine since the various parameters appear to be quite sensitive to position. This is in qualitative agreement with available field observations to be presented later in this chapter, which indicate that, to a degree, this condition persists.

4.1.2 Model Sensitivity

The two layer analytical model was computed for a number of geometrical configurations and physical conditions in an attempt to check the sensitivity of the solution. As seen by the amplitudes and velocities predicted for the two cases just discussed, the model is very sensitive to changes in the interfacial depth and /or changes in density. Consequently, an attempt to quantify the importance of these and other variables has been completed through a sensitivity analysis. The results are presented herein.

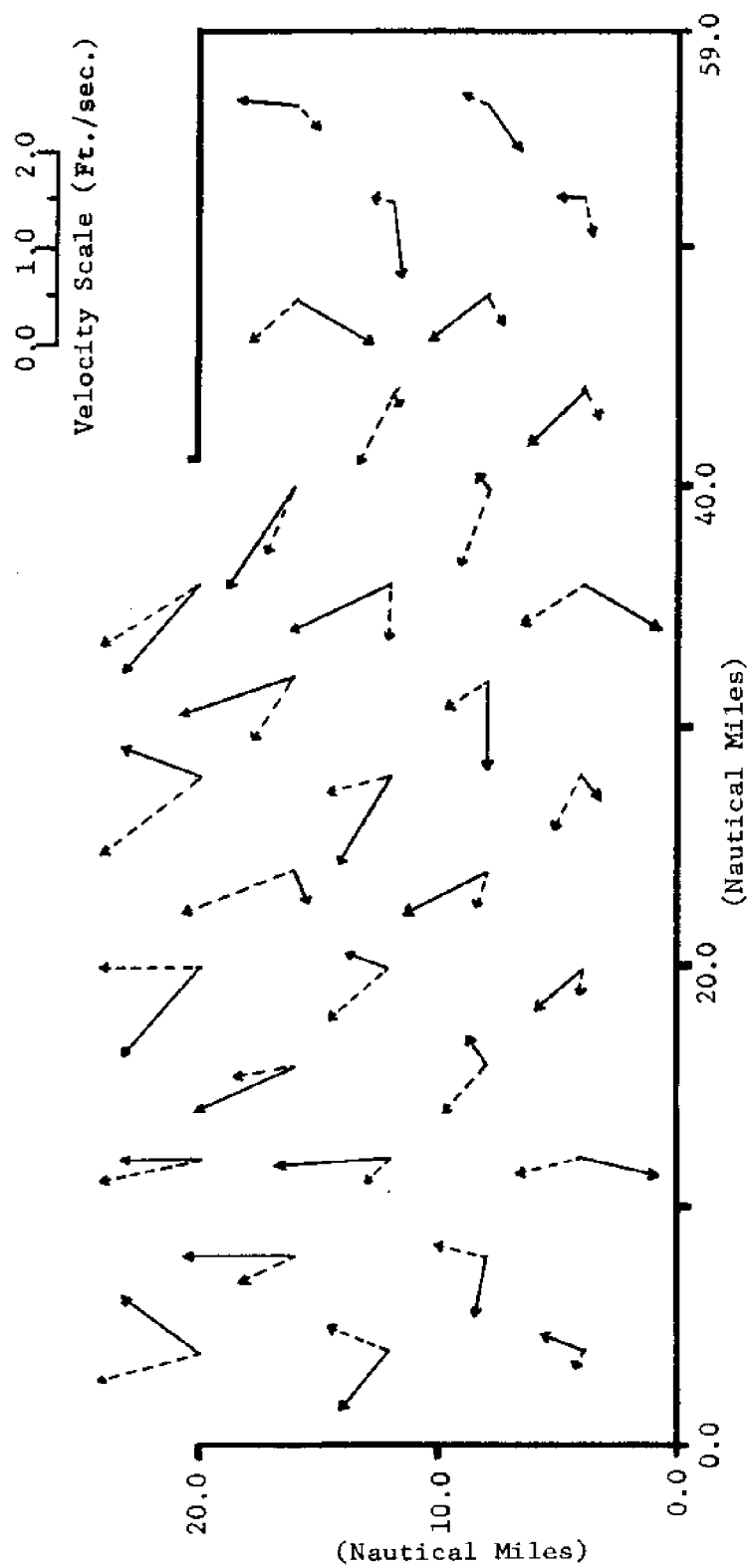


Figure 4-D: Two Layer Model of Massachusetts Bay.
Velocities at Maximum Ebb in Ft./sec.

U_2 (Upper Layer) ———
 U_1 (Lower Layer) - - - - -
 $h_2 = 40.0$ Ft., $\rho_2 = 1.0000$ g/cm³
 $h_1 = 80.0$ Ft., $\rho_1 = 1.0050$ g/cm³

The two constants A_0 and B_0 that were required in the general solution for η_2 shall be first discussed. As pointed out in Section 4.1.1, the constants are generally determined through the application of field data prior to their introduction into Equation (2.30). Also noted was the fact that the value of A_0 primarily governs the surface profile, η_2 , while the value of B_0 is the determining factor in the shape of the interface, η_1 . In checking the sensitivity of the two, it was found that by varying the constant A_0 the surface and interface reacted by the same order of magnitude while a small change in the constant B_0 brought almost no change to the surface profile although creating interfacial disturbances of significantly different magnitudes. Thus, it can be concluded that, in determining the value of B_0 , the initial conditions specified for the interface must be chosen carefully and as precisely as possible. The following clearly demonstrates the situation and the sensitivity of the interface to B_0 :

Constant Conditions:		$h_1 = 80.0 \text{ ft.}$	$\rho_1 = 1.0050 \text{ g/cm}^3$	
		$h_2 = 40.0 \text{ ft.}$	$\rho_2 = 1.0000 \text{ g/cm}^3$	
Specified Elevations @ $x = 10.0 \text{ NM}$, $y = 5.0 \text{ NM}$		Resulting Constants		Maximum Interfacial Wave Height
$\eta_1(\text{ft.})$	$\eta_2(\text{ft.})$	A_o	B_o	$H_1(\text{ft.})$
3.0	4.5	4.684	-0.00790	50
3.5	4.5	4.685	-0.00491	28
4.32	4.5	4.670	0.0	7

Table 4-1: Sensitivity of B_0 to the Choice of Interfacial Amplitude

As a consequence of the large interfacial variations shown in the results of the two layer model and in view of the above information concerning the constants A_0 and B_0 , it is apparent that the model is very sensitive to the location at which η_1 is initially specified. In the two cases presented for the two layer model, both the surface and interfacial amplitude were specified at the coordinates $x = 10.0$ NM, $y = 5.0$ NM. From Figure 4-A and Figure 4-C it can be seen that this position is approximately mid-way between the trough and the crest of the interfacial standing wave. Obviously then small changes in the interfacial wave amplitude at this point will force the solution for η_1 to predict relatively large vertical displacements in the areas of the troughs and crests. Clearly, the solution to this problem is to first determine, for a particular set of conditions, the locations of the 'highs' and the 'lows' of the interfacial waves. This information can be used in the choice of location where the value of η_1 and η_2 should be measured in order to give the best possible resolution such that the model will give reasonable results and an interfacial wave the least sensitive to errors in the measurements.

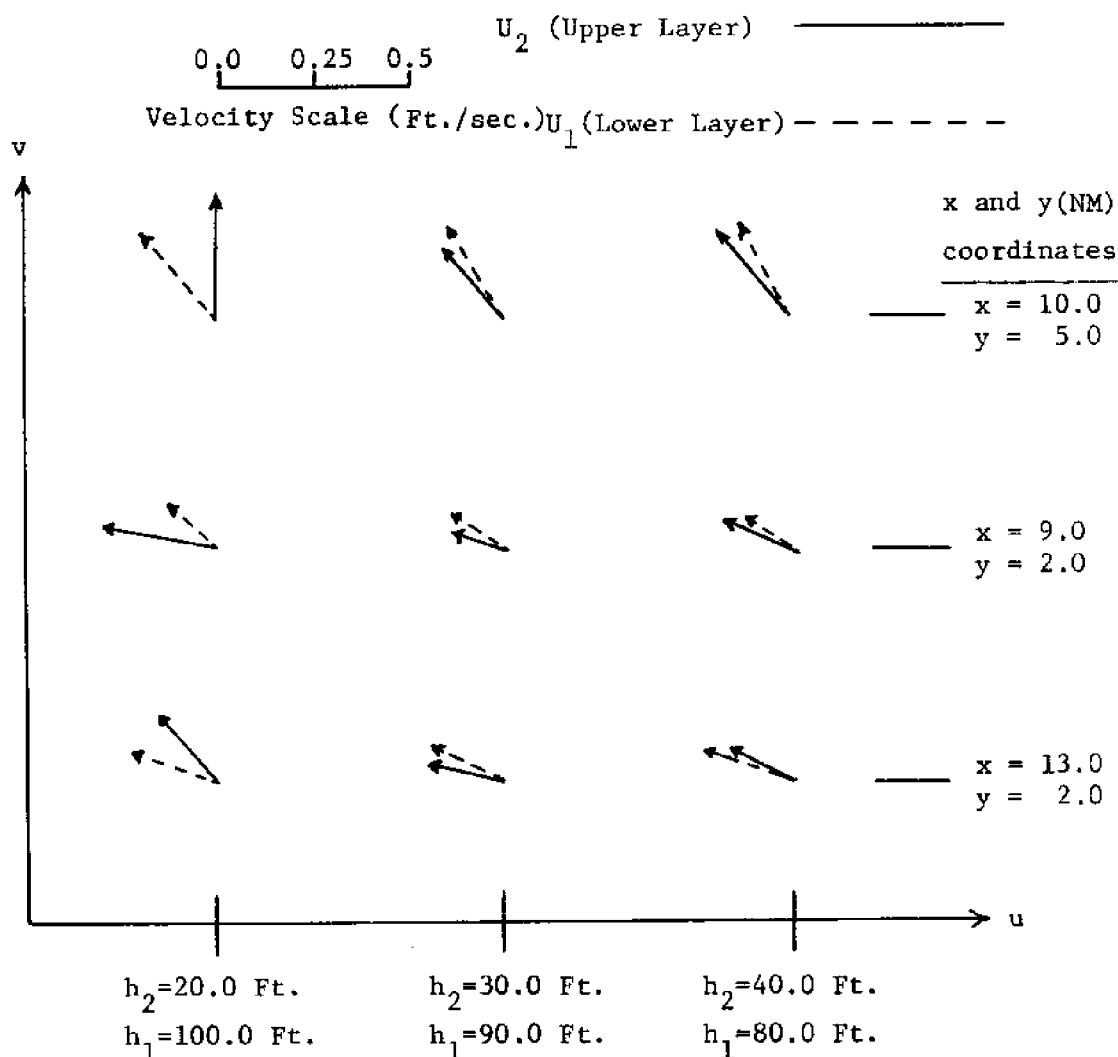
Variation of the geometrical configuration, especially that of the length scale, was an additional criteria which could produce changes in the results. The average length, x_0 , of the Bay was assumed to be of the order 59.0 NM and all the results presented were computed on this basis. To assure that the solution was not sensitive or that no unusual conditions existed in the particular

configuration, the two layer analytical model was run for a number of different lengths. The most important aspect of this analysis was that the results generally indicated that the amplitude and length would be of the same order of magnitude and that, for all practical purposes, a small change in the value of x_0 would produce no unusual results.

Results of density variations have already been indicated by the two cases discussed in Section 4.1.1. The sensitivity of the solution to changes in density are quite pronounced again affecting primarily the profile of the interface. As previously mentioned, the average difference in density found in Massachusetts Bay between the upper and lower layer during stratification is of the order 0.3 per cent. That condition was presented by Figures 4-A and 4-B with the second set of results, Figures 4-C and 4-D, showing $\Delta\rho$ of the extreme value of 0.5 per cent. Differences between the two sets of results cannot be attributed only to the change in $\Delta\rho$ since some influence is possible due to the variation of h_1 and h_2 .

The last set of parameters which merit discussion are the values of h_1 and h_2 . With h_1 representing the thickness of the lower layer and h_2 the thickness of the upper layer, the sum of the two was always equal to 120 feet, the average depth of Massachusetts Bay. Sensitivity of the solution to variations in h_1 and h_2 was checked in a number of cases with the result that by increasing the value of h_1 the interfacial amplitude decreased as did the interfacial wave length.

From (2.20B) it is clear that the influence of changing $\Delta\rho$ and the relative magnitude of h_1 and h_2 are related, in that they combine to give the wave number m_{n_2} . To illustrate the variations with the various parameters, the velocities at selected points are presented in Figure 4-E.



Values of other parameters.

At x=10.0, y=5.0
 $\eta_1=3.5$ Ft., $\eta_2=4.5$ Ft.

$\rho_1=1.02558$ g/cm³
 $\rho_2=1.02250$ g/cm³

Figure 4-E: Velocity Variations as a Function of h_1 and h_2

Most of the discussion concerning the sensitivity of the model to various parameters has been discussed in terms of the changes occurring in the interface. However, the surface profile and velocities in the two layers also exhibit variation as shown in Figure 4-E, although relatively minor, when changes occur in the geometry or in the specified conditions. By far though the most significant example of sensitivity in the model is exhibited by the interface and its reaction to variation of the input parameters.

4.2 Available Data for Comparison

Results of the two layer analytical model can be compared with available field observations for the Massachusetts Bay area. The field data consists mainly of information on the surface profile, temporal and spatial measurements of the temperature and salinity structure, and current drogue measurements. A large number of oceanographic observations have been collected in the Bay by various agencies and institutions during the summer months and the data presented here gives a good overview of the condition present during stratification.

Data compiled in the National Ocean Survey Tide Tables (1973) is used for a comparison with the surface amplitude predicted by the two layer model. This information is taken from observational records at various locations around the Bay perimeter as shown in Figure 3-A.

The vertical structure of temperature over the water column has been one of the most widely studied oceanographic phenomena for

many decades. Temperature observations at Boston Lightship have been taken on a daily basis since 1925 and have afforded many insights into the thermal conditions in Massachusetts Bay. Thus far, the level of the interface has been generally considered a function of the thermocline although this is not strictly true since the variation of salinity also affects the density of sea water. Consequently, with the advent of the newer oceanographic instrumentation, in particular the CTD (Conductivity, Temperature, and Depth), salinity along with temperature can be determined allowing the calculation of a true density profile for each station recorded. Although the thermocline and density gradient normally coincide, neither is discrete but occur as a gradual variation over relatively large vertical distances. Hence, it is difficult to determine, with any precision, the exact depth of the interface and to detect small perturbations that may occur at this level.

As an example of this problem, a sample C.T.D. cast, taken in the vicinity of Boston Lightship, is shown in Figure 4-F. Fortunately though the model predicts relatively large vertical variations of η_1 and consequently the data presented herein will attempt to verify, qualitatively, some of the conditions that may exist.

Oceanographic observations from a buoy located in Stellwagen Basin, approximately 5.5 NM west of Stellwagen Bank, were taken by Halpern in July and August, 1966. Vertical observations of temperature were collected at the position $42^{\circ}16.5'$ N, $70^{\circ}24.5'$ W for a total of 5 days with the result that the temporal variation of the thermocline

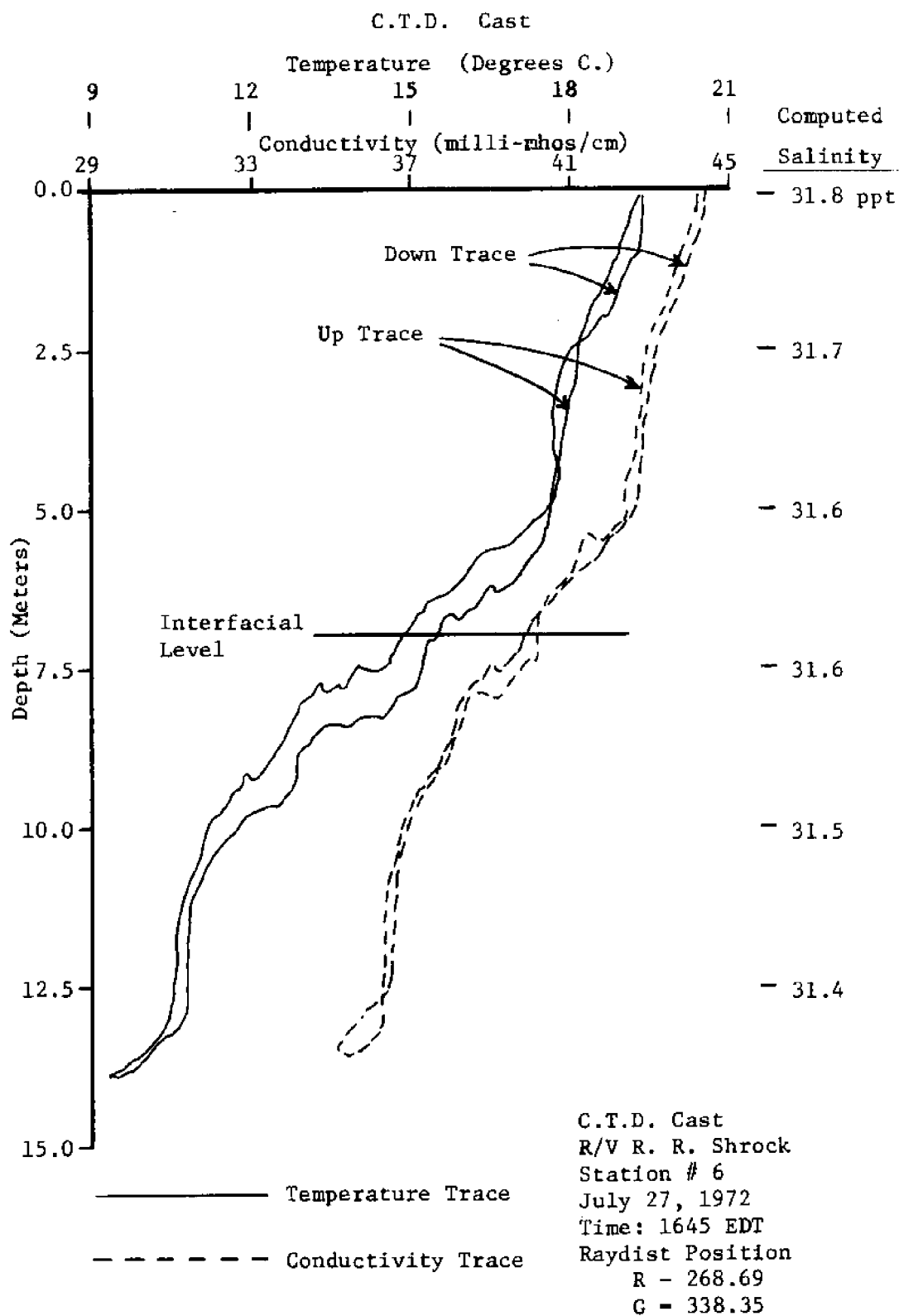


Figure 4-F: C.T.D. Cast Taken in Massachusetts Bay

was well documented at this point of space for a period of time. Halpern reported his observations in a paper on the short-period internal waves in Massachusetts Bay (Halpern, 1971a) and again in a discussion of semidurnal internal tides in Massachusetts Bay (Halpern, 1971b). Concerned primarily with the vertical movement of the thermocline, no information on salinity was obtained and consequently temperature measurements will serve as the primary indicator for the degree and depth of stratification.

Halpern's data locates the average depth of the thermocline approximately 40 feet below the surface with a semidurnal variation of temperature at this depth of approximately 11°F. The most interesting information concerns the vertical displacement of the thermocline, or for our purpose, the interface, with the result that the amplitude of the interfacial wave is of the order 15 feet. Clearly, this is of great interest since the model predicts a periodic motion of a similar magnitude. Although the motion of the interface, from Halpern's observations, is not a purely sinusoidal function, the possibility exists that this is the result of non-linear effects associated with water spilling over Stellwagen Bank on the flooding tide which are also responsible for generation of short period internal waves. However, for our purposes, the information serves to qualitatively confirm some of the predictions given by the two layer model.

A second set of measurements, spatial in nature, are presented to further verify the motion of the interface. In particular,

oceanographic observations, using the C.T.D., have been taken by M.I.T. under the Massachusetts Bay Sea Grant Program. This data has been collected aboard the research vessels R.R. Shrock and Walter E. Phipps allowing a quick on-board determination of the temperature and salinity structure at each station. Almost 20 of these C.T.D. profiles were taken in the Bay on a chemistry cruise conducted on July 25 and 26, 1973. Resultingly, the depth of the interface was determined at a number of locations approximately 5.0 NM apart. The observations used for comparison, although not entirely synoptic, were taken as close to the time predicted for low tide as possible in order to reduce the effects of periodic motion. The 45°F isotherm was used for the depth of the thermocline since it was the temperature at which the largest density gradient occurred. Using this temperature as the indicator for the interface, the results of three of these C.T.D. stations are presented.

C.T.D. Stations - July 26, 1973
Low Tide (NOS Tide Tables) 1432 EDT

Station Number	Time (EDT)	Position Lat. & Long.	x & y (NM) Coordinates	Water Depth (Ft.)	Depth (Ft.) of 45°F Isotherm
14	1300	42°05.8' N 70°31.3' W	x = 32.0 y = 6.0	135	27
15	1340	42°09.8' N 70°31.2' W	x = 28.0 y = 8.0	146	43
16	1430	42°14.0' N 70°37.0' W	x = 22.0 y = 6.0	103	26

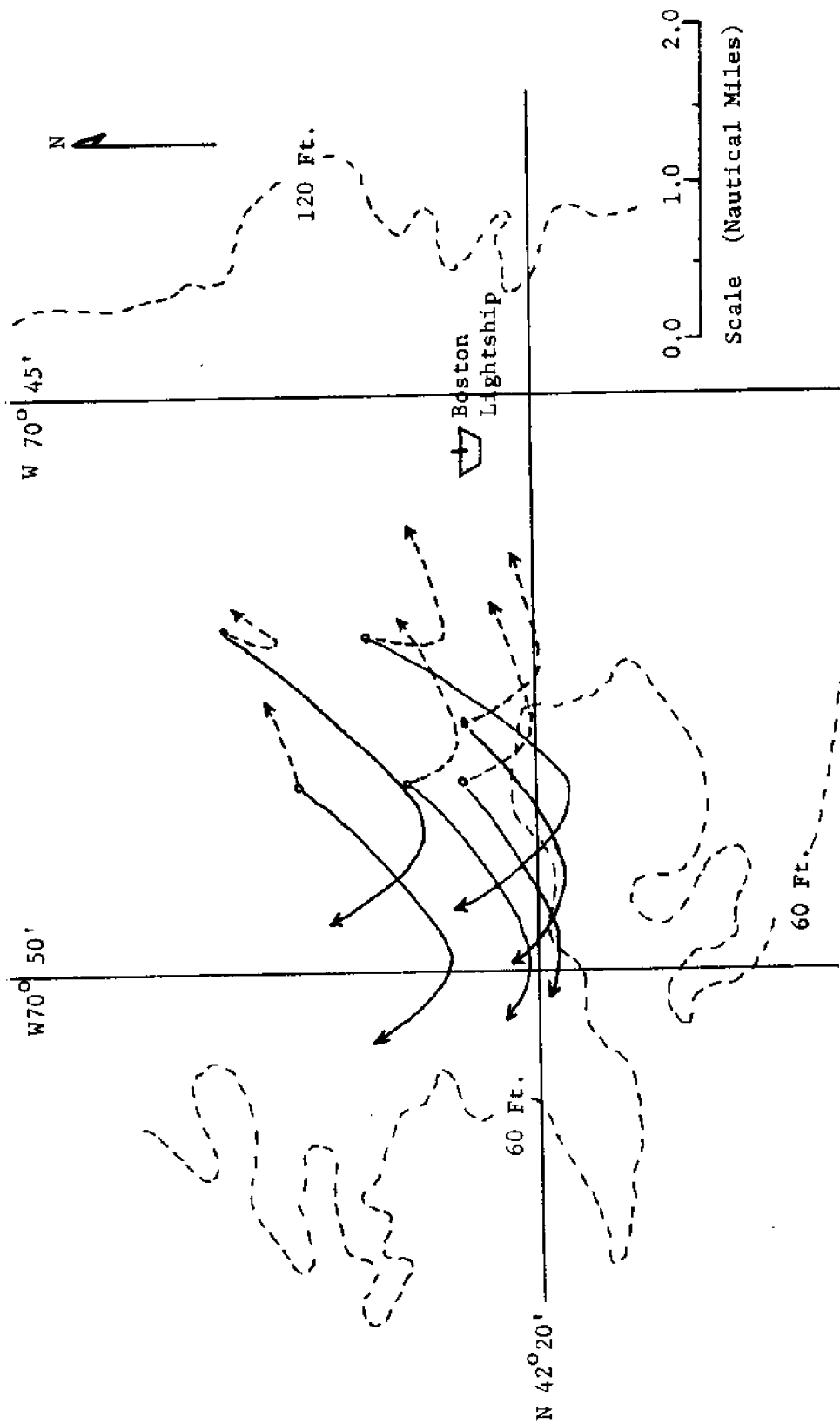
Table 4-2: Observed Spatial Variation in Depth
of Interface below the Surface

These stations, located along the western side of Massachusetts Bay close to the 120 foot contour, point to the fact that vertical variations of the order 17.0 feet occur in the interface over a horizontal distance of approximately 5.0 NM. Obviously this information supports the fact that relatively large interfacial waves can be found in the Bay as predicted by the two layer model and shown in Figure 4-A and 4-C.

Information on the currents in Massachusetts Bay, occurring during stratification, has also been collected by M.I.T. These studies were generally completed through the use of drogues or drifters that employed a large subsurface vane set at a preselected depth and suspended from a relatively small surface float. During stratification, the depth of the vanes was normally determined as a function of the level of the interface with one set of vanes placed in the upper layer and a second set in the lower layer. By following the path of the surface floats the speed and direction of the currents could be computed for the two depths. With this information some idea of the velocity profile could be determined as well as the variability in speed and direction of the two layers.

One such current study was conducted on July 27, 1972 aboard the M.I.T. research vessel R.R. Shrock. Through the C.T.D. casts taken on this cruise, one of which is shown in Figure 4-F, the depth of the thermocline was estimated at approximately 20.0 feet. Average densities for the two layers were computed from the temperature and salinity information with the result that $\rho_1 \approx 1.02558 \text{ g/cm}^3$ and $\rho_2 \approx 1.02250 \text{ g/cm}^3$. It should be noted that these were the conditions

specified in the two layer model shown by Figures 4-A and 4-B. Results of this current drogue study are given in Figure 4-G and it can be seen that the drogue depths were selected so as to be representative of the conditions existing in the two layers. Shown are the directions and velocities of the currents for a seven hour duration taken during an ebbing tide from high to low water. It can be seen that for approximately half of the duration the drogues in the upper layer proceeded southwesterly while those in layer one moved more in a southerly direction and at a slower velocity. During this time the Bay was considered to be in a steady state condition since a 5 to 10 knot wind had been blowing from the northeast for the past 18 hours. However, at approximately the mid-point of the observations, the wind shifted to the southeast 5 to 10 knots and continued in that direction for the remainder of the day. At this time it can be seen that the drogues changed direction such that the surface layer reacted directly to the wind stress. The lower layer apparently also reacted by moving in a northeasterly direction which is to be expected if the interface was forced down as a result of the thickness of the surface layer increasing due to the wind setup. It is the steady state condition for which model predictions of the currents in the two layers can be made. Consequently it is the first half of the drogue observations that is of interest for comparison with the model results as will be discussed in the next section. However, the results point out the great importance of wind driven currents. The last field data to be considered will be



Drogue Depth, 6.5 Ft. _____
 Drogue Depth, 33.0 Ft. -----
 Interface Depth ≈ 20 Ft.

Figure 4-G: Current Drogue Study of Massachusetts Bay, July 27, 1972. Ebbing Tidal Cycle. Average Velocity Upper Layer ≈ 0.35 Knots. Average Velocity Lower Layer ≈ 0.20 Knots.

that taken during a second drogue study conducted for M.I.T. on July 31, 1972. Although the C.T.D. was inoperable this particular day, it can be assumed that approximately the same density conditions and interfacial depth exist as were recorded from the study completed on July 27. Again the Bay can be assumed in steady state since the wind, for the past 18 hours, was generally from the south at 5 to 10 knots. Only a slight wind shift to the southwest was observed during the drogue observations and this was considered to have a negligible effect on the currents.

Results of this study are shown in Figure 4-H where the observations were taken from low to high tide during the flooding situation. Although the currents in the lower layer maintained a relatively constant speed and direction, the upper layer revealed a slow change in direction swinging from almost east to around to south-southwest. The important consideration in these observations is that, for most of the time, there is an angular difference between the currents in the two layers. In addition, both drogue studies show that, it is indeed observed that, the currents in the upper layer can proceed in a direction quite different from that normally expected during either a flooding or ebbing tide if only a one layer model is considered.

4.3 Discussion of the Model Results

The need to include the effect of a two layer model has been seen by the conditions existing in Massachusetts Bay during the summer months. The results of this model have been shown and can now

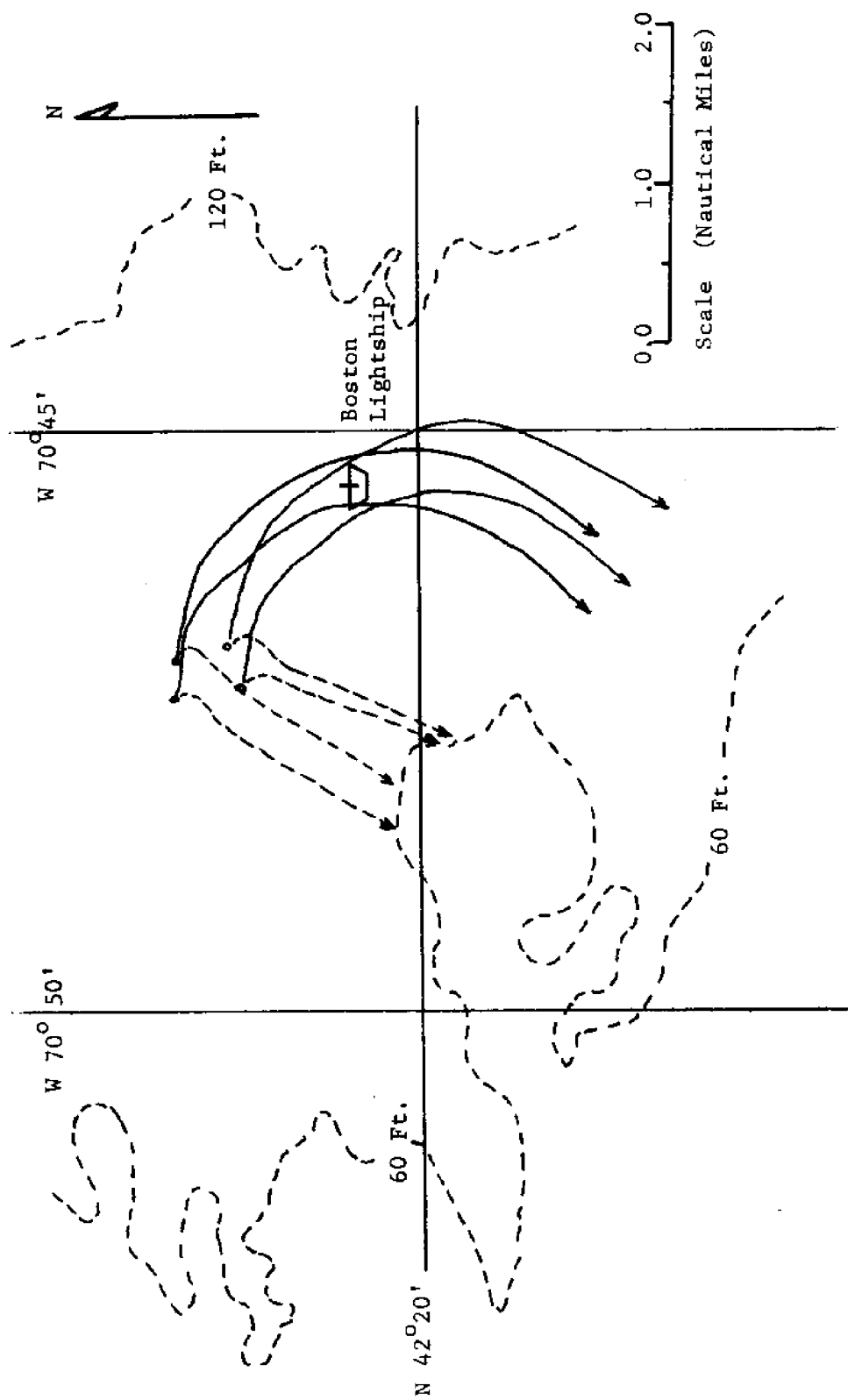


Figure 4-H: Current Drogue Study of Massachusetts Bay, July 31, 1972.
 Flooding Tidal Cycle.
 Average Velocity Upper Layer $\approx .55$ Knots
 Average Velocity Lower Layer $\approx .25$ Knots

Drogue Depth, 6.5 Ft. ———
 Drogue Depth, 33.0 Ft. - - - - -
 Interfacial Depth ≈ 20 Ft.

be compared with field observations of both currents and elevations. However, the comparisons will generally show agreement only in a qualitative sense since the interface separating the two layers in the Bay is rarely well defined and generally can only be determined within certain limits. This uncertainty is reflected in our arbitrary choice of specifying the interfacial amplitude at $x = 10$ NM, $y = 5$ NM. Consequently the comparisons will be qualitative in nature but will serve to demonstrate the ability of the two layer model to explain some of the conditions that have been observed in Massachusetts Bay.

The results of the surface and interfacial profiles will be compared first with the available field data. Similar to the profile for η given in the one layer model for a fully open channel, Figure 3-B, the surface profile shown in Figure 4-A compares quite closely with the observed tidal amplitudes around the Bay. The surface profile given in Figure 4-C does not, in the details, compare as well with the results of the one layer model presented in Figure 3-B. Thus, the large interfacial waves result in a significant variation in the surface contours. This large difference in surface contours is, however, not of great significance when considering the fact that the contours are drawn for intervals of 0.1 feet. Thus, in terms of actual surface elevation, the predictions are not drastically different between the one and two layer models.

The interfacial profile, given by the solution for η_1 exhibits the most dramatic and somewhat unexpected characteristics. The

results shown in Figures 4-A and 4-B are the amplitude and velocities predicted for the same densities and interfacial depth as observed in Massachusetts Bay during the current drogue study of July 27, 1972. Resultingly the predicted interfacial profile is considered to be fairly representative of the physical situation that could exist. However, due to instrument problems, only a limited number of C.T.D. casts were taken during the drogue study. Consequently, the model predictions will be compared with vertical observations taken by Halpern in Stellwagen Basin and by the M.I.T. C.T.D. stations of July, 1973.

The total vertical variation of the thermocline, as observed by Halpern, was of the order of 30 feet giving an interfacial amplitude of approximately 15 feet. Comparing this value with the results in Figure 4-A shows that the order of magnitude is certainly reasonable since the model also predicts an η_1 of 15 feet. In fact, considering the sensitivity of the model to changes in h_2 and without further knowledge of the conditions surrounding Halpern's data, the prediction for η_1 can actually be considered reasonably good.

The information obtained from the C.T.D. casts, taken by M.I.T. in July, 1973, verify the fact that interfacial waves exist in Massachusetts Bay. This data was synoptic in the sense that it was taken as close to low tide as possible when hopefully slack conditions existed. Unfortunately, the actual wave length, L_1 , of the interface could not be computed from the limited field data taken although the model predicts an L_1 of the order 11.0 NM as seen in

Figure 4-A. It should be mentioned that a similar condition has been noted and discussed by other investigators under the subject of internal waves. It is obvious that the interfacial waves, qualitatively, predicted by the two layer model, are evidenced both by Halpern's data and M.I.T.'s C.T.D. casts.

Currents predicted in the two layers can be compared directly with current drogue observations shown in Figures 4-G and 4-H. As previously mentioned, the first set of results presented for the stratified model are determined for the same conditions as observed in the field during the drogue studies. These results are presented in expanded form in Figure 4-I and show the variability that can be expected in the currents along the boundary in Massachusetts Bay. It is important to note that the two drogue studies were also completed close to the Boston Lightship and the western edge of the Bay in a location, as shown by the predicted results in Figure 4-I, where currents vary drastically with location and are predicted to flow shoreward during an ebbing tide and seaward during the flood in the upper layer. Although the model results do not predict the exact direction given by the drogues, due probably to the effects of Boston Harbor and the surrounding geometry in addition to the neglect of Coriolis force, it is obvious that the model shows that a large difference in current directions is possible during stratification in this area. This is in qualitative agreement with observations as shown in Figures 4-G and 4-H.

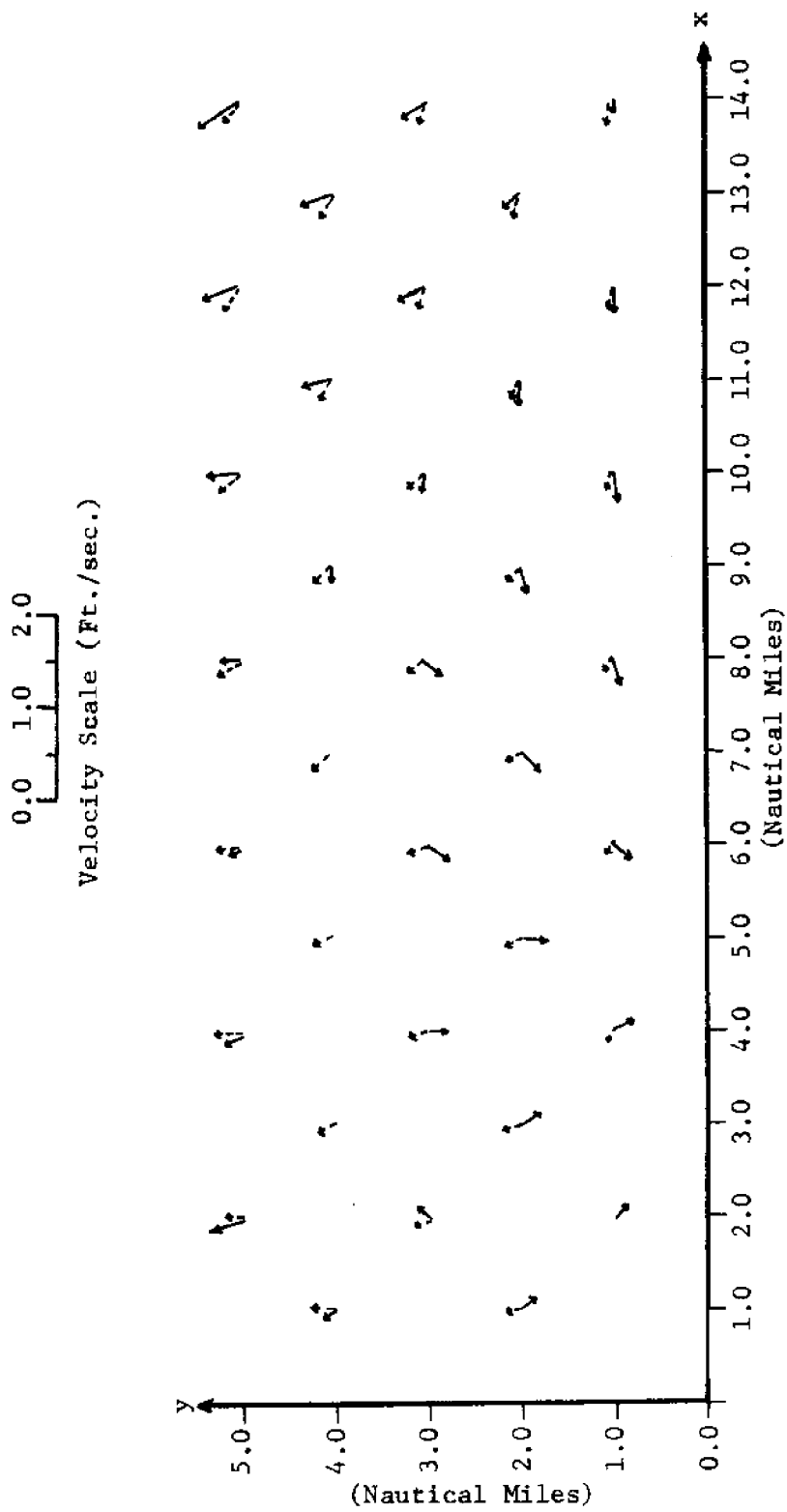


Figure 4-I: Two Layer Model of Massachusetts Bay.
Velocities at Maximum Ebb in Ft./sec.

$$h_2 = 20.0 \text{ Ft.}, \rho_2 = 1.02250 \text{ g/cm}^3$$

$$h_1 = 100.0 \text{ Ft.}, \rho_1 = 1.02558 \text{ g/cm}^3$$

In addition to showing an angular difference in the current direction in the two layers, it demonstrates the sensitivity of the observations to location, especially when close to the boundary. From the results of the two layer model shown in Figure 4-1, an angular change of up to 180° in the current direction in the upper layer can be observed over a distance of only a few miles in the Bay

CHAPTER V

CONCLUDING REMARKS

Two analytical models have been derived for a geometrical configuration similar to that of Massachusetts Bay. A simplistic approach was taken in the theoretical development of the models by depth averaging the linear long wave equations in two dimensions. By neglecting Coriolis force, bottom friction, and wind stress the models were able to represent the tidal circulation for both the uniformly well mixed and stratified case and to explain qualitatively some of the conditions encountered during field observations. Results of the two models were presented for a number of geometrical variations and physical conditions and compared with various types of field observations for verification of the model predictions.

The one layer model, representing the situation generally found during the winter, was discussed first and compared with tidal data and current observations. Comparison of the results of the model with tide gauge observations demonstrated the ability of the model to predict, quite closely, the surface profile for Massachusetts Bay. Velocities of the tidal currents also compared favorably with field data in a qualitative sense, and generally were the same order of magnitude. Current direction was the most difficult to verify as current meter records were often quite variable in this respect showing the effects of localized conditions.

Results of the two layer analytical model were considered more revealing in the sense that insight was gained into the conditions present during stratification. These results were compared with various types of field observations in an attempt to verify qualitatively the significance of using a two layer model to predict interface and surface profiles and currents. Reasonably good agreement was found when comparing the predicted surface profile with the observed tidal amplitudes. Differences between the predicted tidal amplitudes of the one layer model are minor and the differences between the two models and the observed tidal amplitudes can be attributed to the effects of Boston Harbor, the Cape Cod Canal, and the sloping bottom of the lower Bay.

Comparisons of the interfacial profile and current velocities predicted by the model with available field data are generally more qualitative since the physical conditions, especially the depth of the interface as well as the amplitude of the interfacial wave, that govern the solution cannot be determined very accurately. However, observations by both Halpern and M.I.T. verify the existence of interfacial waves and show the amplitude of the same order of magnitude as that predicted by the two layer model.

Currents predicted by the model were the most difficult to verify by field measurements since the physical observations clearly exhibit a high degree of variability over the tidal cycle. The drogue studies were apparently subject to variations due to relatively small changes in wind direction and, in the area surveyed, the observations are

probably affected by the flux in and out of Boston Harbor. In view of these existing conditions only a qualitative comparison can be made. This comparison however shows that the velocities predicted by the model are within the order of magnitude of those measured in Massachusetts Bay, also the observed curiosity of having shoreward current in the upper layer during an ebbing tide is made plausible by a similar prediction by the two layer model.

The two layer analytical model has clearly demonstrated its ability to explain qualitatively observed phenomena as well as giving an insight into conditions that are not readily apparent. Although it represents a highly simplified approach to a rather complex physical problem, it produces useful information on Massachusetts Bay and can assist the coastal engineer in solving problems related to the ocean environment.

Obviously, the development of more sophisticated one and two layer models would be advantageous. It was shown in the theoretical development that Coriolis force exerts some influence and from comparing model results with field data it can be seen that including Boston Harbor, the Cape Cod Canal, and introducing a wind stress would more realistically describe the physical conditions. However, the objective was to develop a simple analytical model of Massachusetts Bay and thereby demonstrate that if current predictions are desired one should indeed have a two layer model. This goal has been achieved in the qualitative agreement of predicted and observed phenomena in Massachusetts Bay.

BIBLIOGRAPHY

- Butman, B. (1971) "Some Short Term Current Observations in Massachusetts Bay", M.I.T., Department of Earth and Planetary Sciences, Unpublished Report.
- Christodoulou, G.C. and Leimkuhler, W.F. (1973) "Report of NOMES Current Observations", M.I.T., Department of Civil Engineering, Unpublished Report.
- Conner, J.J. and Wang, J.D. (1973) "Finite Element Modeling of Two Dimensional Hydrodynamic Circulation in Shallow Water Masses", M.I.T., Department of Civil Engineering, Technical Report No. 171.
- Day, C.G. (1959) "Oceanographic Observations, 1957, East Coast of the United States", U. S. Department of the Interior, Special Scientific Report -- Fisheries, No. 282.
- Doret, S. D. and Madsen, O. S. (1972) "Special Studies Dealing with Run-Up on Impermeable Breakwaters", M.I.T., Department of Civil Engineering, Unpublished Report.
- Frankel, S. L. and Pearce, B.R. (1973) "Chemistry Data Report on the Massachusetts Bay Area", M.I.T., Department of Civil Engineering, Unpublished Report.
- Grubert, J.P. and Abbott, M.B. (1972) "Numerical Computation of Stratified Nearly Horizontal Flows", Journal of the Hydraulics Division, A.S.C.E., Vol. 98, No. HY 10.
- Halpern, D. (1971,a) "Observations on Short-period Internal Waves in Massachusetts Bay", Journal of Marine Research, Vol. 29, No. 2.
- Halpern, D. (1971,b) "Semidiurnal Internal Tides in Massachusetts Bay", Journal of Geophysical Research, Vol. 76, No. 27.
- Ippen, A.T. and Goda, Y. (1963) "Wave Induced Oscillations in Harbors: The Solution for a Rectangular Harbor Connected to the Open Sea", M.I.T., Department of Civil Engineering, Technical Report No. 59.
- Pedersen, F.G. (1972) "Gradually Varying Two-Layer Stratified Flow", Journal of the Hydraulics Division, A.S.C.E., Vol. 98, No. HY 1.
- U.S. Department of Commerce, NOAA (1972) "Tide Tables High and Low Water Predictions, 1973", U.S. Government Printing Office, Washington, D.C.

APPENDIX A

LISTING OF THE PROGRAM USED FOR THE COMPUTATIONS PRESENTED IN CHAPTER IV

The program used for the computation of the solution for the two layer model is presented along with a sample of the output. The "comment cards" should make the program self-explanatory.

```

C TWO LAYER MODEL OF MASSACHUSETTS BAY
C SIMPLE RECTANGULAR GEOMETRY, OPENING ALONG ONE SIDE FROM X1 TO X2
C AVERAGE BAY DEPTH ASSUMED TO BE 120 FEET
C PROGRAM COMPUTES AMPLITUDES AND VELOCITIES FOR TWO LAYER FLOW
C REAL K, M1, M2, MC1, MC2, MN1, MN2
C DIMENSION K(100), A(100), B(100)
C SPECIFY BAY CONDITIONS (RH01, RH02, H1, H2) ON NEXT FOUR CARDS
RHO1=1.02558
RHO2=1.0225
H1=100.0
H2=20.0
C SPECIFY INPUT CONDITIONS AT A GIVEN LOCATION
C I.E. (ETA11 AND ETA22 AT X AND Y COORDINATES)
ETA11=3.5
ETA22=4.5
X=10.0
Y=5.0
C END OF INPUT CONDITIONS
C *****
C SPECIFIED CONSTANTS FOR MASSACHUSETTS BAY
X=X*6076.1
Y=Y*6076.1
RHO3=(RHO1-RHO2)/RHO1
G=32.1725
PI=3.1415926535
W=(2.*PI)/(12.4*3600.)
C=(RHO3*G*H2)/W**2
XC=59.0*6076.1
X1=0.0
X2=41.0*6076.1
Y0=20.0*6076.1
M1=((W**2*(H1+H2))/(G*P2*RHO3*H1))-((W**2)/(G*(H1+H2)))
M2=((W**2)/(G*(H1+H2)))
MC1=M1*.5
MC2=M2*.5
C COMPUTES A0 AND B0 BY ITERATION

```

```

1C      AC=-C.01
2C      BC=4.0
        AINC=0.01
        EINC=0.1
        AC=AC+AINC
        BC=BC+BINC
        F5=C.0
        F6=C.0
        F7=0.0
        N=0
5C      N=N+1
        K(N)=(N*PI)/X0
        MN1=M1-K(N)**2.
        MN2=M2-K(N)**2.
        IF (MN1) 7C, 7C, 65
        CCNTINUE
65      MN1=MN1**.5
        MN2=(-MN2)**.5
        ANL2=(-.5*MN1*SIN(MN1*YC))
        BAL2=(.5*MN2*SINH(MN2*YC))
        C1=(-MN1*SIN(MN1*YO))
        C2=C*(K(N)**2*MN1*SIN(MN1*YO)+MN1**3*SIN(MN1*YO))
        ANL1=C1+C2
        C1=MN2*SINH(MN2*YO)
        C2=C*(-K(N)**2*MN2*SINH(MN2*YO)+MN2**3*SINH(MN2*YO))
        BAL1=D1+E2
        F5=CCS(MN1*Y)
        F6=COSH(MN2*Y)
        GC TC 8C
        CCNTINUE
7C      MN1=(-MN1)**.5
        MN2=(-MN2)**.5
        ANL2=.5*MN1*SINH(MN1*YC)
        BAL2=.5*MN2*SINH(MN2*YC)
        E1=MN1*SINH(MN1*YO)
        E2=C*(-K(N)**2*MN1*SINH(MN1*YO)+MN1**3*SINH(MN1*YO))

```

```

80      ANL1=E1+E2
        F1=MN2*SINH(MN2*Y0)
        F2=C*(-K(N)**2*MN2*SINH(MN2*Y0)+MN2**3*SINH(MN2*Y0))
        BAL1=F1+F2
        F5=CCSH(MN1*Y)
        F6=COSH(MN2*Y)
        CCNTINUE
        G1=(-2.*W**2*(SIN(K(N)*X2)-SIN(K(N)*X1))/(G*H1*(X2-X1))*K(N))
        G2=SIN(MC1*YC)*((1/MC1)-(G*H2*MC1)/W**2)
        G3=SIN(MC2*YC)*((1/MC2)-(G*H2*MC2)/W**2)
        ACL1=G1*G2
        ECL1=G1*G3
        G4=(SIN(K(N)*X2)-SIN(K(N)*X1))/(X2-X1)*K(N)
        ACL2=(-MC1*SIN(MC1*YC))*G4
        BCL2=(-MC2*SIN(MC2*YC))*G4
        G5=AC*ACL1+BC*BCL1
        G6=A0*ACL2+BC*BCL2
        A(N)=(G5/PNL1-G6/BNL2)/((ANL1/BNL1-ANL2/BNL2)
        B(N)=(G5/ANL1-G6/ANL2)/((BNL1/ANL1-BNL2/ANL2)
        H5=COS(K(N)*X)*(A(N)*F5+B(N)*F6)+H5
        F6=K(N)**2*CCS(K(N)*X)*(A(N)*F5+B(N)*F6)+H6
        F7=COS(K(N)*X)*(A(N)*MN1**2*F5+B(N)*MN2**2*F6)+H7
        IF(50-N) 85, 50, 50
        CCNTINUE
85      ETA2=H5+(A0*CCS(M01*Y)+EC*CCS(MC2*Y))
        ETA1=ETA2-(G*H2/W**2)*((H6+H7+A0*M1*CCS(M01*Y)+B0*M2*CCS(M02*Y)))
        IF (BC-6.C) 6,33,33
        CCNTINUE
        6
        IF (ETA2-ETA22) 20, 35, 29
29      IF (BINC-C.OCC1)35, 35, 30
30      PC=BC-BINC
        BINC=BINC/10.C
        IF (BINC-C.OCC1)35,35,20
33      IF (AC-1.C)7, 7, 45
7      CCNTINUE
35      IF (ETA1-ETA11) 10, 45, 40

```

```

40 AC=AC-AINC
   AINC=AINC/10.C
   IF (AINC-0.00001) 45,45,10
45 CONTINUE
   AC=AO+AINC
   EC=BO+BINC
58 FORMAT (I11,'          AC =',F7.4,20X,'BC =',F8.5,/)
   WRITE (6,58) BC, AC
59 FORMAT (I10,' COMPUTES AN AND BN FOR N = 1 TO 50 ',/)
   WRITE (6,59)
   C
   C COMPUTES AN AND BN FOR N = 1 TO 50
   DO 185 N = 1, 50
   K(N)=(N*PI)/X0
   M1=M1-K(N)**2.
   M2=M2-K(N)**2.
   IF (M1) 170, 170, 160
160 CONTINUE
   M1=M1**0.5
   M2=(-M2)**0.5
   ANL2=(-0.5*M1*SINH(M1*YC))
   BNL2=(0.5*M2*SINH(M2*YC))
   C1=(-M1*SINH(M1*YO))
   C2=C*(K(N)**2*M1*SIN(M1*YO)+M1**3*SIN(M1*YO))
   ANL1=C1+C2
   D1=M2*SINH(M2*YO)
   D2=C*(-K(N)**2*M2*SINH(M2*YO)+M2**3*SINH(M2*YO))
   BNL1=D1+D2
   GO TO 180
170 CONTINUE
   M1=(-M1)**0.5
   M2=(-M2)**0.5
   ANL2=0.5*M1*SINH(M1*YC)
   BNL2=0.5*M2*SINH(M2*YC)
   E1=M1*SINH(M1*YO)
   E2=C*(-K(N)**2*M1*SINH(M1*YO)+M1**3*SINH(M1*YO))
   ANL1=E1+E2

```

```

180      F1=MN2*SINH(MN2*Y0)
      F2=C*(-K(N)**2*MN2*SINH(MN2*Y0)+MN2**3*SINH(MN2*Y0))
      BNL1=F1+F2
      CCNTINUE
      G1=(-2.*W**2*(SIN(K(N)*X2)-SIN(K(N)*X1))/(G*H1*(X2-X1)*K(N))
      G2=SIN(MC1*YC)*(1/MC1)-(G*H2*MC1)/W**2)
      G3=SIN(MC2*YC)*(1/MC2)-(G*H2*MC2)/W**2)
      ACL1=G1*G2
      BCL1=G1*G3
      G4=(SIN(K(N)*X2)-SIN(K(N)*X1))/(X2-X1)*K(N))
      ACL2=(-MC1*SIN(MC1*YC))*G4
      BCL2=(-MC2*SIN(MC2*YC))*G4
      G5=A0*ACL1+BC*BCL1
      G6=AC*ACL2+B0*BCL2
      A(N)=(G5/BNL1-G6/BNL2)/((ANL1/BNL1-ANL2/BNL2)
      E(N)=(G5/ANL1-G6/ANL2)/((BNL1/ANL1-BNL2/ANL2)
      WRITE (6, 60) N, A(N), E(N)
      FORMAT (10X, I4, 10X, E12.5, 10X, E12.5)
      CCNTINUE
      COMPUTES ETA 1 AND ETA 2
      COMPUTES VELOCITIES U1, V1, U2, V2
      Y=2.0*6076.1
      WRITE (6, 115)
      FORMAT (1F1, 5X, ' COMPUTES ETA AND VELOCITIES FOR TWO LAYER
      IED FLAG')
      WRITE (6, 120)
      FORMAT (1H0, 5X, 'X (NM)', 5X, 'Y (NM)', 10X, 'ETA-1 (FT)', 5X, 'U1 (FPS)',
      1, 5X, 'V1 (FPS)', 10X, 'ETA-2 (FT)', 5X, 'U2 (FPS)', 5X, 'V2 (FPS)')
      X=-6076.1
      X=X+6076.1
      P1=C.0
      P2=C.0
      P3=C.0
      P4=C.0
      P5=C.0
      P6=C.0

```

```

H7=C.0
CC 220 N = 1, 50
M1=M1-K(N)**2
M2=M2-K(N)**2
IF (M1-K(N)**2) 200, 19C, 190
CCNTINUE
M1=M1**5
M2=(-M2)**5
P1=(-K(N)*SIN(K(N)*X)*(A(N)*COS(MN1*Y)+B(N)*CCSH(MN2*Y)))+P1
P2=(COS(K(N)*X)*(-A(N)*MN1*SIN(MN1*Y)+B(N)*MN2*SINH(MN2*Y)))+P2
E2XX=X*K(N)**3*SIN(K(N)*X)*(A(N)*COS(MN1*Y)+B(N)*COSH(MN2*Y))
E2YY=X*A(N)*MN1**2*COS(MN1*Y)-B(N)*MN2**2*COSH(MN2*Y)
F3=E2XX+K(N)*SIN(K(N)*X)*E2YY+P3
E2XXY=A(N)*MN1*SIN(MN1*Y)-B(N)*MN2*SINH(MN2*Y)
E2YYY=A(N)*MN1**3*SIN(MN1*Y)+B(N)*MN2**3*SINH(MN2*Y)
P4=X*K(N)**2*COS(K(N)*X)*E2XX+COS(K(N)*X)*E2YY+P4
F5=COS(MN1*Y)
F6=COSH(MN2*Y)
CC TC 210
CCNTINUE
M1=(-M1)**5
M2=(-M2)**5
P1=(-K(N)*SIN(K(N)*X)*(A(N)*COSH(MN1*Y)+B(N)*COSH(MN2*Y)))+P1
P2=(COS(K(N)*X)*(-A(N)*MN1*SINH(MN1*Y)+B(N)*MN2*SINH(MN2*Y)))+P2
E2XX=X*K(N)**3*SIN(K(N)*X)*(A(N)*COSH(MN1*Y)+B(N)*COSH(MN2*Y))
E2YYX=-A(N)*MN1**2*COSH(MN1*Y)-B(N)*MN2**2*COSH(MN2*Y)
P3=E2XX+K(N)*SIN(K(N)*X)*E2YY+P3
E2XXY=-A(N)*MN1*SINH(MN1*Y)-B(N)*MN2*SINH(MN2*Y)
E2YYY=A(N)*MN1**3*SINH(MN1*Y)+B(N)*MN2**3*SINH(MN2*Y)
P4=X*K(N)**2*COS(K(N)*X)*E2XX+COS(K(N)*X)*E2YY+P4
F5=COSH(MN1*Y)
F6=COSH(MN2*Y)
CCNTINUE
F5=COS(K(N)*X)*(A(N)*F5+B(N)*F6)+H5
F6=X*K(N)**2*COS(K(N)*X)*(A(N)*F5+B(N)*F6)+H6
H7=COS(K(N)*X)*(A(N)*MN1**2*F5+B(N)*MN2**2*F6)+H7

```

```

220 CONTINUE
D=G**2*RT+C3*H2/W**3
ETA2=H5+(AC*CCS(M01*Y)+EC*CCS(M02*Y))
ETA1=ETA2-(G*H2/W**2)*((H6+H7+AC*M1*CCS(M01*Y)+8C*M2*CCS(M02*Y)))
L2=(-G/W)*P1
V2=(-G/W)*(P2+(-A0*M01*SIN(M01*Y)-B0*M02*SIN(M02*Y)))
U1=U2-D*(P3)
V1=V2-D*((AC*M01**3*SIN(M01*Y)+B0*M02**3*SIN(M02*Y))+P4))
X5=X/6076.1
Y5=Y/6076.1
WRITE (6, 230) X5, Y5, ETA1, U1, V1, ETA2, U2, V2
230 FORMAT (5X,F5.2,6X,F5.2,11X,F8.4,7X,F8.4,10X,F8.4,7X,F8.4,
15X,F8.4)
IF (X-(58.*6076.1)) 140, 140, 240
CONTINUE
240 STOP
300 END

```

SAMPLE OF COMPUTER PROGRAM OUTPUT

A_o = -0.058
 B_o = 4.686

COMPUTES ETA AND VELOCITIES FOR TWO LAYERED FLOW

<u>X (NM)</u>	<u>Y (NM)</u>	<u>ETA-1 (FT)</u>	<u>U1 (FPS)</u>	<u>V1 (FPS)</u>	<u>ETA-2 (FT)</u>	<u>U2 (FPS)</u>	<u>V2 (FPS)</u>
10.00	10.00	4.1789	- 0.1582	0.1886	4.4359	- 0.1615	0.1886

